UNIVERSITA' DEGLI STUDI DI PADOVA
FACOLTÀ DI INGEGNERIA

CORSO DI LAUREA MAGISTRALE IN INGEGNERIA ELETTRICA

TESI DI LAUREA MAGISTRALE

CHARACTERISATION OF A HYDRAULIC INSULATING BREAK PROTOTYPE FOR ULTRAPURE COOLING WATER CIRCUIT OF HIGH VOLTAGE COMPONENTS FOR NUCLEAR FUSION EXPERIMENTS

CARATTERIZZAZIONE DEL PROTOTIPO DI UN ISOLATORE IDRAULICO PER CIRCUITI DI RAFFREDDAMENTO AD ACQUA ULTRAPURA DI COMPONENTI IN ALTA TENSIONE PER ESPERIMENTI DI FUSIONE NUCLEARE

RELATORE: CH. MO PROF. PIERGIORGIO SONATO
DIPARTIMENTO DI INGEGNERIA ELETTRICA

CORRELATORI: ING. ANDREA RIZZOLO
ING. MARCO BOLDRIN
CONSORZIO RFX

LAUREANDO: DIEGO CRIVELLARI

ANNO ACCADEMICO 2011-2012

Alla mia famiglia, a Giulia e a Marianna

Contents

Sommario

Oggetto di questa tesi è la caratterizzazione del prototipo di un isolatore idraulico (passante idraulico o break) che avrà lo scopo di addurre acqua ultrapura (avente resistività maggiore di 2 MΩ*cm) per il raffreddamento di componenti in alta tensione (fino a 110 kV in corrente continua) per esperimenti di supporto alla fusione nucleare.
La caratterizzazione è stata preceduta da uno studio della configurazione elettrostica del break mediante analisi agli elementi finiti.
Successivamente, dal punto di vista sperimentale, si è proceduto come segue:

1. è stata eseguita una prova di tenuta dielettrica applicando la piena tensione di funzionamento al break privo di acqua;
2. si è provveduto a mettere a punto il sistema di produzione dell'acqua delle caratteristiche di resistività richieste (superiore a 2 MΩ*cm) tramite filtrazione di acqua deionizzata disponibile in commercio con resistività iniziale dichiarata superiore a 300 kΩ*cm;
3. quindi i prototipi di break oggetto dello studio, preventivamente puliti e successivamente flangiati, sono stati riempiti con tale acqua, per sua stessa natura aggressiva e perciò incline a sciogliere le sostanze con cui entra in contatto, con conseguente riduzione della resistività; in questa fase è stato monitorato l'andamento nel tempo della resistività senza applicazione di tensione;
4. infine, una volta sostituita l'acqua degradata, è stato registrato il decadimento nel tempo della resistività imputabile ai fenomeni elettrochimici prodotti dalla circolazione imposta di corrente elettrica attraverso la colonna d'acqua del break, similmente a quanto previsto nel funzionamento in impianto.

Il lavoro svolto ha verificato l'idoneità dal punto di vista dielettrico dell'attuale disegno dei break per l'uso previsto.
Ha altresì evidenziato il rapido degrado della resistività dell'acqua in esso contenuta, degrado accentuato dalla presenza di fenomeni elettrochimici che si instaurano con la circolazione di corrente elettrica attraverso la colonna di acqua.

Abstract

The aim of this degree thesis is the characterization of a hydraulic insulating break prototype which will be used to adduce ultrapure water (with resistivity greater than 2 MΩ), used to cool components under high voltage (up to 110 kV DC of voltage) for nuclear fusion experiments.
Before the characterization it has been necessary a preventive study of electrostatic configuration of the breaks using Finite Elements Method analysis.
From the experimental point of view, we proceeded as follow:

1. It has been performed a full voltage test (150 kV) to study the dielectric strength of empty breaks;
2. It has been provided to prepare a system to purify water in order to obtain ultrapure water with suitable resistivity (ρ > 2MΩ*cm) using specific filters that purify deionized water (ρ >300 kΩ*cm).
3. The break prototypes, after a preventive cleaning process, have been flanged and filled with the ultrapure water obtained during the purification process; the aggressive nature of this water causes the dissolving of substances that enter in contact with this matter, and this provoke the decay of resistivity. During this process, the decay of resistivity, without applying voltage, has been monitored.
4. Once replaced water with low resistivity with new water purified, it has been monitored the decay of resistivity due to the electrochemical effect caused by the flow of a current imposed by a power supply. This will represent the operative conditions where the breaks will be employed.

The results showed that the break prototype can assure a good electric strength during tests with voltage applied.
It has been also noticed that the fast decay of resistivity of ultrapure water when inserted on break prototypes; this phenomenon of decay became more marked due to electrochemical effect caused by a current that flows on the column of water.

Introduction

In the last years the need to find new sources of energy to provide the increasing lack of energy, which is still not tied to fossil fuels, has led to an intense and strong research to the development of those clean sources that can have an impact on the electric energy market in line with the other sources still exploited.
In this sense, the development of thermonuclear fusion recently had an important impulse, this source represent the future of electric and thermic energy production.
This text, even if is not directly connected to thermonuclear fusion, treats topics that are as much distinctive and will have a large range of applications inside the field of fusion; in particular it will be discussed about the use of ultrapure water to cool down high voltage components that will be affected by heavy heat loads.
On chapter I it will be presented the thermonuclear fusion from the physical aspects, providing a brief introduction and overview of fusion machines, closing with ITER, the principal experiment that is under construction in the south of France. The aim of ITER is to show that fusion could be used to generate electrical power, and to acquire the necessary data to design and operate the first electricity-producing plant. To reach high temperatures that need to heat the plasma and then supply energy it will be necessary to use additional heating systems, as the Neutral Beam Injector, that accelerates, neutralizes and injects neutral fuel particles inside the plasma.
Chapter II introduces the experiments that will be prepared in Padua: SPIDER and MITICA. This last is the first prototype of the Neutral Beam Injectors that will be installed on ITER. One of the critical aspects that need to be considered concerns the cooling of high voltage components. The ultrapure cooling water will be brought from ground potential to the high voltage components by means of insulating pipes, facing considerable problems to assure its resistivity requirements against deterioration phenomena (erosion, corrosion …).
Chapter III will take care about the purification of water and the studies on this delicate element.
Chapter IV will introduce the electrostatic analysis performed on these electric-hydraulic insulators using a FEM method.
Chapter V will provide the full description of interaction among ultrapure water and the breaks used for the tests, with and without voltage applied in order to simulate the operative conditions that would be if these breaks will be installed on injector experiments.

Chapter I : Thermonuclear Fusion

This chapter will show the principal aspects of thermonuclear fusion, giving a simple point of view, starting from the origins and coming to the various applications and further developments of this significant process.

1.1. History of the term "plasma"

In the mid-19th century the Czech physiologist Jan Evangelista Purkinje (1787-1869) introduced use of the Greek word plasma (meaning "formed" or "moulded") to denote the clear fluid which remains after removal of all the corpuscular material in blood. Half a century later, the American scientist Irving Langmuir proposed in 1922 that the electrons, ions and neutrals in an ionized gas could similarly be considered as corpuscular material entrained in some kind of fluid medium and called this entraining medium plasma. However it turned out that unlike blood where there really is a fluid medium carrying the corpuscular material, there actually is no "fluid medium" entraining the electrons, ions and neutrals in an ionized gas. [a]

1.2. Overview

In nuclear physics, nuclear fusion is the process where two, or more, atomic nuclei are joint together to form a single heavy nucleus; this process called fusion is usually accompanied by the release or absorption of large quantities of energy.
Due to conservation of energy and momentum, the energy released by the reaction is distributed among the two, or more, fusion products in quantity inversely proportional to their masses.
Generally, when dealing with light elements, like Hydrogen or Helium for example, the lower the ratio of atomic mass to mass number is, the heavier the nucleus is. This is known as mass defect.
This lost mass is present in the released energy in accordance with $E=mc^{2.}$ Most of the excess binding energy is released as kinetic energy of the resulting particles.

1.3. Principal reactions

As said before, for thermonuclear fusion are used light elements, the least difficult fusion reaction to initiate in earth is that between the hydrogen isotopes D and T:

$$D + T \longrightarrow {}^{4}He\ (3.5\ MeV) + n\ (14.1\ MeV)$$

in which D stands for Deuterium (the stable isotope of hydrogen with a nucleus consisting of one proton and one neutron) and T for Tritium (the radioactive hydrogen isotope with a nucleus of 2 neutrons and 1 proton); to produce sufficient fusion reactions, the temperature of the plasma has to be on order of 100 to 200 million °C for this reaction. A first generation of future fusion reactors would be based on this reaction. The reaction products are thus an α–particle (helium nucleus) and a very energetic neutron. Twenty percent of the energy is taken by the α–particles which are confined, owning to their charge, and deliver their energy to the background plasma. The kinetic energy of fast neutrons will be converted into heat in a blanket and then into electric energy using conventional technology (steam).
The D-T reaction is not the only possibility for controlled fusion. Other conceivable reactions are:

$$D + D \longrightarrow {}^{4}He\ (0.82\ MeV) + n\ (2.45\ MeV)$$

$$D + D \longrightarrow T\ (1.01\ MeV) + H\ (3.02\ MeV)$$

$$D + {}^{3}He \longrightarrow {}^{4}He\ (3.6\ MeV) + H\ (14.7\ MeV)$$

These are more difficult to achieve and have a much lower power density than the D-T reaction but show even more benign environmental features.
The D-D reaction would eliminate the need for Tritium and produce neutrons with lower energies which are therefore easier to absorb and shield.
The reactions also releases its total energy in the form of charged particles, enabling in principle the possibility of direct energy conversion to electrical energy. However, the prospects for these "advanced" fuels are still too speculative and only the D-T reaction has immediate future prospects.

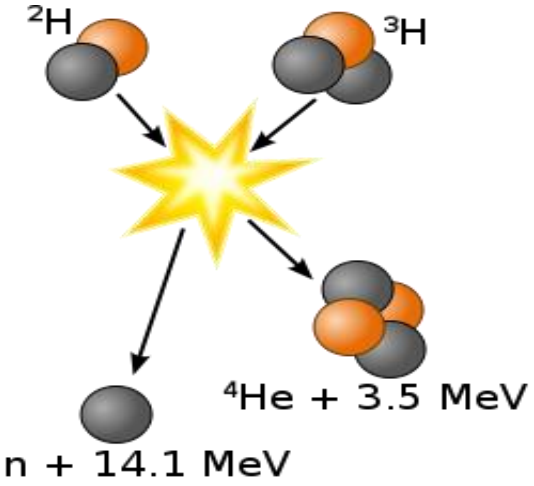

Figure I-1: Fusion of deuterium wit tritium creating helium, freeing a neutron, and releasing 17.59 MeV of energy.

The most obvious advantage of fusion is the virtual inexhaustibility of fuels which are cheap and widely accessible.
Deuterium, a non-radioactive isotope of hydrogen is extremely plentiful as it can be obtained from ordinary water (about 33 g from 1 ton) with cheap extraction techniques using conventional technology. Complete burning of deuterons and the first generation fusion products (T and ^{3}He) results in the overall equation:

$$6D \longrightarrow 2{}^{4}He + 2H + 2n + 43.3\ MeV$$

providing $350*10^{15}$ J/ton D. The Deuterium content of the oceans is estimated at $4.6*10^{13}$ tons, thus equivalent to about $5*10^{11}$ TWyr.
Tritium is the radioactive isotope of Hydrogen. It decays to ^{3}He by emission of an electron:

$$T \longrightarrow {}^{3}He + e^{-} + 18.7\ keV$$

with the rather short half-life of 12.3 years. The quantities available in nature are not sufficient for technical applications. The neutrons produced in the fusion reactions will be used to breed it by bombarding a blanket around the burn chamber containing a lithium compound, according to:

$$^{6}Li + n \longrightarrow {}^{4}He\ (2.05\ MeV) + T\ (2.73\ MeV)$$

$$^{7}Li + n \longrightarrow {}^{4}He + T + n - 2.47\ MeV$$

Thus the real consumables in the D-T fusion process are D and Li, while T is an intermediate fuel.
Lithium, like Deuterium, is a widely available element. There are two isotopes ^{6}Li and ^{7}Li, which occur naturally (7.5% and 92.5% respectively). ^{6}Li is the most useful isotope as it reacts with neutrons in the lower energy range (E<1 MeV).

1.4. Principal parameters

Three fundamentals parameters characterize plasma:

1-The particle density *n* (measured in particles per cubic meter),

2-The temperature *T* for each species (usually measured in eV, where 1 eV=11600 K),

3-The steady state magnetic field *B* (measured in Tesla).

A host of subsidiary parameters (for example Debye length, Larmor radius, plasma frequency, cyclotron frequency, thermal velocity) can be delivered from these three fundamental parameters. [a]

1.5. Fusion on Earth

There exist presently two approaches to realize nuclear fusion on Earth: inertial and magnetic fusion.
Inertial fusion consists of micro-explosions of small fuel pellets by means of powerful lasers or particle beams; confinement of the fuel is based on the inertia of the pellet fuel mass, which resists the natural expansion when it is heated to thermonuclear fusion temperatures.
Magnetic fusion uses magnetic fields to confine the fuel. Seems that this last type of confinement is the most used and developed in Europe due to the important progress made in the last 30 years.
There is a third type of confinement: the gravitational confinement, but it's impossible to reproduce this process because the gravitational confinement happens on the stars where the gravitational force oppose to the expansion due to the very high temperatures reached; the parameters of these plasmas cover an enormous range.

1.6. Fusion machines

1.6.1. Stellarators

The stellarator concept was introduced in 1951 by the astrophysicist Lyman Spitzer. In order to introduce rotational transform in a toroidal configuration he proposed to twist a torus into a shape resembling the shape of the number 8 (figure-eight stellarator).
The first stellarator confinement experiment was built in Princeton (Princeton C stellarator) but was no successful: the plasma lost very quickly. In the same period the tokamak line became the best way to confine plasma so the stellarator concept was pursued only in some places.
An important part in the engineering design of a stellarator is the question how a coil system must produce the desired magnetic field. The classical coil system stellarator consists of groups of interlinked coils (see Figure

I-2): a set of planar coils generating the toroidal field component and four helical coils carrying currents running in alternating directions in neighboring coils responsible for the helical field components**.** [b]

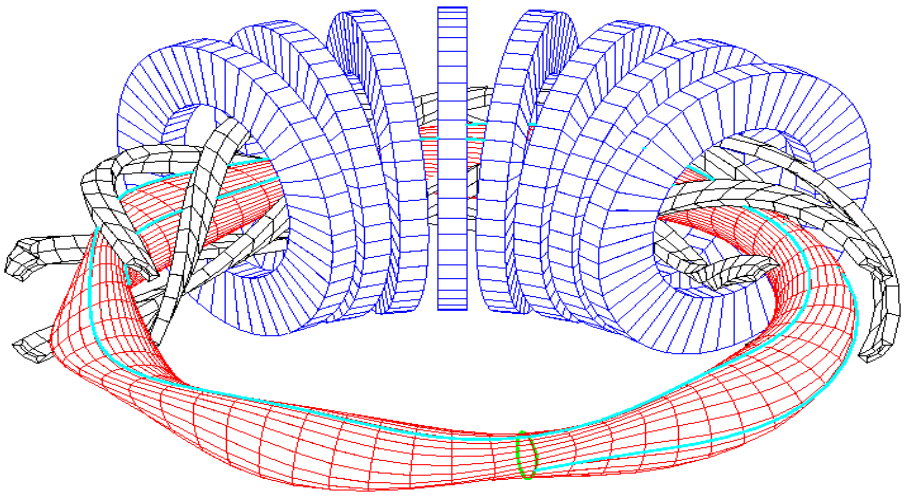

Figure I-2: Classical coil system for stellarators.

Stellarators, in general sense, do not need a large toroidal net plasma current for confinement, and with the advent of powerful auxiliary heating sources they did no longer require the plasma current for ohmic heating.

1.6.2. RFPs

The Reversed Field Pinch (RFP) is an axisymmetric toroidal system in which the plasma is confined by a combination of a poloidal field produced by the plasma current I_φ flowing around the torus and a toroidal field, B_φ, produced by currents flowing both in the plasma and in external coils.
Schematically the system is similar to a Tokamak (see 1.6.3) and consists of a toroidal vessel, in which the plasma is formed, surrounded by a toroidal winding, that generates the initial B_φ, and coupled to a coaxial transformer whose secondary is the plasma current I_φ.
The configuration derives its name from the fact that the toroidal magnetic field in the outer region is reversed with respect to its direction on the axis (see Figure I-3).

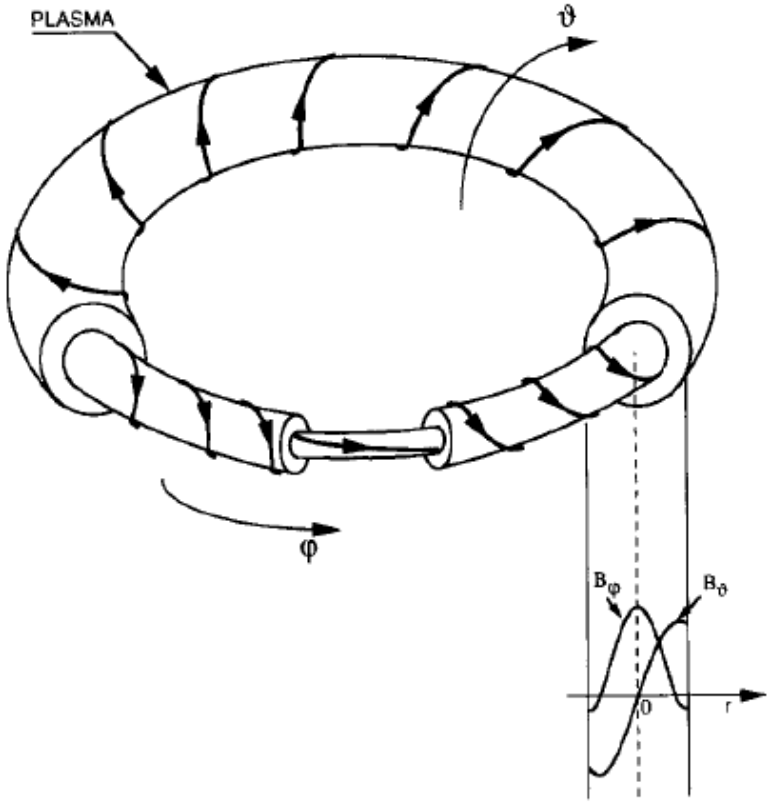

Figure I-3: RFP plasma ring example.

However, while a toroidal current can be efficiently provided by an ohmic transformer, a practical scheme to drive the poloidal current with a similar efficiency is presently lacking.
Experimentally the configuration is realized thanks to a spontaneous dynamo mechanism, driven by global resistive tearing modes resonant on closely spaced magnetic surfaces in the core of the discharge, inside the reversal surface.
In Padua is located one of most important RFP experiment, called RFX where several upgrades has been performed to improve the knowledge of RFP physics and this put emphasis on the capability to operate in conditions more similar to tokamaks.
The most important difference between tokamak and RFP magnetic field configurations is that in the tokamak the toroidal field is much larger than the poloidal field, whereas in RFP the toroidal and the poloidal components are of the same order of magnitude and the toroidal field reverses in the plasma other region.At present, RFP experiments in addition to RFX are underway in Sweden, United States and Japan principally. [c]

1.6.3. Tokamaks

The tokamak is a toroidal plasma confinement system, the plasma being confined by a magnetic field. The word tokamak is derived from Russian word, **to**roidalnaya **ka**mera and **ma**gnitnaya **k**atushka, meaning "toroidal chamber" and "magnetic coil". The device was invented in the Soviet Union in the late 1950's.
The successful development of the tokamak was principally the result of the careful attention paid to the reduction of impurities and the separation between the plasma and the vessel.
The principal magnetic field is the toroidal field. However, this field not alone doesn't allow confinement of plasma. In order to have an equilibrium in which the plasma pressure is balanced by the magnetic forces it is necessary also to have a poloidal field. In a tokamak this field is produced mainly by the current in the plasma itself, this current flowing in the toroidal direction.

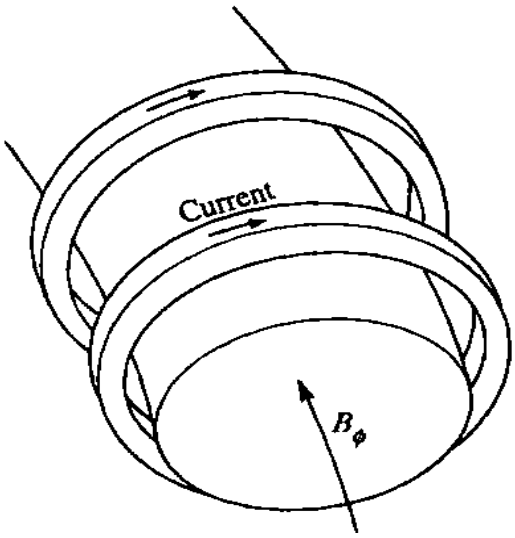

Figure I-4: The toroidal magnetic field is produced by current in external coils.

The toroidal magnetic field is produced by currents in coils linking the plasma, as shown in Figure I-4. The combination of the toroidal field B_ϕ and the poloidal field B_θ gives rise to the magnetic field lines which haves a helical trajectory around the torus as shown in Figure I-5(a) and (b).

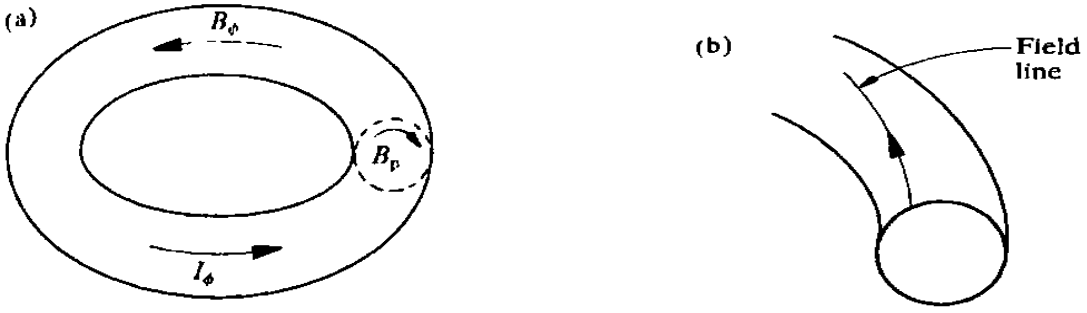

Figure I-5: (a) Toroidal magnetic field B_ϕ, and poloidal field B_θ due toroidal current I_θ. (b) Combination of B_ϕ and B_θ.

The plasma pressure is the product of the particle density and the temperature; the pressure which can be confined is determined by stability considerations and increases with the strength of the magnetic field.
Since the toroidal magnetic field is inversely proportional to the major radius the resulting field at the centre of the plasma would be around 6-8 T.

The toroidal fields in present large tokamaks are somewhat lower than this value.
In present large tokamaks, currents of several megamps are used, a current of 7 MA having been produced in the JET (Joint European Reactor) tokamak. With conservative assumptions a reactor would require a current of 20-30 MA.
In present experiments the plasma current is driven by a toroidal electric field induced by a transformer action in which a flux change through the torus is generated. The flux change is brought about by a current passed through a primary coil around the torus. Control of the shape requires additional toroidal currents, further such currents are required to control the position of the plasma.
These toroidal currents are carried by suitably placed coils (see Figure I-6).

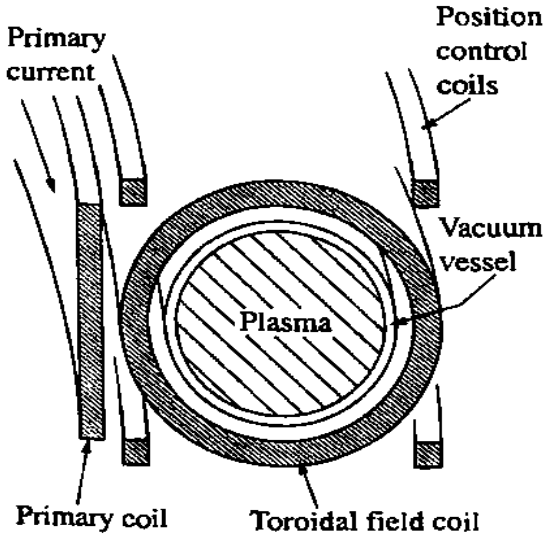

Figure I-6: Arrangement of coils in a tokamak.

An energy confinement time of greater than one second has been obtained in JET. It is found that the energy confinement time increases with plasma current and, unfortunately, decreases with increasing plasma pressure.

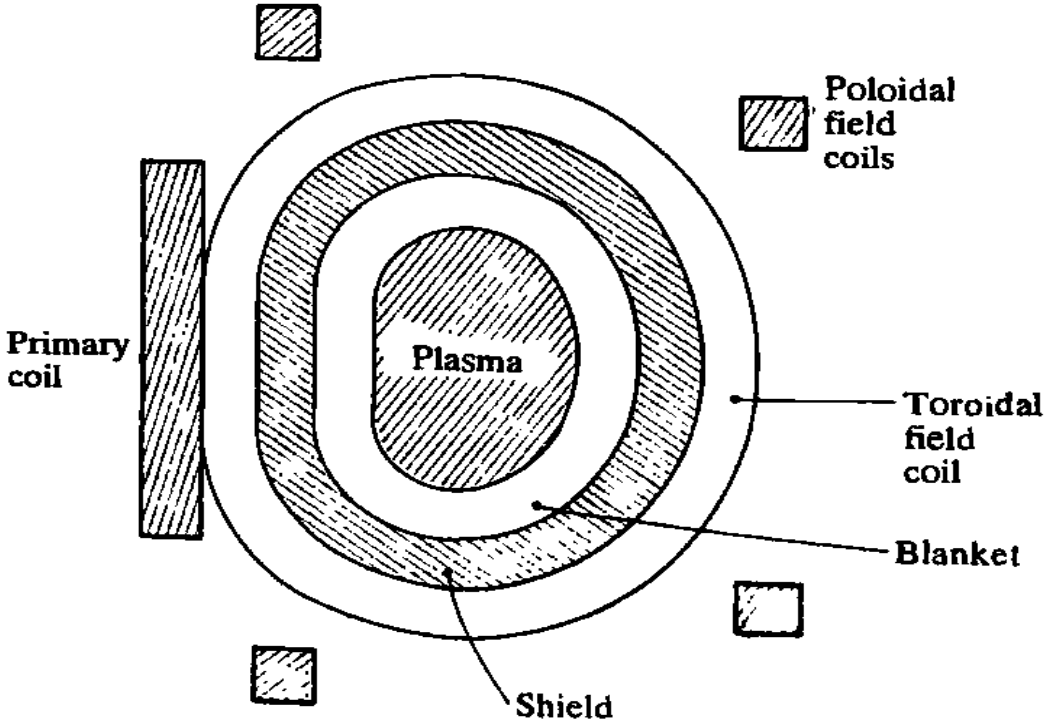

Figure I-7: Layout of principal components in a conceptual tokamak reactor.

The structure of a tokamak reactor is shown in Figure I-7; we can see that the plasma is surrounded by a blanket which has three roles: first, absorb the 14 MeV neutrons transforming their energy into heat which is carried out by a coolant system. Secondly, in absorbing neutrons the blanket shields the superconducting coils and other outer components. Thirdly the blanket allows the necessary breeding of Tritium to fuel the reactor. The blanket is composed by a compound of Lithium: Li_2O.

Ideally the toroidal current in the plasma would be continuous in time. However with the transformer action, the driving electric field is induced by increasing the magnetic flux linking the torus and this can only be continued for a limited period. The transformer action allows pulses of about one hour.

Due to this problem, to achieve a continuous current, a remaining part of the current would be driven by injected neutral particle beams or electromagnetic waves.

In particular, this document will show the problems linked to the cooling of neutral beam injector and give some possibilities to improve this apparatus.

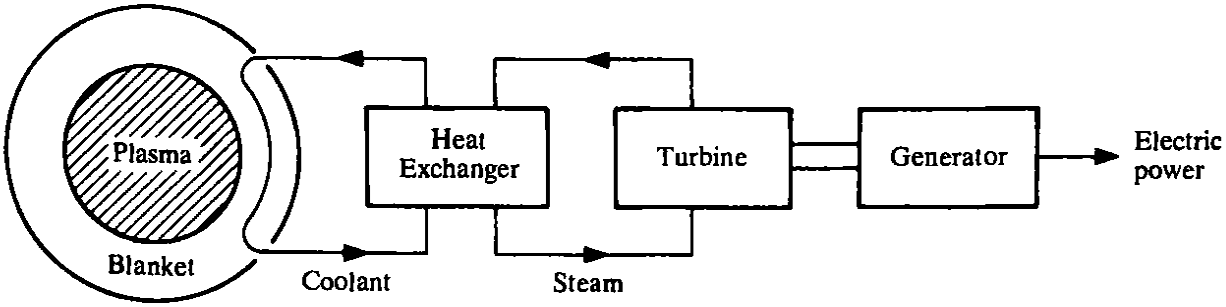

Figure I-8: Thermonuclear power absorbed in blanket would be converted into electric power by conventional means.

1.6.1.1. Additional heating in tokamaks

The two main methods used to increase the temperature to reach the ignition conditions are the injection of energetic neutral beams and the resonant absorption of radio frequency (RF) electromagnetic waves; both of these methods would be capable of providing heating and both have been tested at power levels of tens of MW.
The beams used for injection heating have to be composed of neutral particles because ions would be reflected by the tokamak magnetic field, the heating with neutral beams is a complex process. Ions must first be produced and accelerated to the required energy, they are then neutralized by charge exchange in a gas target and the unwanted residual ions removed. In the plasma the neutral particles become charged again and as a result are confined by the magnetic field; they are then slowed by collisions with the plasma particles, giving up their energy in the process.
As said before, the neutral atoms injected into a plasma travel in straight lines, being unaffected by the magnetic field. The atoms become ionized through collisions with the plasma particles and the resulting ions and electrons are then held by the magnetic field; since the ions and electrons have the same velocity the energy is carried almost entirely by the more massive ions.
Is desirable that the flux of neutral take place in the central region of the plasma.
There are difficulties in producing neutral beams with high energies; the proposed solution is to use negative ion beams, which can be produced and neutralized at higher energies.
A disadvantage of neutral beam systems is the large scale of the equipment and that they have to be in the immediate vicinity of the torus thus they are being subjected to high neutron fluxes and tritium contamination, nevertheless, they can be tested and developed separately from the tokamak itself, and the heating profile can be predicted independently of the magnetic configuration.

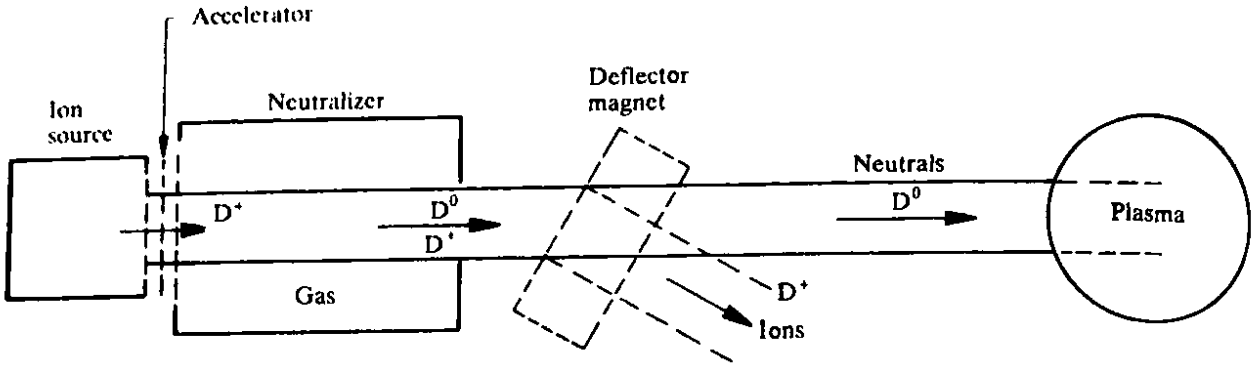

Figure I-9: Layout of neutral injection system.

The first neutral beam injection systems were based on positive ion sources, it was envisaged that the problem of producing high energy beams with a high neutral fraction can be overcame by using negative ion sources. Such sources allow the achievement of much higher neutral fractions at high energy than is possible with positive ion beams.
The goal of the present research endeavours is to extract 40 A of ion current and accelerate it to 1 MeV as to be useful for the ITER experiment. [d]

1.7. ITER experiment

ITER (acronym of **International Thermonuclear Experimental Reactor**) is an international nuclear fusion research and engineering project, which is currently building the world's largest and most advanced experimental tokamak nuclear fusion reactor at Cadarache in the south of France. The ITER project aims to make the long-awaited transition from experimental studies of plasma physics to full-scale electricity-producing fusion power plants. The project is funded and run by seven member entities - the European Union (EU), India, Japan, the People's Republic of China, Russia, South Korea and the United States. The EU, as host party for the ITER complex, is contributing 45% of the cost, with the other six parties contributing 9% each.

The ITER fusion reactor itself has been designed to produce 500 megawatts of output power for 50 megawatts of input power, or ten times the amount of energy put in. The machine is expected to demonstrate the principle of getting more energy out of the fusion process than is used to initiate it, something that has not been achieved with previous fusion reactors. Construction of the facility began in 2007, and the first plasma is expected in 2019. When ITER becomes operational, it will become the largest magnetic confinement plasma physics experiment in use, surpassing the Joint European Torus (JET) located in UK.

The first commercial demonstration fusion power plant, named DEMO, is proposed to follow on from the ITER project to bring fusion energy to the commercial market.

ITER is designed to produce approximately 500 MW of fusion power sustained for up to 1,000 seconds (compared to JET's peak of 16 MW for less than a second) by the fusion of about 0.5 g of deuterium/tritium mixture in its approximately 840 m^3 reactor chamber. Although ITER is expected to produce (in the form of heat) 10 times more energy than the amount consumed to heat up the plasma to fusion temperatures, the generated heat will not be used to generate any electricity.

ITER's mission is to demonstrate the feasibility of fusion power, and prove that it can work without negative impact.

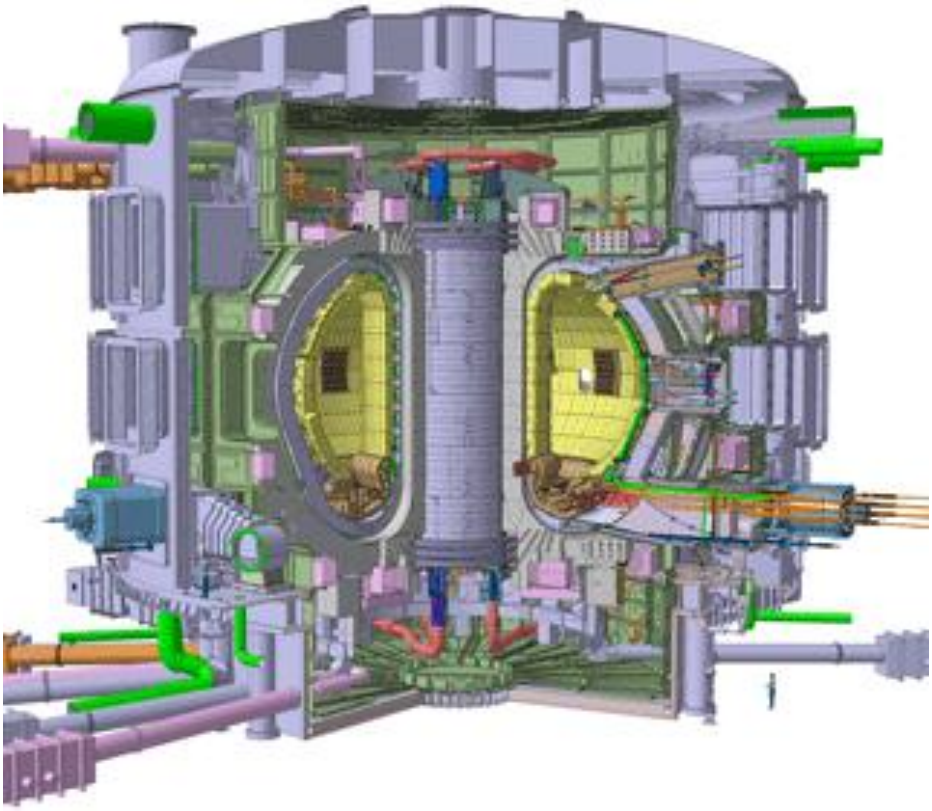

Figure I-10: View of ITER experiment.

The principal characteristics of this tokamak are:

- **Building height**: 24 m;
- **Building length** : 30 m;
- **External radius of plasma**: 6.2 m;
- **Internal radius of plasma**: 2 m;
- **Temperature of plasma:** $1.5*10^8$ K;
- **Output power:** 500÷700 MW;
- **Heating power:** 53 MW;
- **Volume of plasma:** 837 m^3;
- **Surface of plasma:** 678 m^2:
- **Pulse time duration:** 300÷5000 s;
- **Toroidal magnetic field of external radius of plasma:** 5.2 T;
- **Plasma current:** 15 MA
- **Total weight:** 23350 t.

Chapter II : The Neutral Beam Injector: SPIDER and MITICA

Concerning ITER (International Thermonuclear Experimental Reactor) project, the neutral beam injector (NBI) is one of most important part that needs to be studied and developed. ITER will need 2 (+1 optional) NBI, for a maximum power injected in the plasma of about 50 MW.
In Padua will be created a new specific structure to host the first NBI prototype. At this aim, two experiments will be performed.

2.1. The site

The Padua research area where presently the activities of the Consorzio RFX are hosted will also host the two above-mentioned experiments. In Figure II-1, the new buildings for the two experiments are shown. The full size source experiment is located on the left hand side of the building. The main building is divided in two parts: the main and the highest one host the two experimental devices, whereas the adjacent building hosts the experimental service plants, like cooling system, cryogenic systems and power supplies. The whole length of the main building is 110m. A total surface of 7000m^2 of new buildings has been designed to host the two experimental devices. The presently existing power station at 400 kV will be adapted to supply the necessary energy as well as the other conventional services to operate the facility.

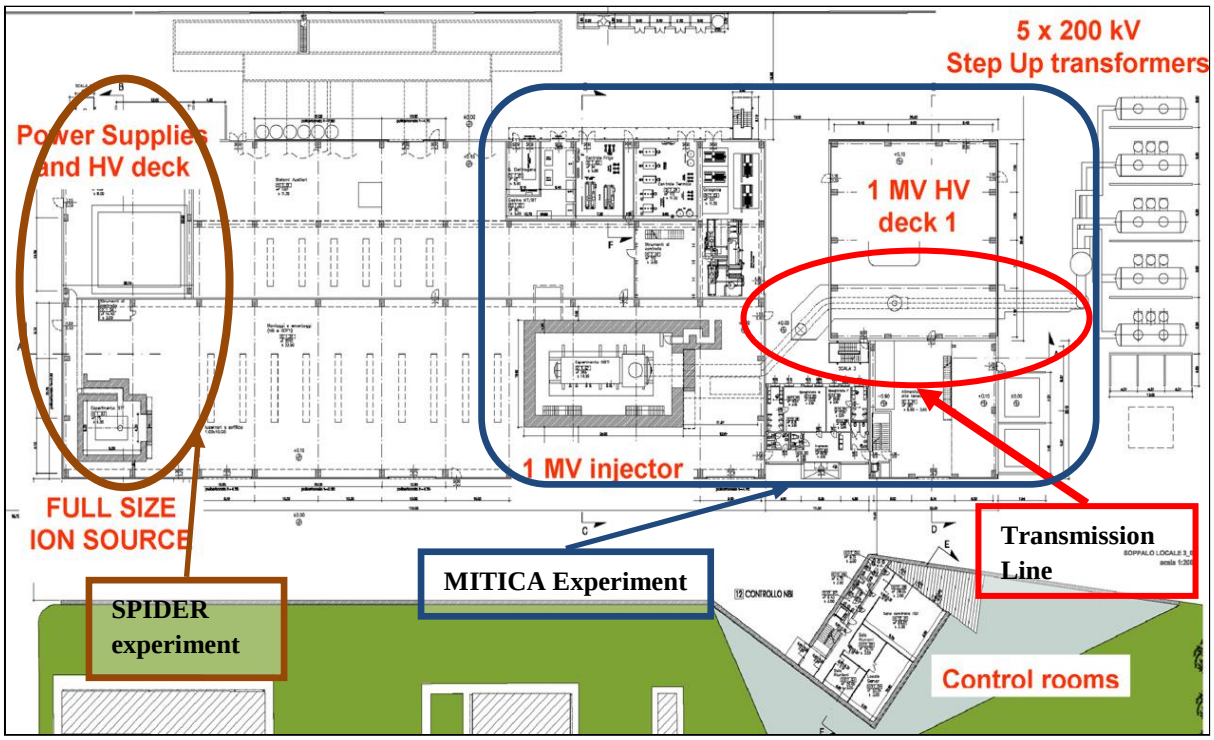

Figure II-1: Neutral beam test facility located in Padua.

2.2. MITICA experiment

MITICA (**M**egavolt **IT**er **I**njector & **C**oncept **A**dvancement) will be the prototype of the Heating Neutral Beam (HNB) injectors and its components will mostly be first of a kind, with some exceptions, to be fully tested before starting the operation at ITER. The ion source and the extractor will be very similar to those of SPIDER (described in the next paragraph). The accelerator is composed of five acceleration stages of 200 keV each.
MITICA will produces a Deuterium neutral beam (D^0) with a maximum power of 16.7 MW, this beam is obtained by a negative ion beam (40A) generated and accelerated by a voltage of 1MV inside the beam source.

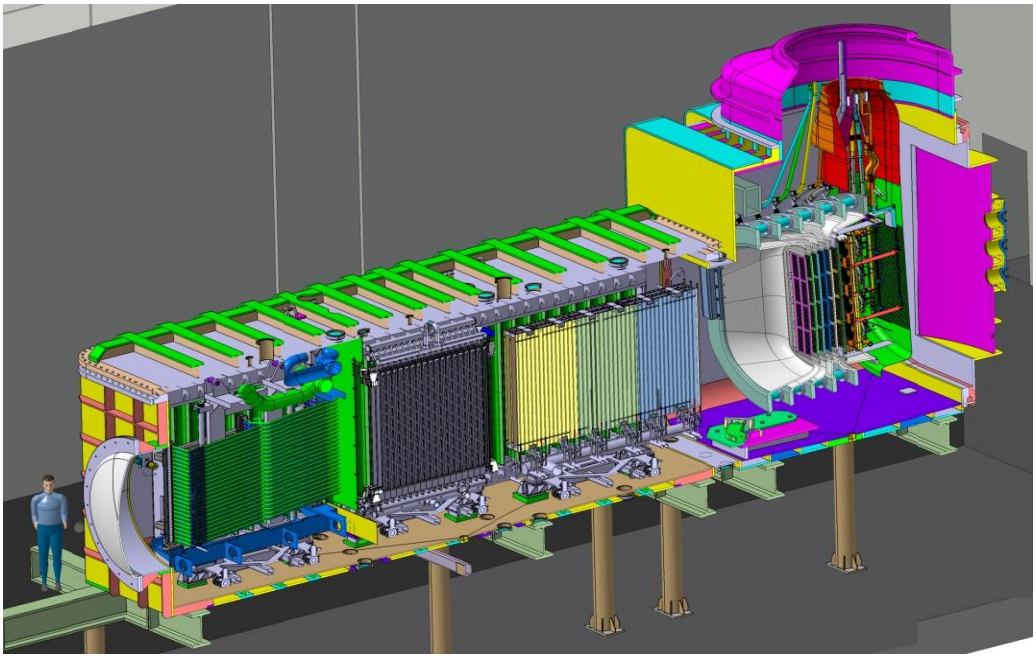

Figure II-2: View of MITICA experiment.

The total dimension of the vacuum vessel is: 15 m long, 5m wide and 9 m height. The 9 m height takes into account also the height of the 1 MV SF_6 to vacuum feedthrough which acts as interface for the electric and hydraulic connections of the source devices set at – 1 MV potential and of the accelerating grids system. The vacuum vessel is dimensioned so that to resist to an inward pressure of 2 bar. The vessel is equipped both with a rear port to access the source and a large port placed on the upper surface of the vessel of the beam components to allow access from above during the mounting and maintenance of the internal components. In ITER, the beam exit port is connected to an interface valve between the injector vacuum vessel and the tokamak vacuum vessel. In MITICA, the same port is closed by a blind flange because the injector is connected to no other vacuum chambers.
The injector must be maintained at a vacuum level of the order of 0.02 Pa in the entire region where the charged and neutralized particle beam travels along.
The pumps must have a huge pumping velocity of the order of about 5000 m^3/s at a pressure of about 0.02 Pa. This high pumping velocity can be obtained only by using helium cryogenic pumps operating in the temperature range between 4.5 and 6.5 K.
The MITICA power supply system has to provide electric power to the accelerating grid system up to 1 MV voltage and has to provide electric power to the negative ion source power supply system, which is set at – 1MV, to the residual ion neutralization system and to other injector auxiliary components.
The power supply system gets the power from the 400 kV electric power line and in the substation the power is distributed to the various systems at a voltage of 22 kV and to sub systems after proper voltage adaptation carried out in a dedicated cabin.

The SF_6 insulated transmission line has to carries conductors from the power supply system to the injector with a level of insulation up to 1 MV and with conductors with intermediate potentials scaled of 200 kV for acceleration grids.
As far as the MITICA power supplies are concerned, the most challenging component within the European scope is the high voltage (1MV) bushing, which takes the conductors of the ion source power supply from the High Voltage Deck (HVD1) down to the 1MV Transmission Line (TL); the interface between the bushing and the transmission line is particularly critical.
At present time it is foreseen that the procurement of the majority of the MITICA components will start between 2011 and 2012. The assembly phase will instead start in the second half of 2014.

2.3. SPIDER experiment

SPIDER (**S**ource for **P**roduction of **I**on of **D**euterium **E**xtracted from **R**f plasma) is a full-size ion source with a 100 kV accelerator, dedicated to the optimization of the negative ion source of the Heating Neutral Beam (HNB) and of Diagnostic Neutral Beam (DNB).
SPIDER is an experiment which will allow to develop the knowledge on negative ions and optimize the maximization and uniformity of negative ion production, before MITICA goes into operation (indicatively 2.5 years before) and in parallel to MITICA operation.
SPIDER will be equipped with a source for negative ion production that, once optimized, will be duplicated for MITICA.
What differs among the two sources is essentially:

- The presence of hydraulic connection and of "flanged type" gas rather than "welded type" gas to allow a higher flexibility to modifications;
- The presence of a different accelerating grid system of the extracted beam. In SPIDER and in MITICA the Bias Plate, the Plasma Grid and the Extraction Grid respond to the same drawings, while the ion beam extracted in SPIDER is accelerated up to an energy of -100 kV through just one accelerating grid placed at zero potential, in MITICA the ions are accelerated up to -1MV with five steps at -200 kV each.

As the accelerating grid is placed at ground potential and the accelerating voltage is -100 kV, SPIDER source is at -100 kV potential with respect to ground.
The beam source of SPIDER is targeted to accelerate a negative ion beam up to 100 keV with a total deuteron current equal to 48A (56A in hydrogen). The ion source is illuminated by eight Radio Frequency drivers and the -100 kV accelerator features a three grid system each composed by 4 planar segments, for a total of 1280 aperture grid. This configuration, with the addition of a filter field, ensures optimal electron filter and suppression, and minimizes the ion beam deflection.
The whole beam source is supported by four insulators attached to an adjustable frame to allow the source alignment. On its back an electrostatic screen will keep the electric field towards ground potential within a safe limit and will allow a residual pressure in the driver region low enough to avoid discharges on the Radio Frequency coils.

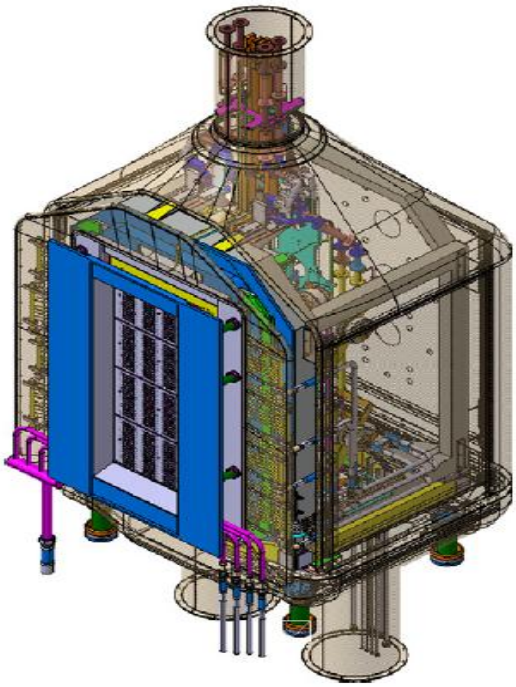

Figure II-3: View of the SPIDER beam source.

All the electrical and gas lines are brought to the source by means of a transmission line which is connected to a bushing placed at the top of the Vacuum Vessel (VV), whereas all the coolant lines are driven to the two hydraulic bushings placed on the bottom side of the VV.
The VV itself is composed by two modules, the beam source module and the pumping module, where all the cryogenic and turbo pumps are placed. The modules are then closed on both sides by two lids and all the VV components are installed on rails in order to easily access the internal components.

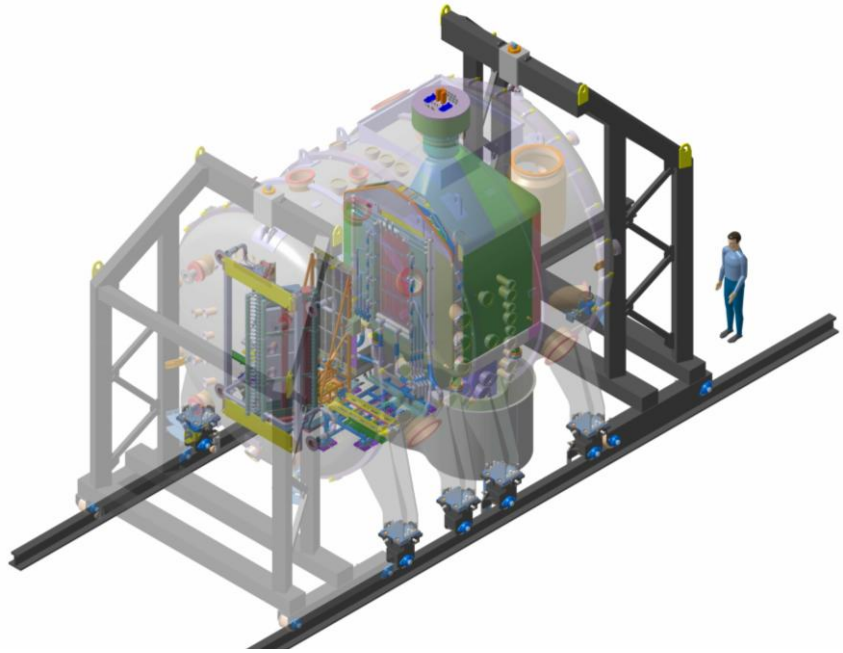

Figure II-4: View of SPIDER.

The total length of Vacuum Vessel is about 5.5 m.

As the beam accelerating voltage is -100 kV, isolating distances in air lead to design a transmission line with reasonable dimensions and no use of isolating fluids having a higher dielectric strength. The transmission line allows feeding the active components of the source that has to be brought to a voltage of -100 kV with respect to the zero potential reference.
The power supply system of SPIDER is conceptually the same of the MITICA one, with the evident difference coming from the fact that the beam accelerator is of -100 kV.
The experiment will be equipped with a complete set of diagnostics that includes those embedded in the components, such as thermocouples, electrostatic probes and calorimetric probes, and those which will be devoted to diagnose the beam.
The design of the SPIDER components and the simulation of its physical and electrical behaviours have been accomplished by using several computer simulations.
It is foreseen to start the experiments on SPIDER in the first half of 2014.

2.4. Cooling Plant

The total power to be removed by the Cooling Plant (CP) from both the experiments (SPIDER and MITICA) and the auxiliary systems is up to 70 MW.
The cooling plant will be composed by three main heat transfer systems that exchange thermal power between them, the experiment test facilities for cooling and the environment.
The primary heat transfer system will be directly connected to the test facilities for cooling and thermal control of vessel and auxiliaries. A secondary heat transfer system will act as a confinement barrier for safety purpose and it will transfer the thermal power from the primary heat transfer system to a tertiary heat transfer system via water, with large amount of stored energy in order to reduce the active installed power of heat rejection equipment. The tertiary heat transfer system will transfer the thermal power from water to environment through cooling towers and air coolers.
During the experiments it will be possible to adjust the inlet water temperature of some components in the range of 35÷45°C by means of electrical heaters. Other components will operate at the temperature of 55°C in order to store a big amount of energy by using the water temperature variation.
The maximum calculated thermal powers are:

- ✓ 11.1 MW for SPIDER (9.7 kW from experiment and 1.4 MW from the power supplies);
- ✓ 58.4 MW for MITICA (54.6 MW from the experiment and 3.8 MW from power supplies).

Different levels of purity are necessary for the deionized water, depending on the electrical potential of the cooled components:

- ✓ Water used in the operative range of 5÷10 MΩ*cm resistivity at 25°C;
- ✓ Water used in the operative range of 1÷2 MΩ*cm resistivity at 25°C;
- ✓ Water used in the operative range of 3.3÷5 MΩ*cm resistivity at 25°C;
- ✓ Demineralized water used in the operative range of 0.05÷ 0.1 MΩ*cm resistivity at 25°C. [e]

2.5. Ultrapure water in fusion machines

In the last paragraphs it has been discussed about the most important fusion machines and system for additional heating. All of these machines use ultrapure water for heat transfer and electric insulation.
The most important problem concerning ultrapure water is that, this element is not hard to obtain (using specific filters and purification plants) but it is difficult to maintain the characteristics that permit to the water to be pure and remain insulating, because every single trace of impurity inside the pipes will decrease drastically the resistivity, this is only one of problems.
To bring coolant fluids from ground potential to high voltage components, insulating pipes (electric-hydraulic insulators or breaks) with suitable length are necessary to limit leakage currents due to fluid conductivity.
In addition, the leak current circulating through the water column produces electrolytic effects that, combined with corrosion due to water velocity, lead to deterioration of water quality with a strong resistivity decrease.
This text will be focused on the characterization of a possible realization of the electric-hydraulic insulators for SPIDER experiment.
They have to feed ultrapure water with a resistivity value in the range from 1 to 2 MΩ*cm at 25°C with simultaneous applications of about -110 kV DC (one flange connected at ground potential, the other one at -110 kV).

Figure II-5: Sample of an insulator that will be tested.

The insulators that have been characterized are made by a heat resistant rubber tube with an inner diameter of 50 mm and an outer diameter of 60 mm, with a length of 40 cm, jointed at the end with two flanges UNI 2284-67 Pn 40 Dn 50 made by stainless steel AISI 316L type, for a total length of 60 cm.
The rest of the cooling plant in which they will be connected is made by stainless steel AISI 316L type.
Assuming that:

- ✓ Water characterized by a resistivity of 2 MΩ*cm @ 25°C of inlet temperature;
- ✓ The column of water is fixed at 40cm;
- ✓ The voltage is -110 kV.

The internal surface of break is:

$$S = \pi * r^2 = \pi * \left(\frac{50}{2}\right)^2 \cong 20\ cm^2 \tag{1}$$

The resistance of column of water (with ρ=2 MΩ*cm) will be:

$$R = \rho * \frac{l}{S} = 2 * 10^6 * \frac{40}{20} = 4 * 10^6 M\Omega \tag{2}$$

Then the current that will flow in these conditions, using the Ohm's law will be:

$$I = \frac{V}{R} = \frac{110 * 10^3}{4 * 10^6} = 27.5 * 10^{-3} A = 27.5 mA \tag{3}$$

Thus on SPIDER, these prototypes will have to absorb a current of 27.5 mA. For the tests that will be performed, the power supply used can reach a maximum current of 8 mA, then all the tests that foresee the presence of a current will be done with the application of 6 mA maximum to avoid overcurrent protection that occurs when 8 mA are reached. The results will be studied to understand principally the behaviour of ultrapure water when is subjected to a flow of a current.

Figure II-6: Particular of one flange.

Chapter III : Ultrapure water

3.1. The water for cooling circuit

3.1.1. Ultrapure water characteristics

Ultrapure water has a theoretical resistivity of 18.3 MΩ*cm at 25°C, but, as a matter of fact, during all the operations, the water temperature becomes higher, specially on Neutral Beam Injector experiments, with a remarkable conductivity increase, logically the power losses increases at the same way.

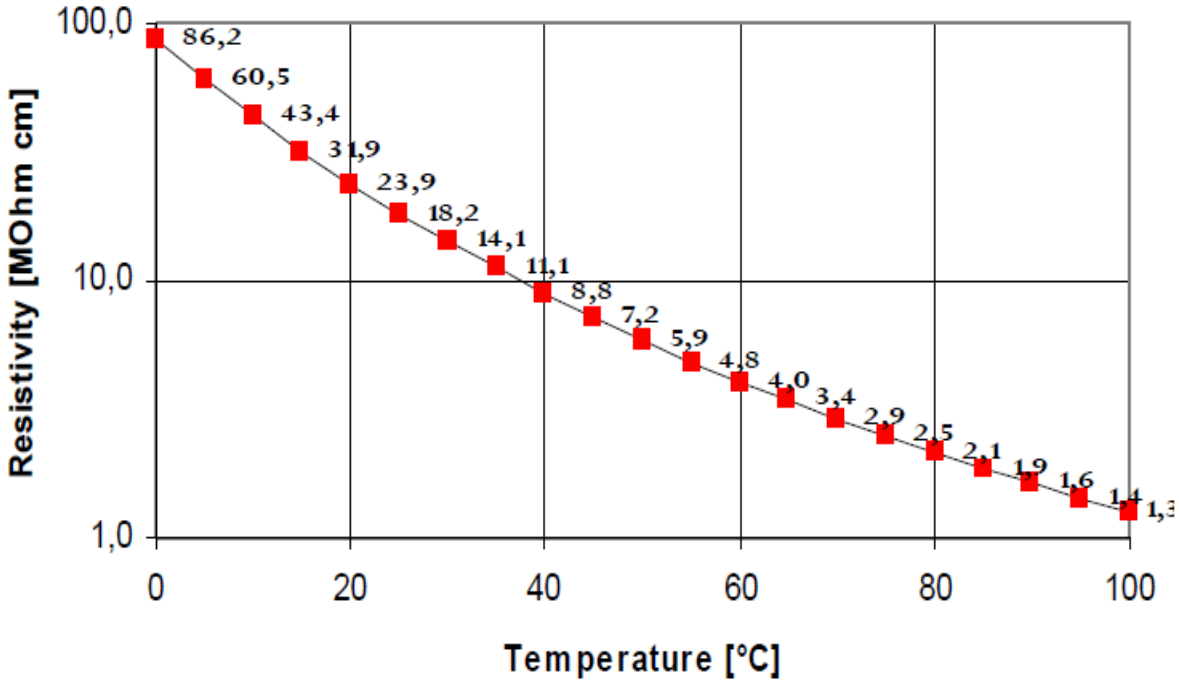

Figure III-1: Trend of ultrapure water resistivity versus the temperature.

It is clear, studying the Figure III-1 that the conductivity increases up to 10 times if 100°C are reached.
These tests will not reach high temperatures, but this will be a problem that requires further studies.
On appendix are shown some information concerning ultrapure water and various theories about ultrapure water measurement and about the cell used during the tests performed.

3.1.2. Ultrapure water treatment

In order to study the behaviour of ultrapure water before the interaction with breaks, a specific circuit, part of an experimental plant called ICE (see 3.3 for plant description), for the purification of water has been set-up.

The aim is to obtain ultrapure water with a stable value of resistivity (ρ> 2 MΩ*cm), that will be used to fill the breaks described on previous chapter and to study the progression of resistivity and temperature after several hours of tests that can be with or without voltage applied.

The specific plant dedicated to the purification of water, is composed by a set of three water filters (filled with cationic resin that use the ionic exchange process) and one dust filter; this section is completed by a volumetric pump and a inox tank that contain the water that need to be purified (see Figure III-2).

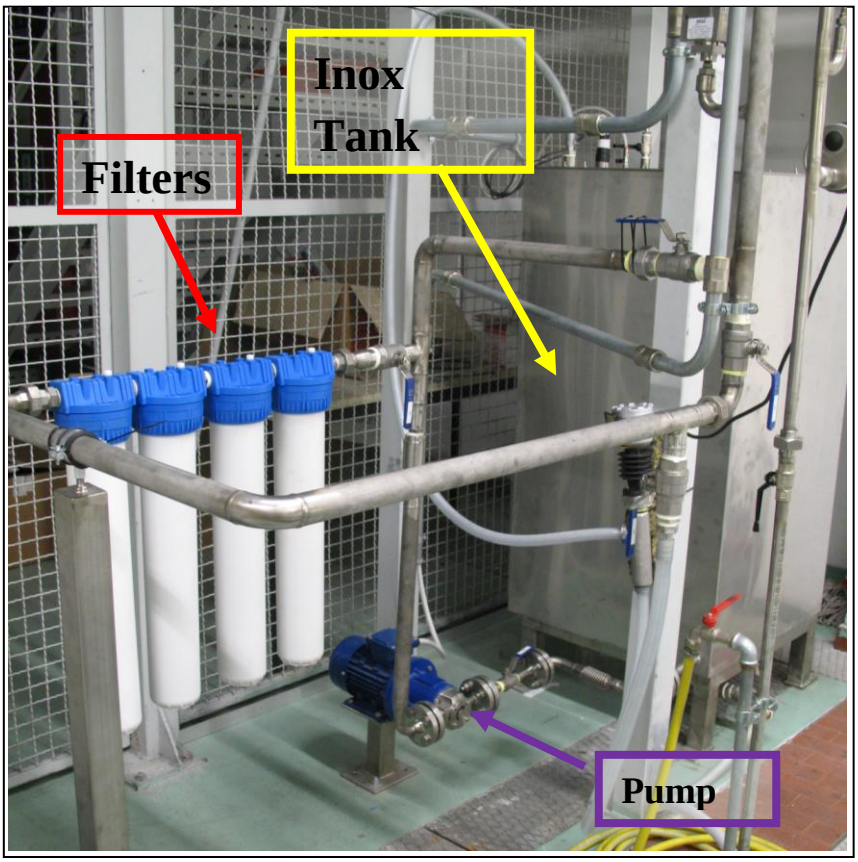

Figure III-2: Purification section of plant.

The water before any operation is demineralized water with resistivity close to 300 kΩ*cm.

For first, is mandatory to find a start value of resistance, the starting value is about 830 kΩ*cm, obtained measuring for several minutes the water flowing along the purification circuit without the filters connected, this value is maintained for some minutes (see Figure III-3).

For these particular set of tests, the sensor used for measurement of resistivity and temperature is in series with the circuit.

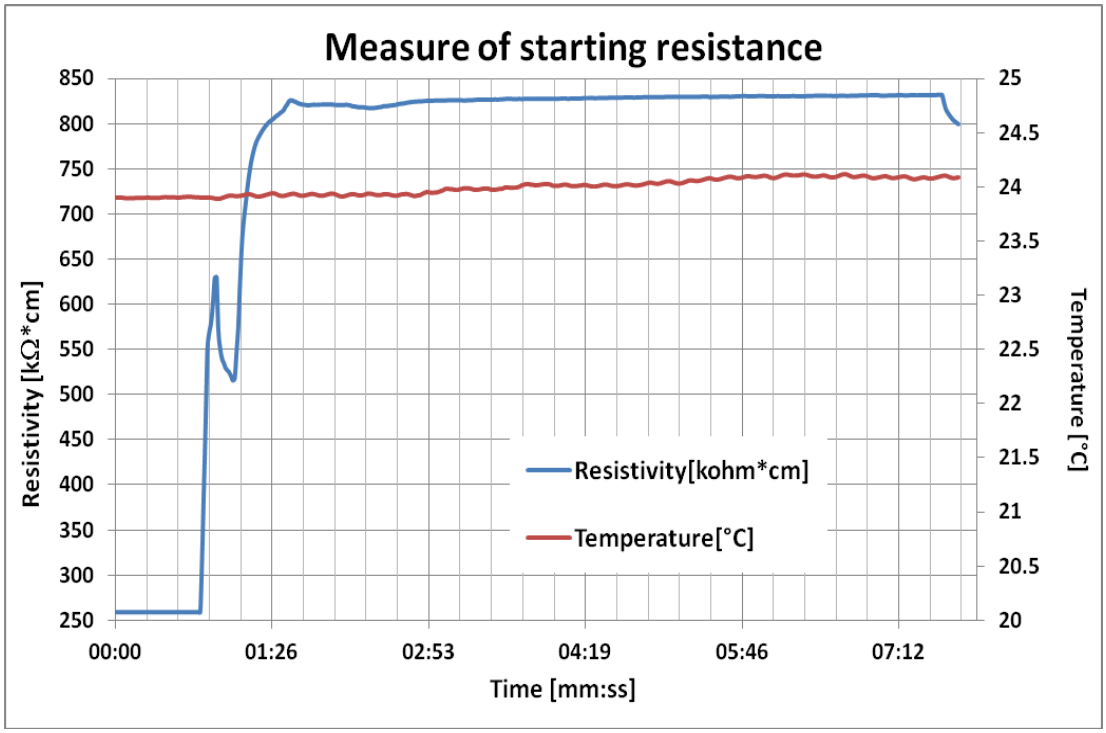

Figure III-3: Measure of starting resistance

The value of 830 kΩ*cm is maintained for more than 5 minutes, that can be enough to confirm the starting value of purification tests (see Figure III-3).

The set of purification tests foresee a combination of several hours of circulation of water in the circuit with and without the filters in series with the same circuit, in order to understand if the water, when is purified, can maintain its resistivity.

The series began with a cycle of one hour with filters in series with the purification circuit and alternatively one hour, excluding the filters, to evaluate the degradation of water flowing without filters.

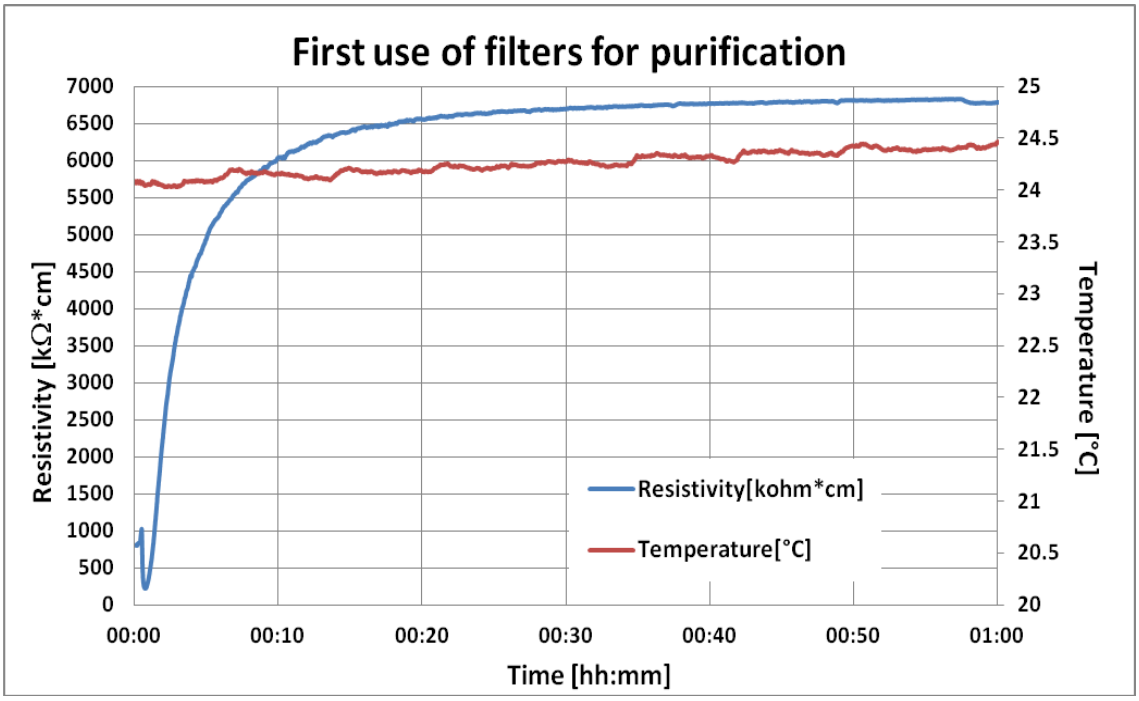

Figure III-4: Results after one hour of purification cycle.

Almost after one hour of working, the filters can assure a good grade of purification reaching the maximum value of 6840 kΩ*cm (see Figure III-4).

The second set of measures is based on the flow of water through the filters for one hour and next hour with the filters excluded, stopping the pump only for few seconds to move the valves that can permit to change the circuit status; this is necessary to have the real value that we have obtained after the first set of tests.

Figure III-5 can give the idea of how the resistivity changes, looking the Figure III-6 it is possible to see that the resistivity decreases more than a half.

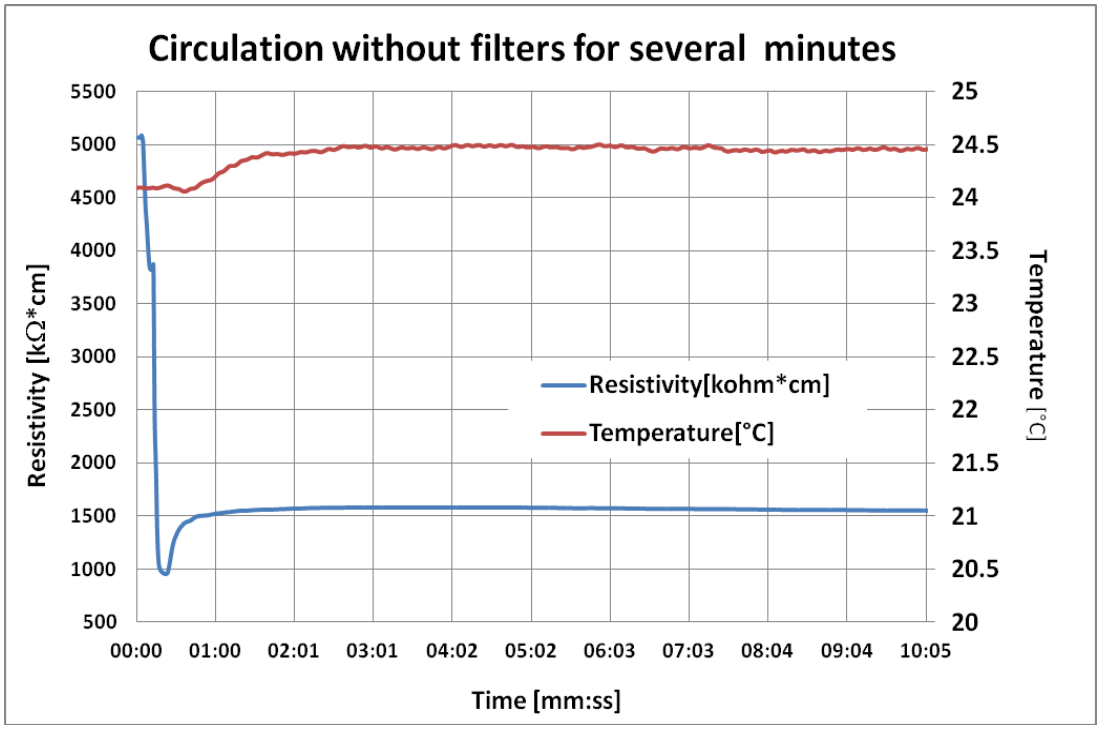

Figure III-5: Decay of ultrapure water during several minutes with filters excluded from circuit.

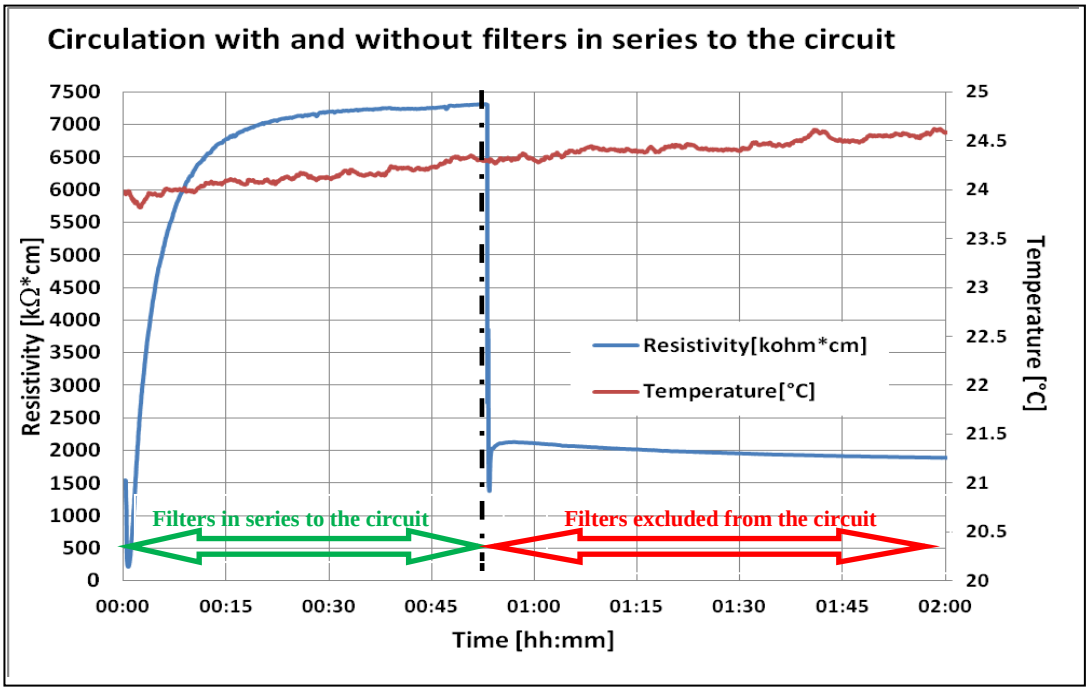

Figure III-6: Trend of resistivity during combined cycle (with and without filters connected to the circuit).

Next cycles have been dedicated to improve the purification of water, increasing the circulation time, this served to refine the ultrapure water as it is possible to see in Figure III-7; where, comparing with Figure III-6Figure III-7 the resistivity of the figure below is higher than before.

This stable value obtained can permit to pass to further two steps: fill the break with ultrapure water without and with voltage applied, respectively.

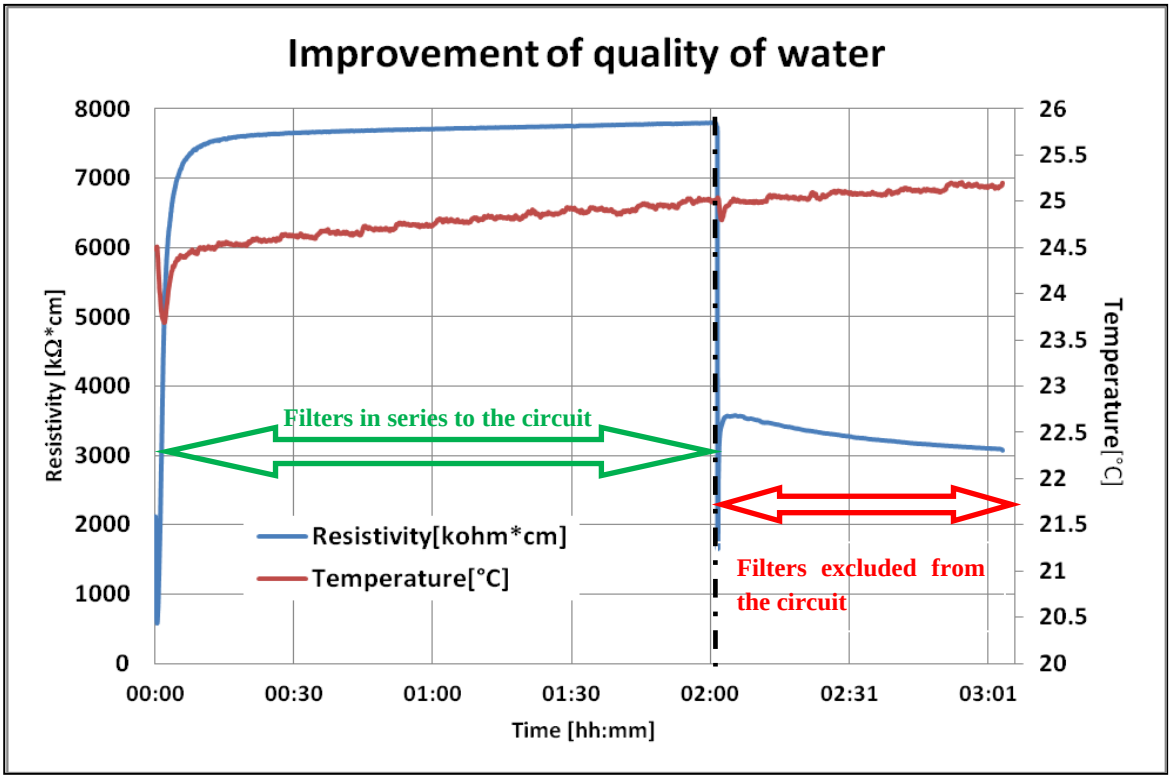

Figure III-7: Values obtained increasing the circulation time during purification process**.**

Up to now it has not been discussed about the temperature, this because this important parameter did not change for more than 2°C. This is probably due to the pump heating that transmits the heat to the water, nevertheless the temperature does not affect, during the tests, the resistivity of ultrapure water.

3.2. Process of Water purification

On paragraph 2.4 it has been discussed about the different kind of water purification, now we will try to give a short description of the three principal methods used to purify water:

- Ultra-filtration,
- Electrodeionization,
- Reverse osmosis.

The next figure will show the various type of filtration in order to obtain ultrapure water.

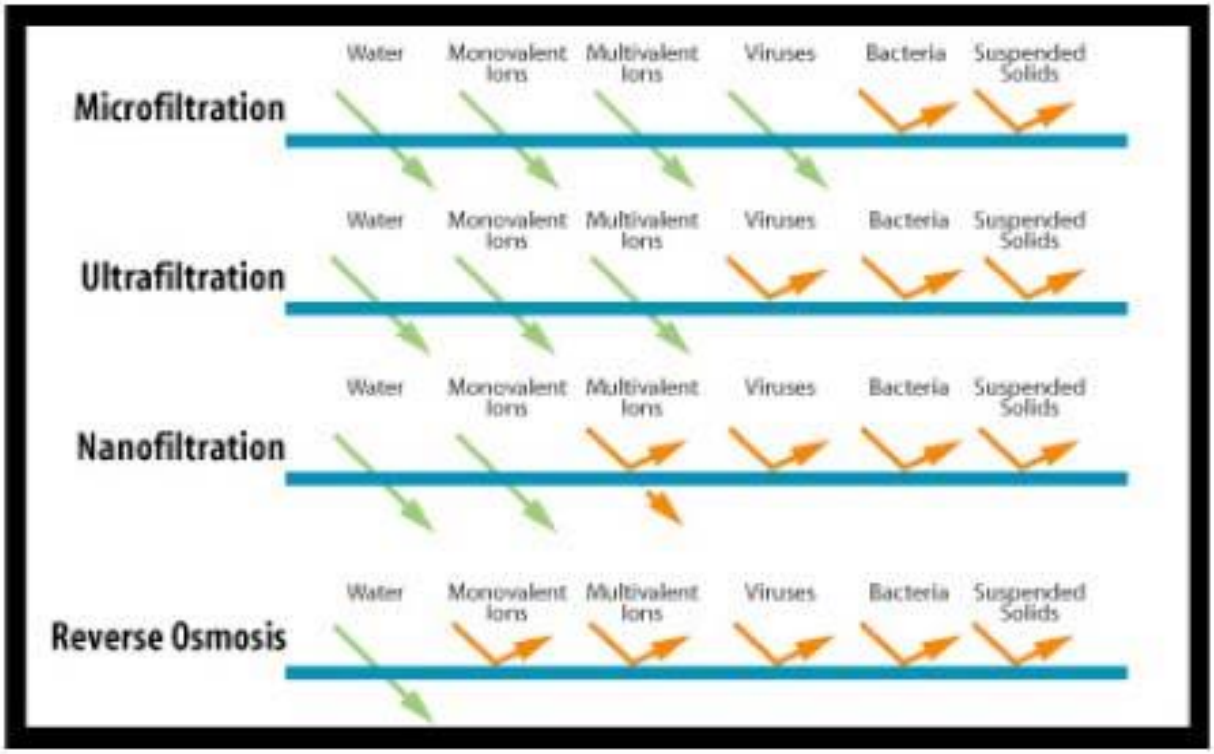

Figure III-8: Membrane process characteristics.

3.2.1. Ultra-filtration

Ultra-Filtration (UF) is a kind of membrane filtration method. It is a filtration process which utilizes trans-membrane pressure differential to separate particles according to molecular weights.
By using hollow fibres UF membrane as filtration media, raw water particles which are smaller than "pore" of UF membrane will permeate through and collected as permeate; whilst, particles which are larger than UF membrane pore size will be separated as concentrate under certain pressure applied.
UF membrane is an asymmetric semi-permeable membrane made of high molecular material by special technology. It is hollow fibre tube cover densely by micro-pores which allow solution flowing in or out the membrane under the influence of pressure. UF membrane pore size range from 0.1 to 0.005 μm.
Generally, it is used to remove high molecular-weight substances, colloidal materials, bacteria, organic and inorganic polymeric molecules.
UF system requires only 20% energy consumption of reverse osmosis system. Low operating pressures are sufficient to achieve high flux rates from UF membrane. UF is usually used as Reverse Osmosis Pre-Treatment.
In the next table are showed the various fields of operation of Ultra-filtration:

Table III-1: Examples of ultra-filtration applications.

Application	Permeate	Concentrate	Benefits of UF
Potable water	Potable water free of suspended solids, turbidity, bacteria and large viruses	Water, particulate solids	Certified for 4-log removal of bacteria and viruses from drinking water.
Oily wastewater	Oil free (<50 mg/litre) water	Water, suspended solid, insoluble metal hydroxides, etc.	Consistent permeate water quality even when feed composition subject to upsets. Highly concentrated oil emulsion for waste disposal.
Electrocoat paint	Water, dissolved salt and solvents	Water, paint resins and pigments	Allows the recovery of valuable paint resins and pigments
Reuse of municipal wastewater	Water free of suspended solids, bacteria & viruses	Water particulate solids	Polished biologically treated municipal effluent for discharge, reuse, or feed to reverse osmosis
Industrial MBR, e.g. malting industry	Suspended solids < 0,1 mg/litre	Malting wastewater, activated sludge	Meet stringent effluent discharge requirements, eliminate solids, reduces wastewater discharge fees, and requires less space than conventional wastewater treatment

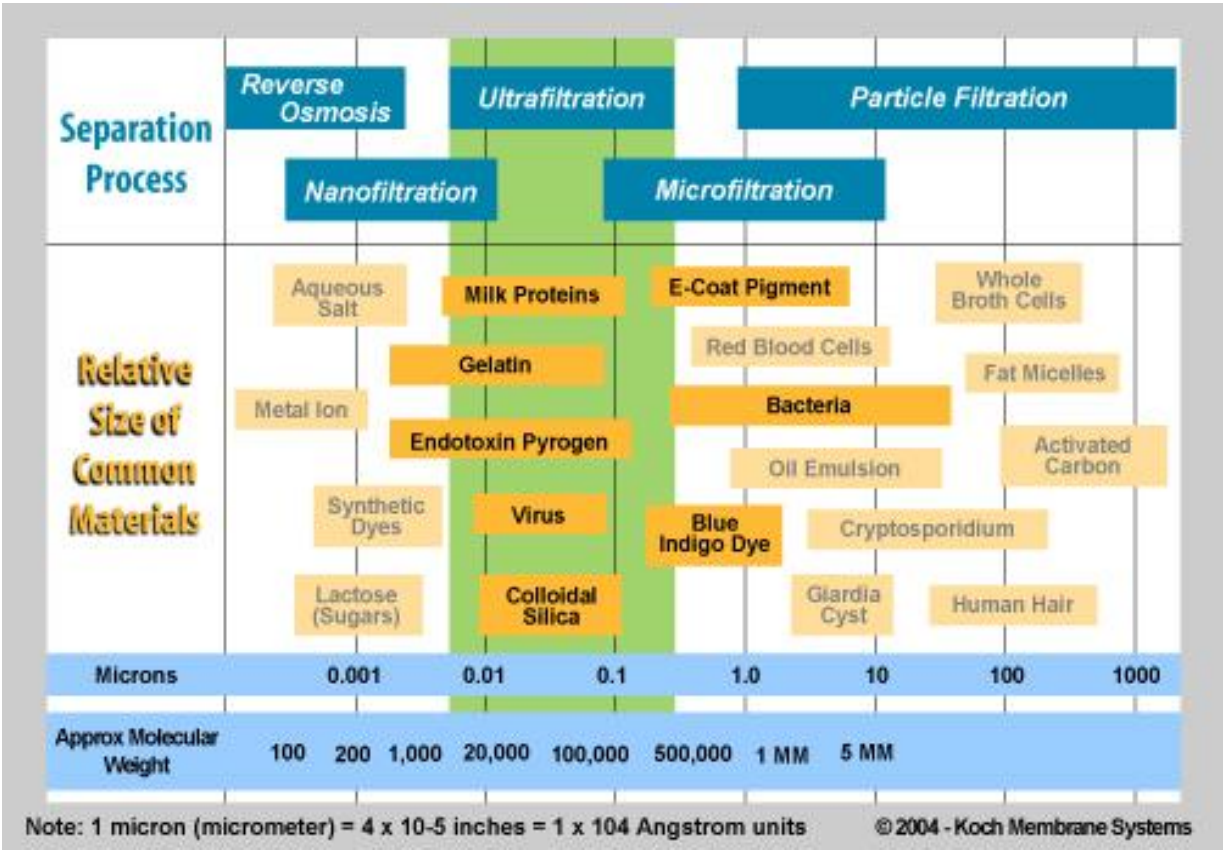

Figure III-9: Ultrafiltration range of work.

3.2.2. Electrical deionization

Electrical deionization (EDI) is a new modern technology of ultra-clear water preparation which combines the technology of filtration through semi-permeable membranes (RO) and the ion-changer technology, and thus it achieves a high efficiency in the demineralization process. In the area between the membranes, EDI uses a mixture of cation and anion exchange resins which markedly accelerate the movement of ions and facilitate removal of salts also from highly diluted solutions.

The EDI process makes use of an electrical field for a continuous regeneration of the ion exchanger system, as well as the field capability of reducing ions on the basis of their charge. Thus it is possible to save a large quantity of acids and other caustic materials necessary for resin regeneration.

The use of the EDI technologies saves consumption of energy (normally 0.1 to 0.5 kWh/m³) as well as operation costs for production of ultra-clear water, it saves as much as 95% of chemical substance consumption, and therefore it means a lot of environmental benefits as well.

Deionized water has the ionically charged minerals removed by ion exchanged. Usually two ion exchange resins are used. One resin (cation) removes positively charged ions (calcium +, magnesium + +, sodium + etc.) and releases an equivalent amount of hydrogen ions (H+). The second resin (anion) removes the negatively charged ions (chloride $^{-}$, sulphide $^{-}$ $^{-}$ etc.) and releases an equivalent of hydroxide ions (OH $^{-}$). The hydrogen and hydroxide ions combined to form water.

The dissolved minerals are attached to the resin beads and must be removed (regenerated) using, hydrochloric acid and sodium hydroxide. Since this is a highly toxic process, it is rarely or never done in the lab. Regenerated tanks are ‘exchanged’, new for used.
The next two figures are similar, and show how EDI works.

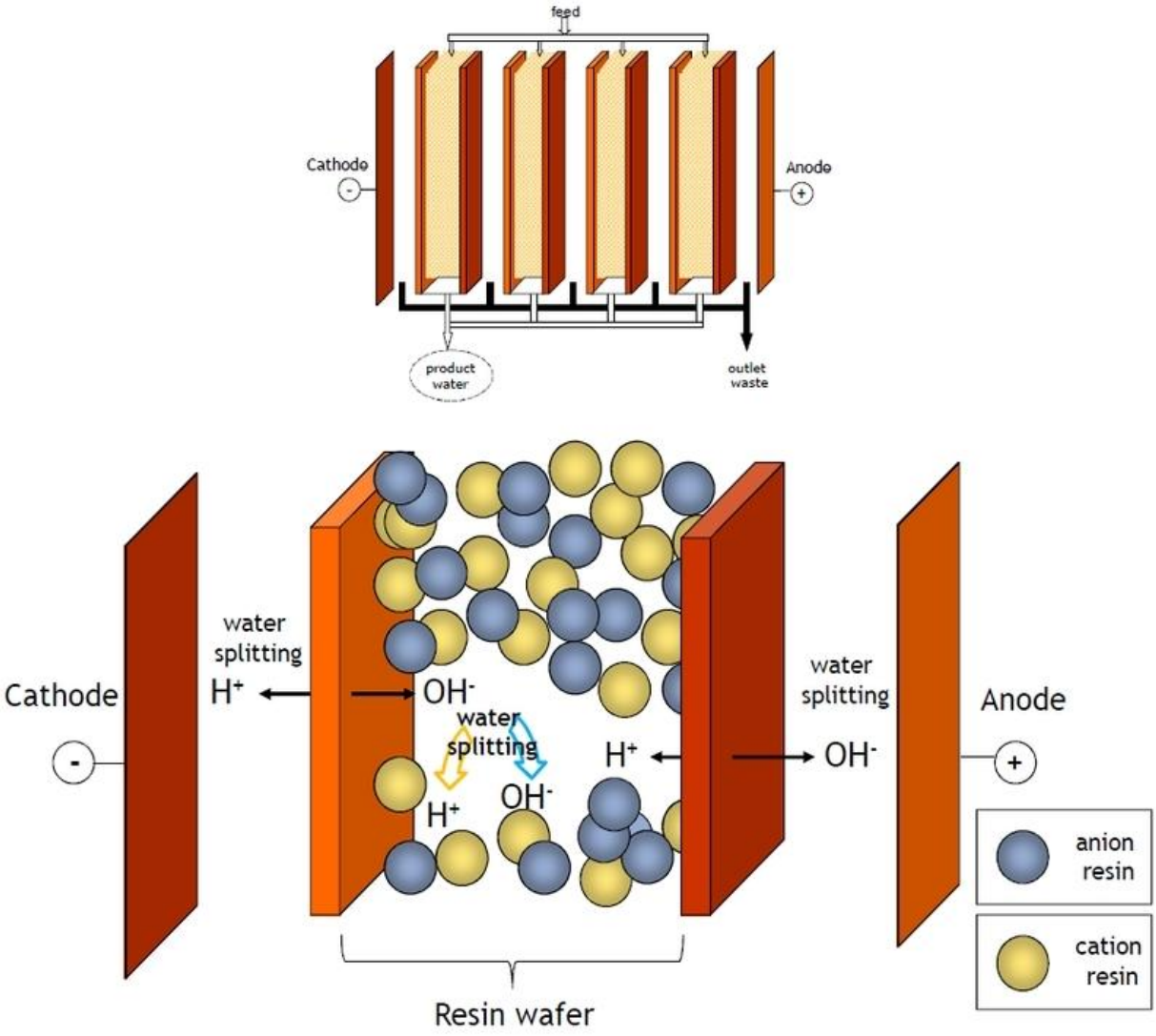

a)

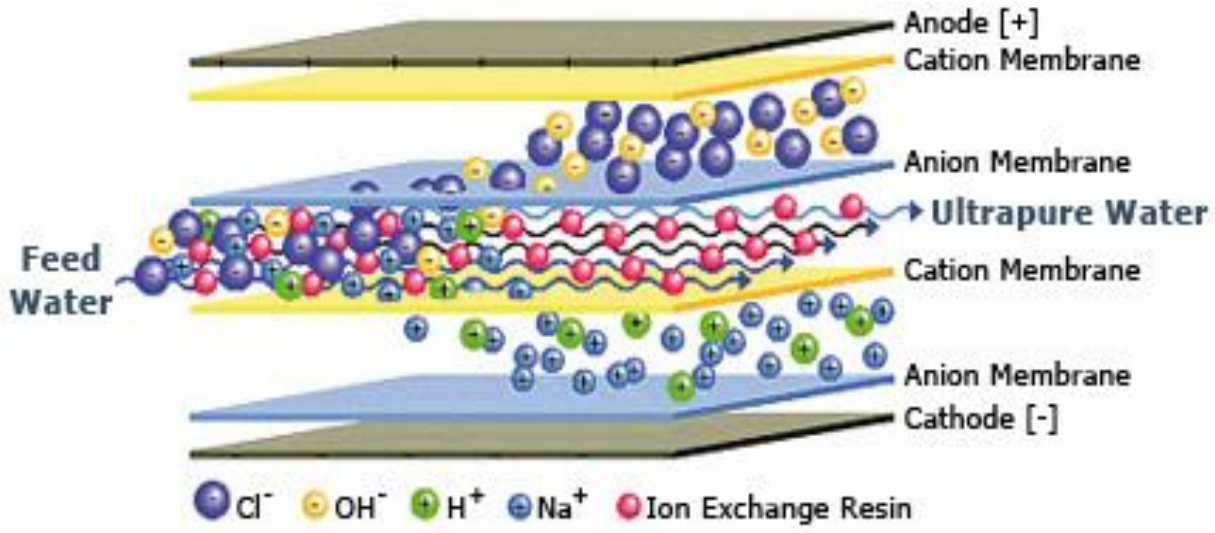

b)

Figure III-10a) and b): Electrical deionization process.

3.2.3. Reverse Osmosis

When we distil water, we use the fact that water can move from a liquid to a gas. By adding heat, we create a vapour and by cooling, we turn it back into a liquid. Only the dissolved minerals are left behind in the boiling chamber. Reverse osmosis (RO) is also a demineralizing technology. To understand reverse osmosis, it is helpful to understand osmosis. Osmosis is the movement of a solvent through a semi-permeable membrane from a lower to a higher concentration.

The cells of our body will move needed nutrients through the cell wall (semi-permeable membrane) to supply nutrients. Gore-Tex is an example of a semi-permeable membrane; it contains a plastic layer with pores large enough to let vapour out, but too small to not let liquid in.

With reverse osmosis, we use the pressure to force a solvent (water with dissolved impurities) through a semi-permeable membrane from a higher to a lower concentration. Under pressure, the water flows down into the pores of the membrane and works its way to permeate or product water side. Charged ions (mineral salts) are repelled from the membrane surface and are transported away (rejected) with main flow of water (reject water). Reverse osmosis uses water to make water. The amount of water used versus the amount of product water produced is measured as a percentage called 'percent recovery'. Newer designed systems can run from 50% to 75% recovery and do not 'waste' water. In fact, some water is often recycled to the RO feed side or even used in other plant operations with little or no 'waste'.

RO as a demineralization technology is always a part of a system that combines treatment technologies, including micro filtration and carbon pre-treatment.

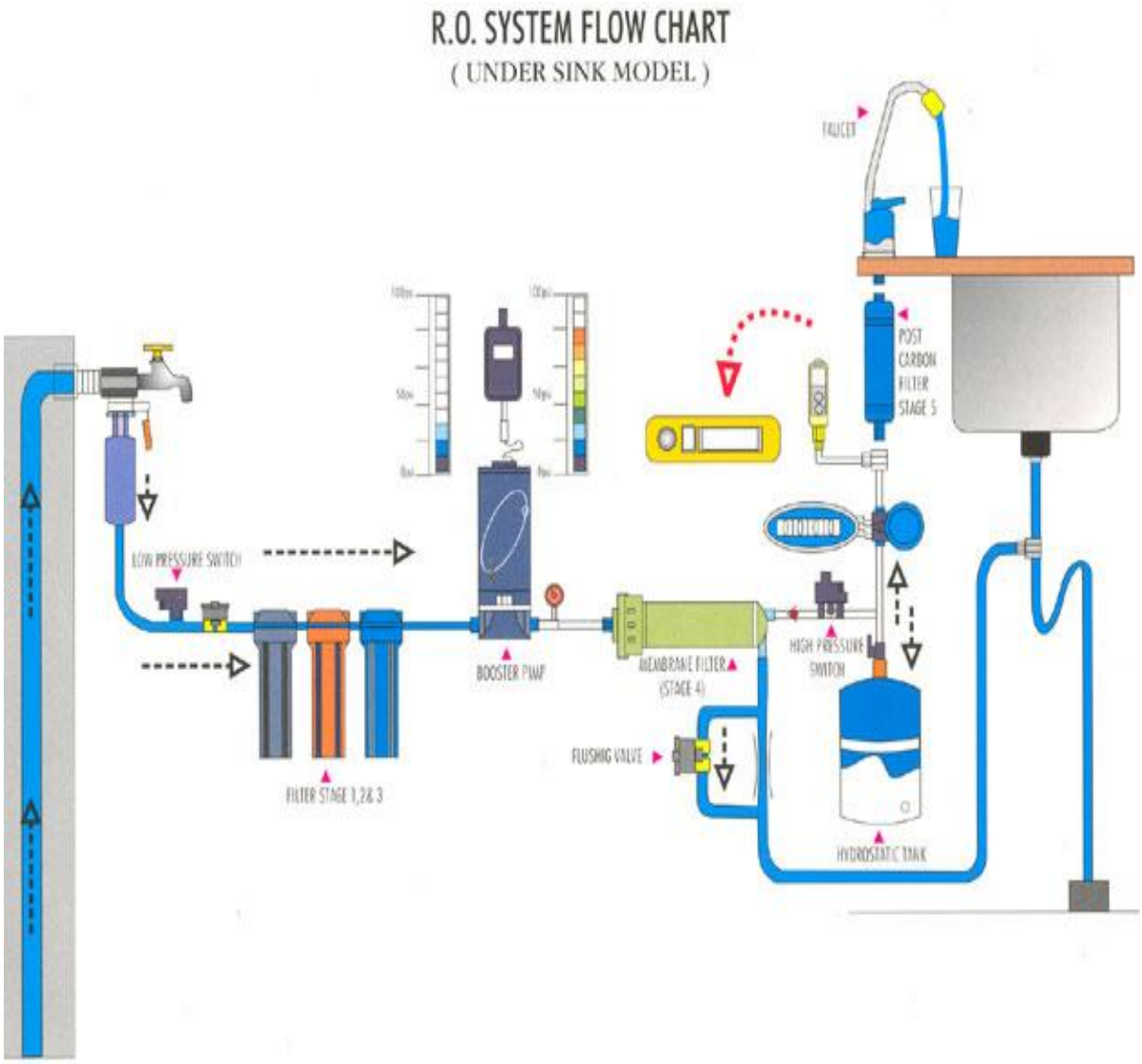

Figure III-11: Flow chart of reverse osmosis process.

3.2.4. Other process of deionization

The Figure III-12 shows other process for purify water similar to Figure III-8 but some names are different, now we will describe the remaining process with few words:

- **Microfiltration:**
  Filtration to a size of 1 µm for removal of dispersed particles. The main application is a pre-treatment process for hyperfiltration [RO systems] and drinking water filtration.

- **Nanofiltration:**
  The nanofiltration principle is the same as in the case of reverse osmosis. The nanofiltration systems are often used as an alternative to a classical water softening process, also for the reason that operation costs of nanofiltration are lower because the necessity of regeneration of water softener with a large quantity of salt is fully eliminated. It is used to remove bivalent ions (Fe^{++}, Ca, Mg) from water. The main use is given by water treatment at water heating systems, cleaning of boilers, production of foods and drinks, water processing and applications in high-performance cooling towers.

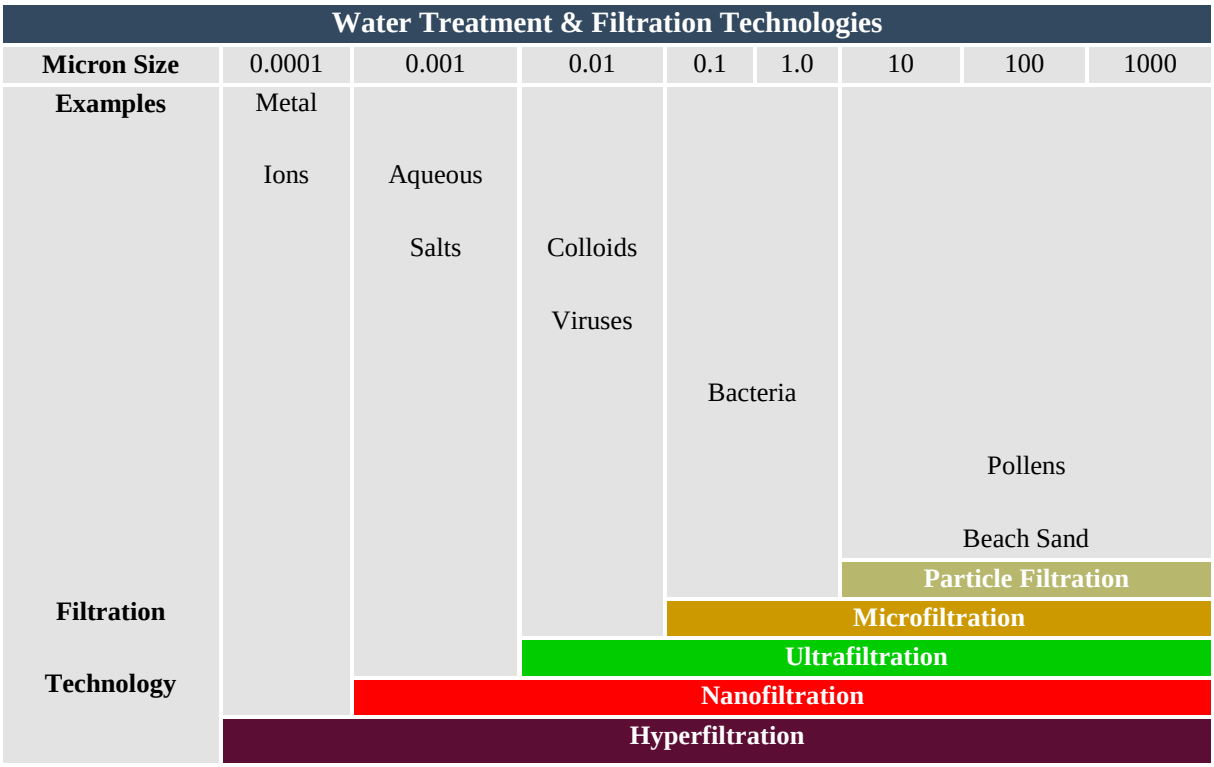

Figure III-12: Other process of water purification.

3.3. ICE description

ICE is the acronym for Insulation and Cooling Experiment at Consorzio RFX, this specific plant is built with two different test sections: one where the ultrapure cooling water resistivity and degradation are measured and tested, and one section for thermo-hydraulic experiments.
Both two sections share services like water pumps, reservoirs and heat exchangers to distribute the coolant fluid with controlled temperature and flow rate to the inlet of the test sections. The two parts are driven by a variable speed motor, in this way the flow rate can vary from 100 to 8000 kg/h.
The circuit is filled with ultrapure water stored into a dedicated electro polished stainless steel reservoir.
The thermo-hydraulic test section is set-up in order to perform thermo-fluid dynamics investigations and conditions relevant for SPIDER and MITICA.

Figure III-13: Test section for thermo-electric investigation.

The section, on Figure III-13, will not be used for these test, nevertheless this part will be used in the next step, where ultrapure water will be heated and then circulated into ICE Plant. It is possible to see that, on this specific section are used the break that are object of this script.

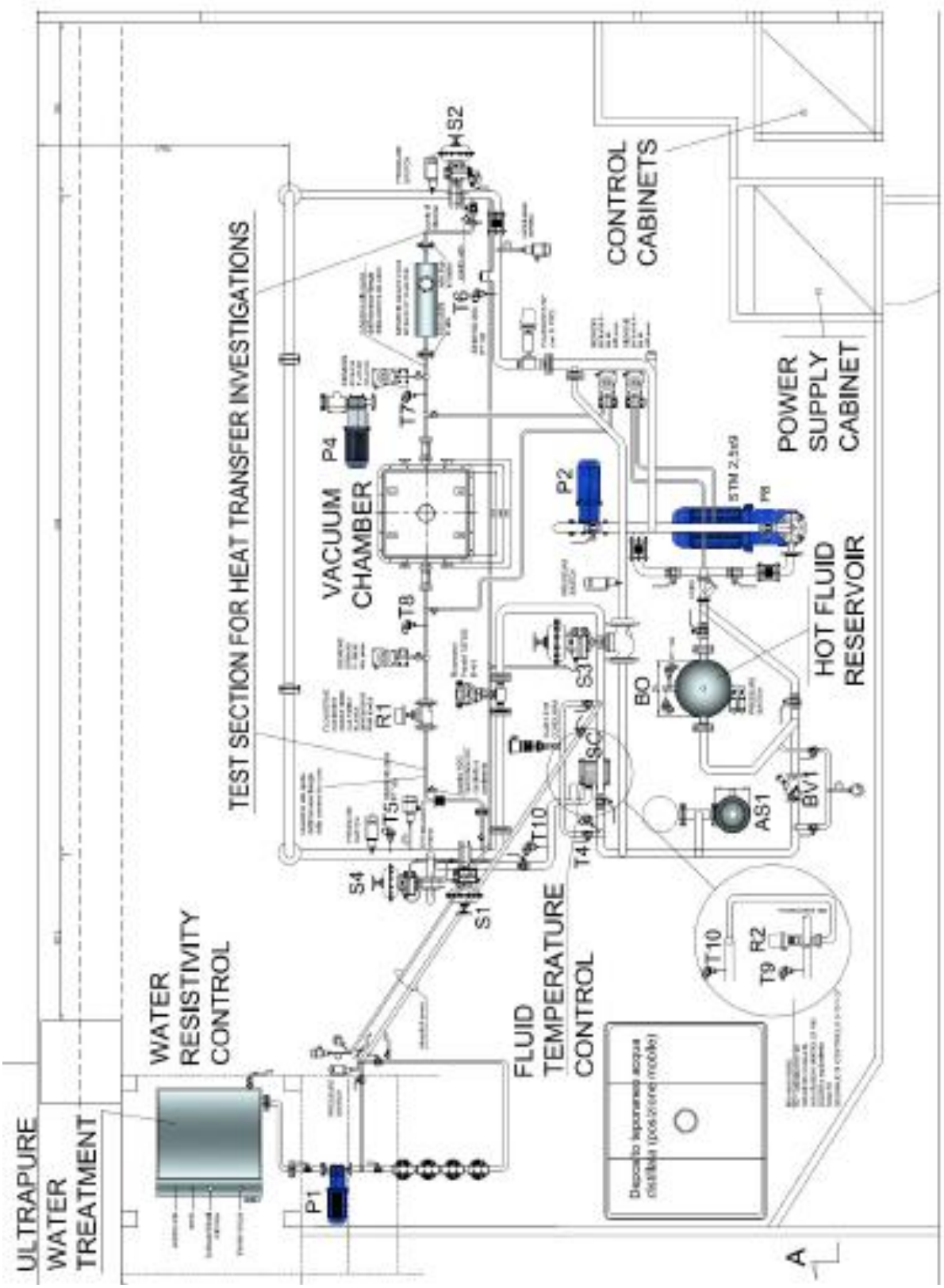

Figure III-14: Plant view of ICE plant.

3.3.1. Sensors used

The instrumentation used have a double purpose: to keep under control important parameters for correct and safe operation of the plant (temperature and pressure for example) and to be able to acquire all the data measured. The parameters that will be kept under control are:

- ✓ temperature;
- ✓ pressure;
- ✓ mass flow rate;
- ✓ water electrical conductivity.

3.3.1.1. Water electrical conductivity sensor

In order to study the water behaviour in terms of electrical resistivity, a conductivity measurement cell has been installed. With this instrument it's possible to keep under control the values of the cooling medium resistivity and monitor the degradation process of water resistivity.
Measurements under high voltage and/or high temperature conditions can be done in the ultrapure water test section.

Figure III-15: Water conductivity sensor display.

The display shown on Figure III-15 is directly connected to the cell shown on Figure A.7 and Figure A.8.

Chapter IV : Electrostatic analysis on break sample

4.1. Introduction

Preliminary electrostatic analyses have been performed to simulate the behaviour of the break under voltage applications and to identify possible corrective actions to improve the configuration, if necessary. At this aim a suitable 2D Finite Element Method (FEM) described in the following was used.

4.2. Electrostatic analysis

4.2.1. FEM Model

The specific software that has been used to perform the *Finite Element Method* (FEM) analyses is COMSOL Multyphysics.
The cylindrical symmetry gave the possibility to study the problem using 2D axial-symmetric. The variable dependent for the electrostatic analysis is the voltage.
Below, on Figure IV-1, it is possible to see a break prototype on the right and on the left the relative simplified drawing with relative quotes that will be used for the analysis. The joints of the flanges have been represented chamfered in order to get the worst condition for the analysis.

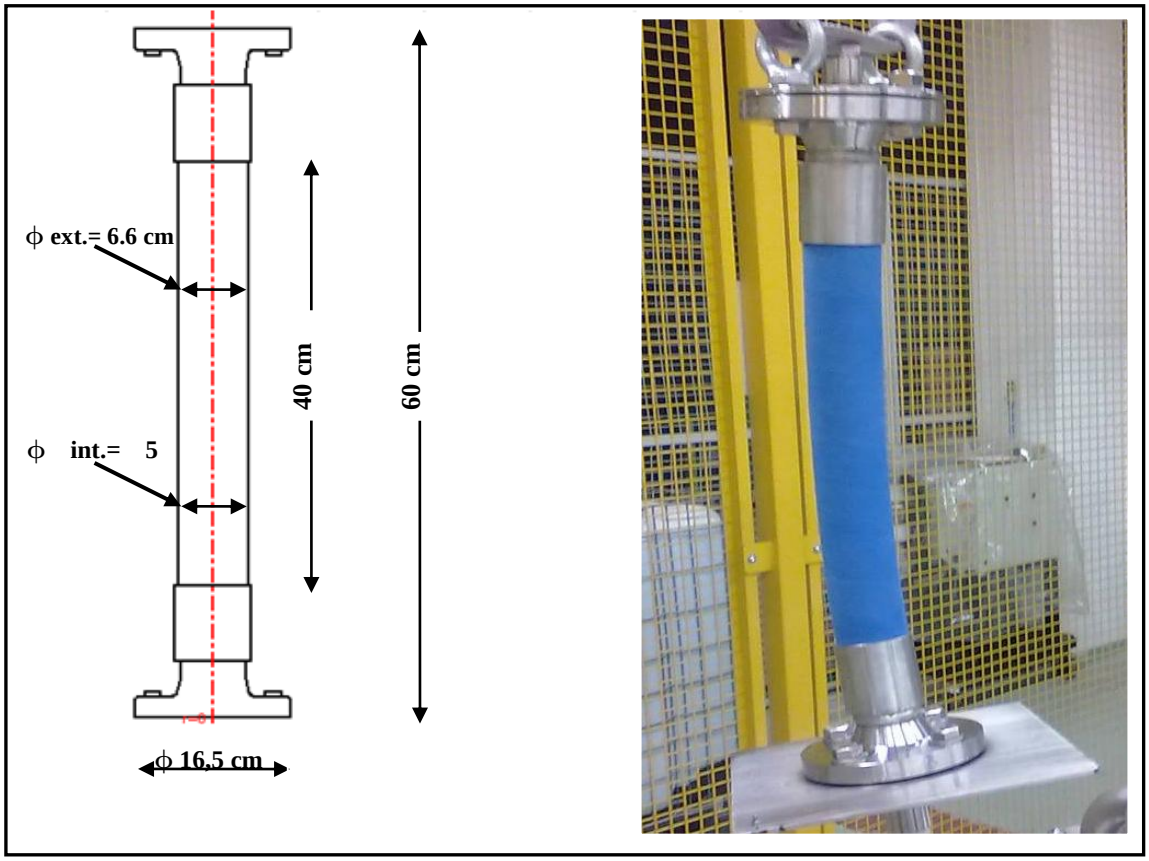

Figure IV-1: Simplified view of the break prototype used for the analysis on the left, a break prototype on the right.

Due to the cylindrical symmetry, for the electrostatic analysis it will be necessary only to study half break and show the internal connection to understand the layout of different materials inside the break (see Figure **IV-2**).

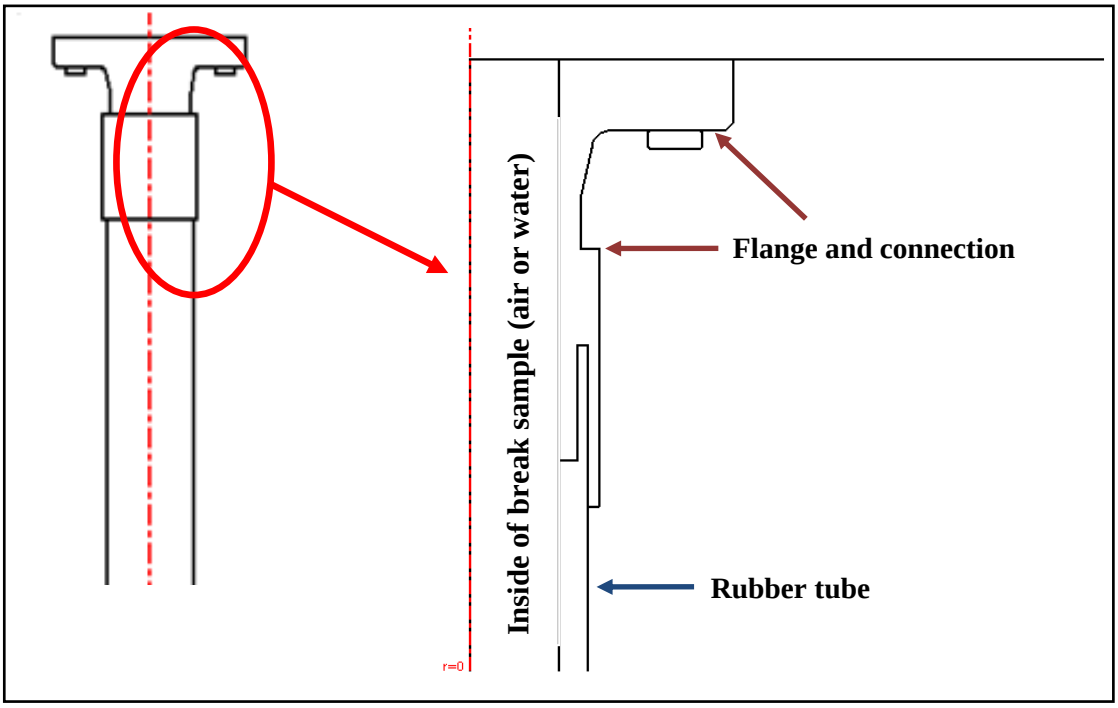

Figure IV-2: Particular of connection among different materials on break sample.

The materials that have been defined are shown in Figure IV-3.

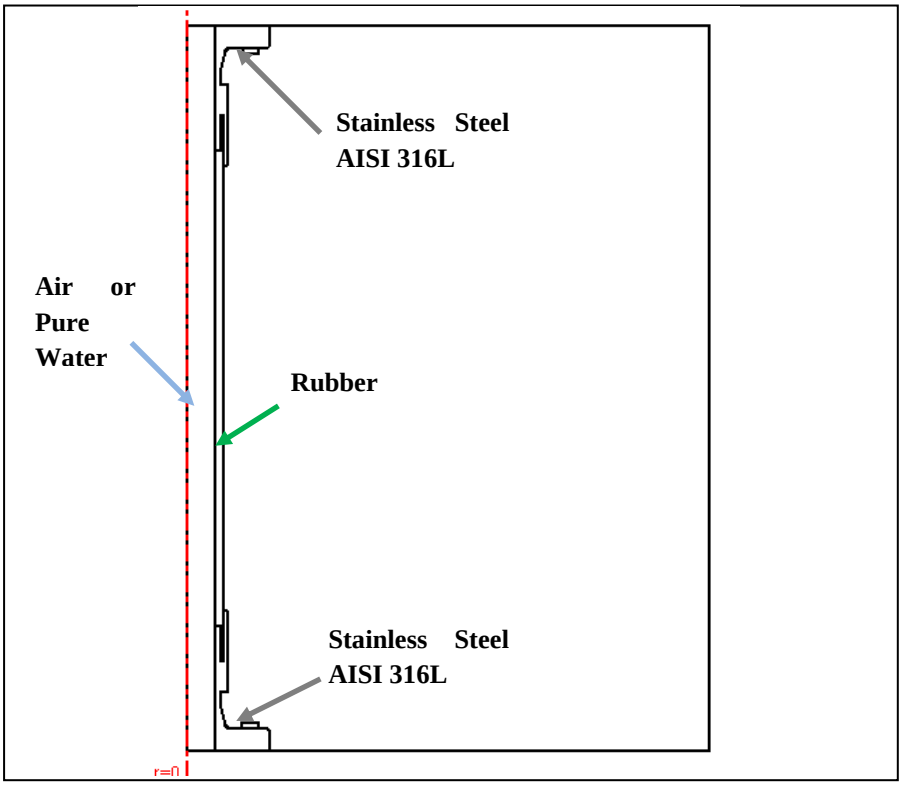

Figure IV-3: Materials defined for the electrostatic analysis.

The following table defines the values of relative permittivity ε_r for each material shown on Figure IV-3.

Table IV-1: Relative permittivity of materials used for the analysis.

Material	Relative permittivity
Air	1
Water	82
Rubber	4
Stainless Steel	-

The stainless steel will not be taken into account during the electrostatic analysis because it is a conductive material.

The contour conditions assigned to the analysis are shown on Figure IV-4: where the axial-symmetric condition has been assigned to the axis of the break; the electric potential of -110 kV has been assigned to the upper flange of the break and the metallic part jointed to the same prototype; the electric potential of 0 kV has been assigned to the lower side of the break, to the upper and lower surface of the analysis; electric displacement has been assigned to the surfaces that corresponds to the rubber tube surface; no charge condition has been assigned to the remaining surface of the analysis on the hypothesis that a reasonable distance the equipotential lines are parallel to each other.

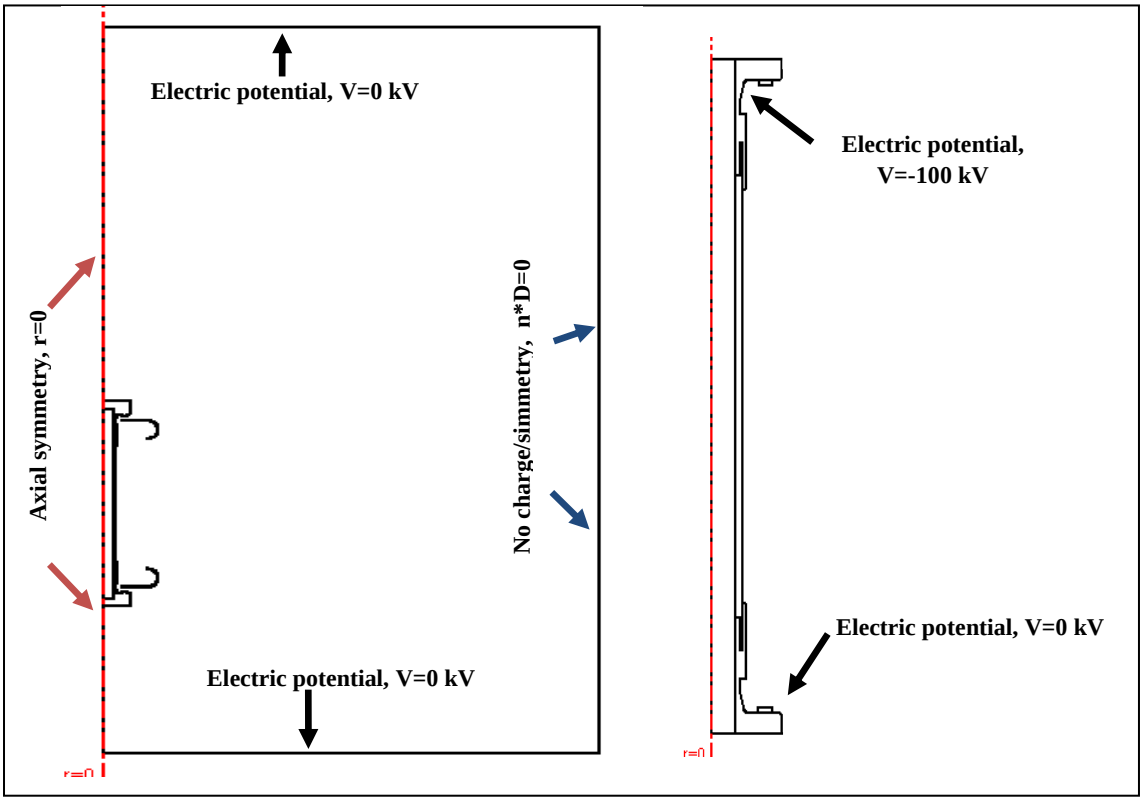

Figure IV-4: Contour conditions assigned before electrostatic analysis.

4.2.1.1. Results with break empty

Figure IV-5 reports the equipotential lines map of the electric field.

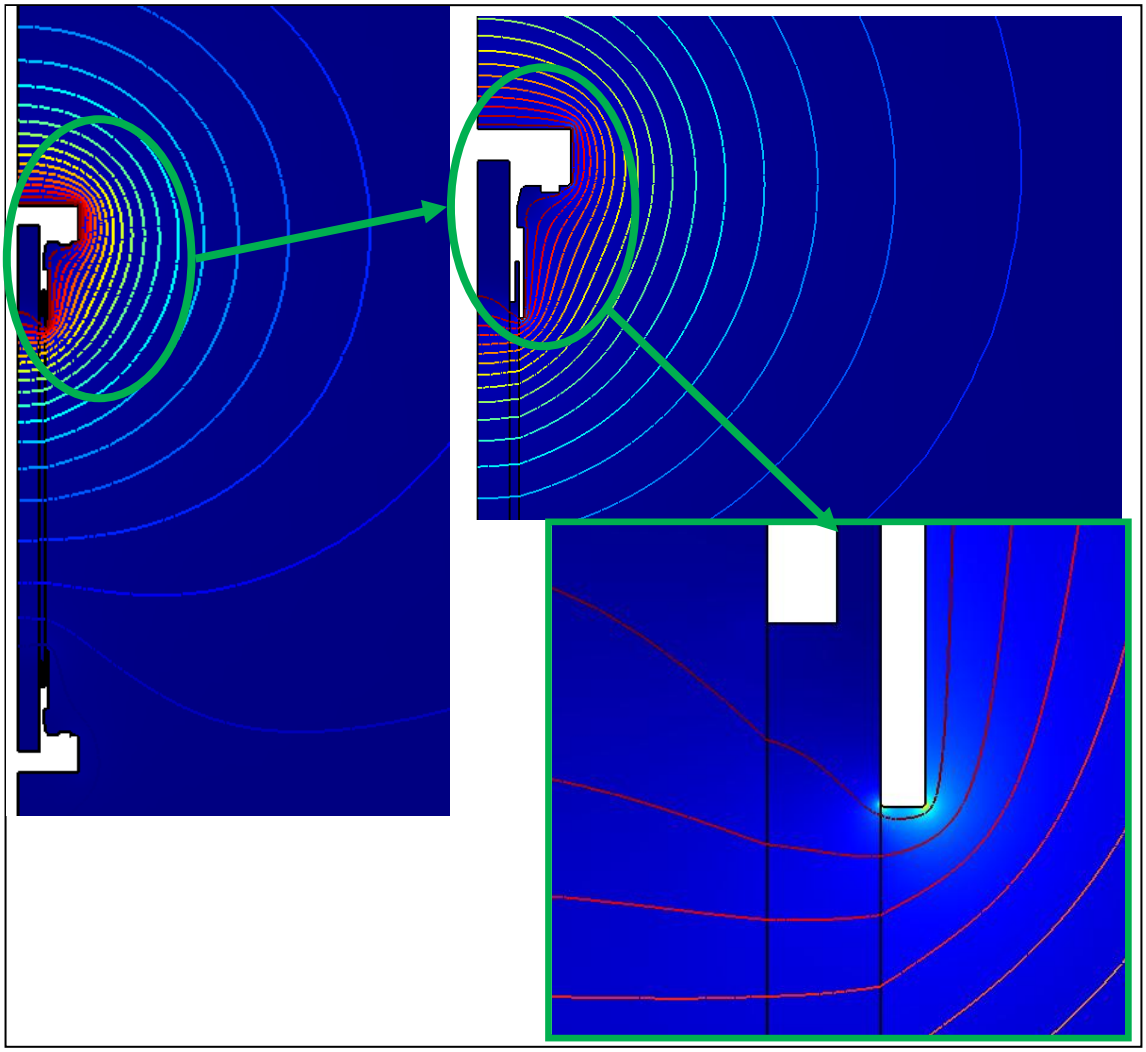

Figure IV-5: Solution of first case of 2D electrostatic problem.

An analysis about the meshing has been performed in order to study the variation of maximum value of electric field calculated by COMSOL to reach which size of mesh can assure a suitable result.
The analysis, done on Figure IV-5 has been solved with three different mesh sizes in order to evaluate the number of meshes and the value of electric field reached.

The first analysis has been solved with a coarse meshing size, and the results are shown on Figure IV-6:

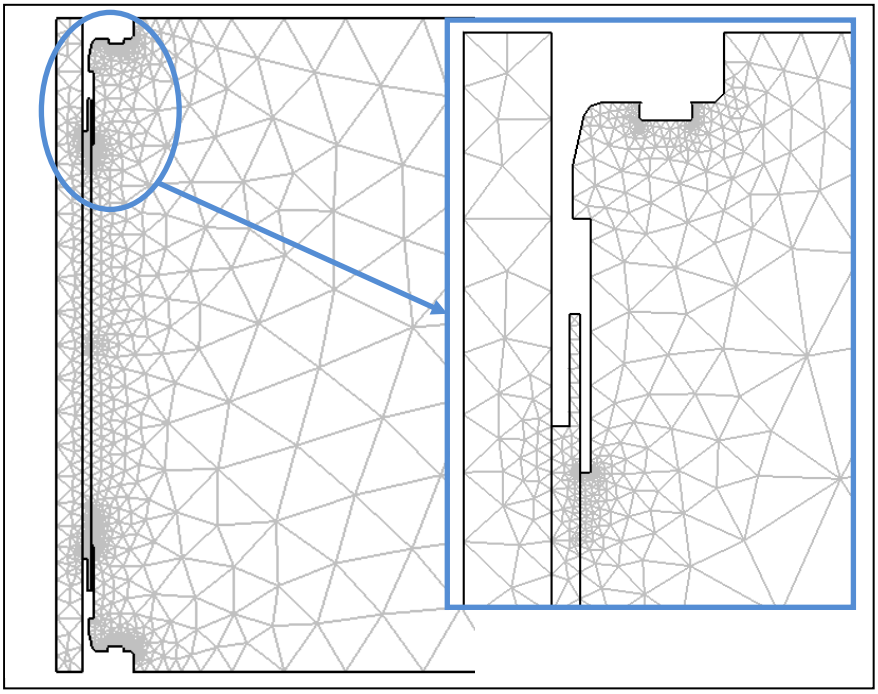

Figure IV-6: Analysis done with a coarse meshing size.

The results obtained with this kind of meshing size are shown on Figure IV-7:

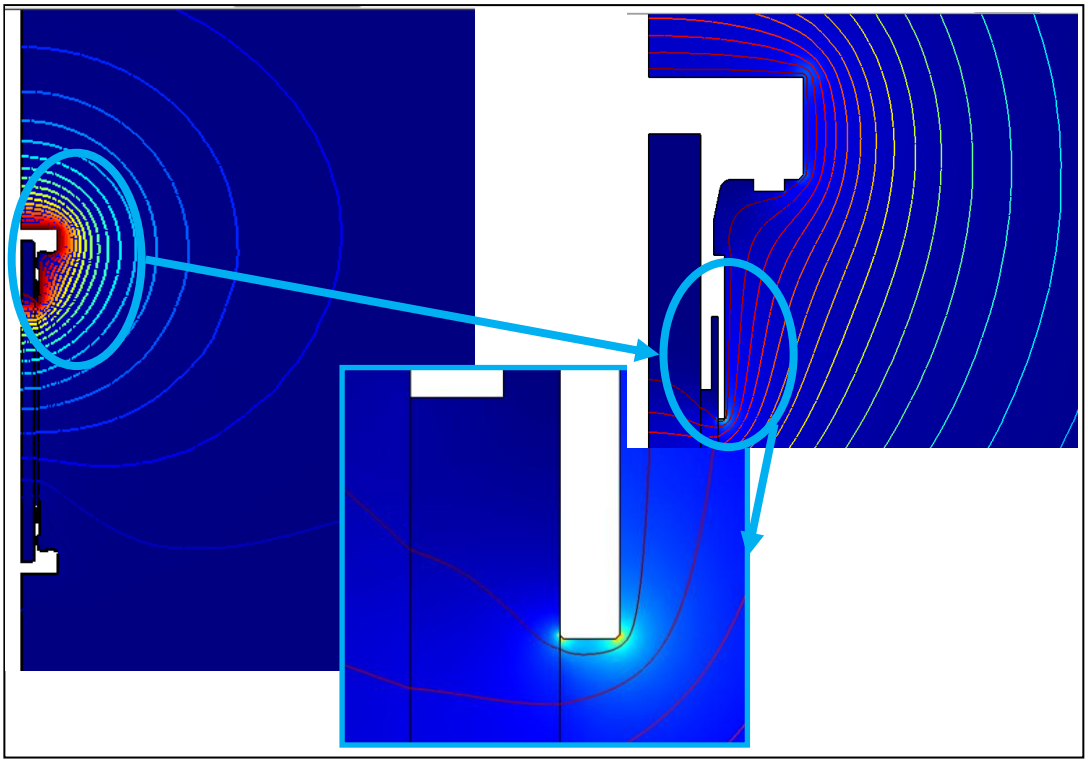

Figure IV-7: Results obtained with coarse meshing size.

The coarse meshing size used 3531 elements and the maximum electric field reached the value of $10.6*10^6$ V/m that equals to 10.6 kV/mm located in the area shown on Figure IV-7.

The further analysis foresees a normal meshing size, as it is possible to see on Figure IV-8:

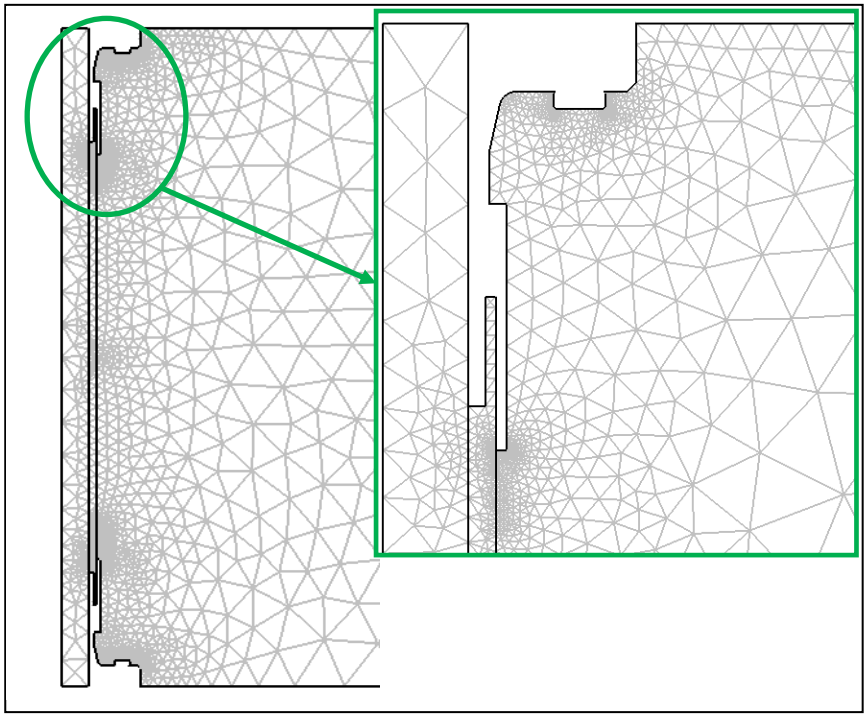

Figure IV-8: Analysis done with a normal meshing size.

The results, with this meshing size showed that the number of meshing element was 4805, and the value of electric field reached was $11.69*10^6$ V/m that equals to 11.69 kV/mm, see Figure IV-9:

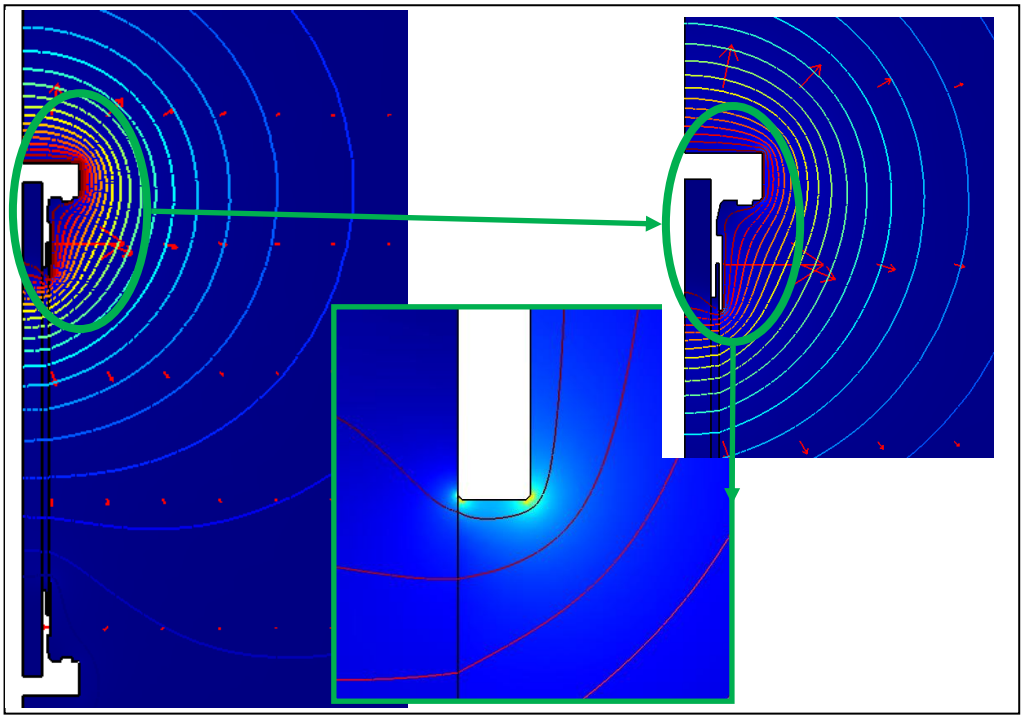

Figure IV-9: Results obtained with normal meshing size.

The last analysis foresees a fine mesh size and the meshing are shown on Figure IV-10:

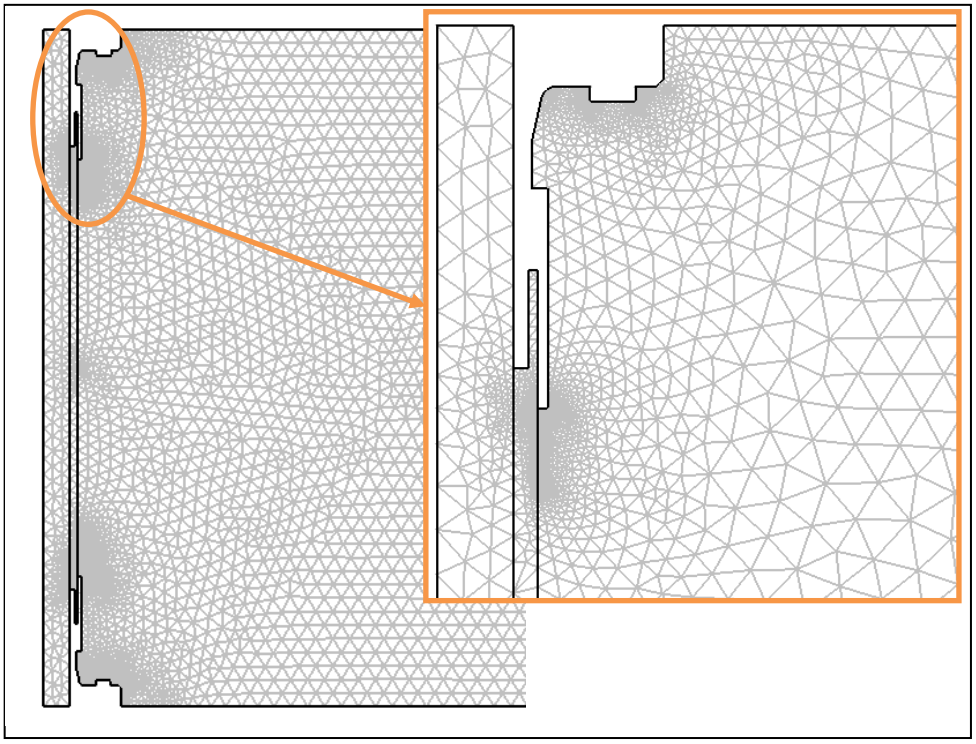

Figure IV-10: Analysis done with a fine meshing size.

This kind of meshing size used 5710 elements and the maximum value reached was $11.8*10^6$ V/m, that equals to 11.8 kV/mm, as it is possible to see in the next Figure IV-11:

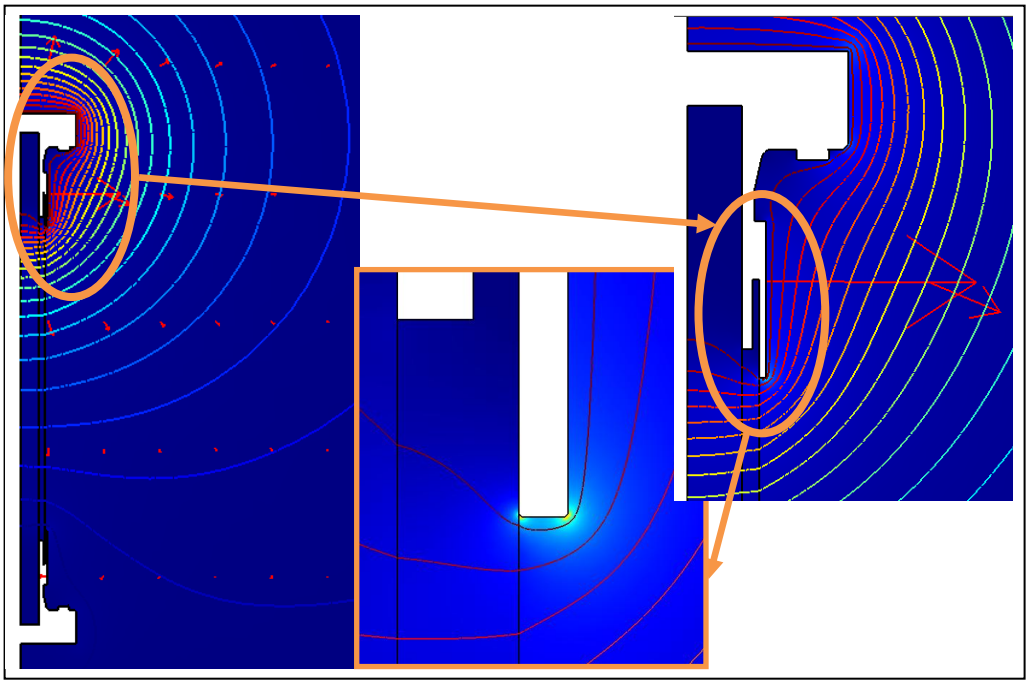

Figure IV-11: Results obtained after fine meshing size.

Summarizing the results obtained in the Table IV-2:

Table IV-2: Results obtained with three different meshing sizes.

Meshing size	Number of elements	Electric Field [kV/mm]	Maximum electric field point
Coarse	3531	10.6	Between stainless steel and rubber
Normal	4805	11.69	Same of coarse meshing
Fine	5710	11.8	Same of precedent meshing

It has been decide to use, in the further analysis done with COMSOL, a normal meshing size because the number of element is sufficient to make a good analysis.
The point where the maximum electric field is reached is the same for all the meshing sizes, and this is an edge point where the electric field could reach an infinite value for the solver. Thus the normal meshing could be enough for our purposes.
All the meshing sizes shown that the maximum electric field reached is higher than the dielectric strength of dry air that is 3 kV/mm, than it will be necessary to study a solution that decreases this electric field on the break and avoid possible electric discharges.
To prevent electric discharges and limit corona effect, a possible solution was to use two circular shields made of aluminium, see Figure IV-12:

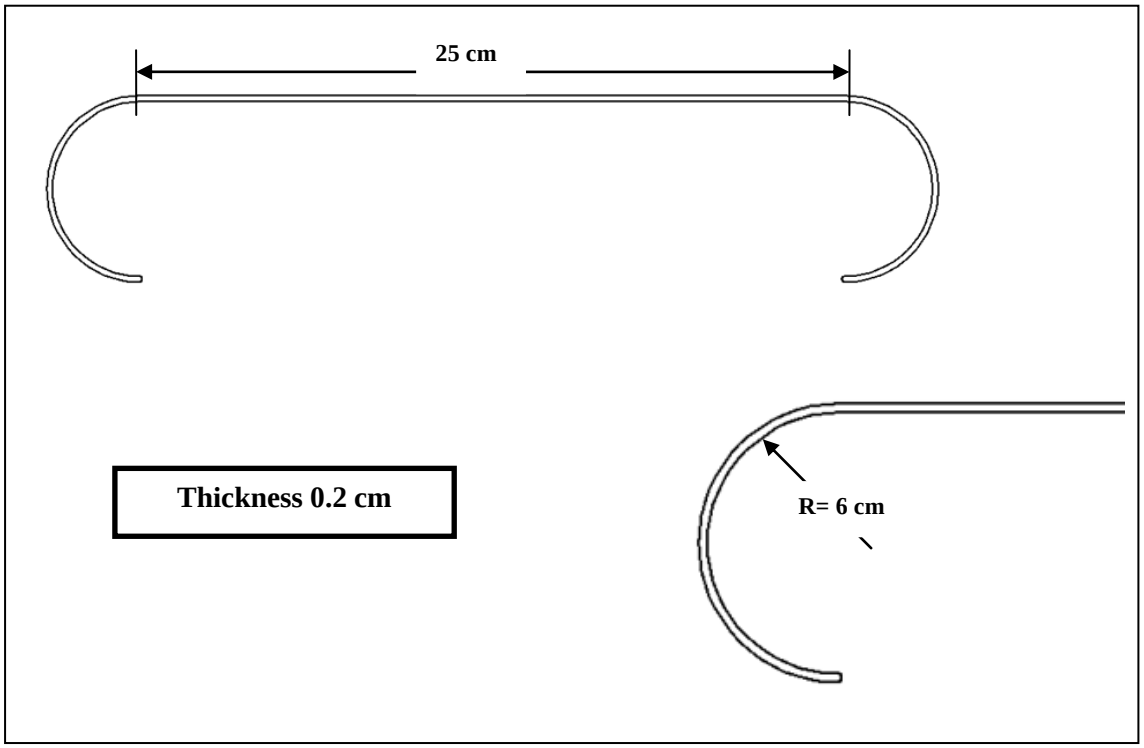

Figure IV-12: Shields used for the analysis.

The COMSOL analysis with the shields foresees two different cases: one where the distance between the shields and the flanges varies (on Figure IV-13 only y varies), and one where is the distance between the break and the shield varies (on Figure IV-13 x and y varies) in order to study the variation of maximum electric field and if the point where the electric field is found is different among the various analysis (Point A and B are the possibilities).

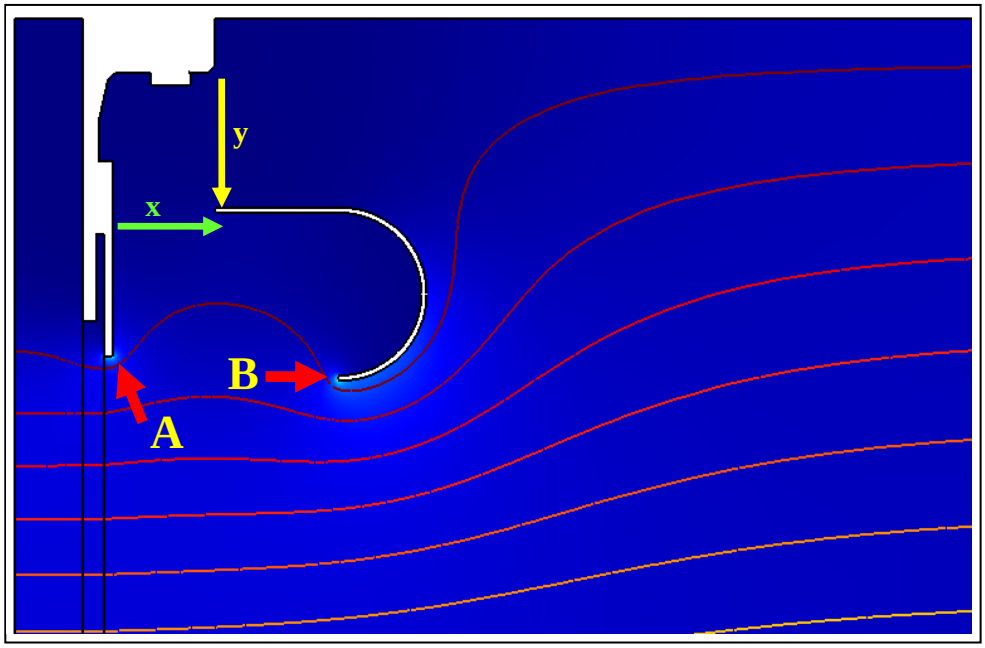

Figure IV-13: Variation of shield distance to perform different electrostatic analysis.

For the first case various distances have been evaluated in order to study the variation of electric field, on Figure IV-14 and Figure IV-15 it is possible to see a general case with the shield is in an intermediate position.

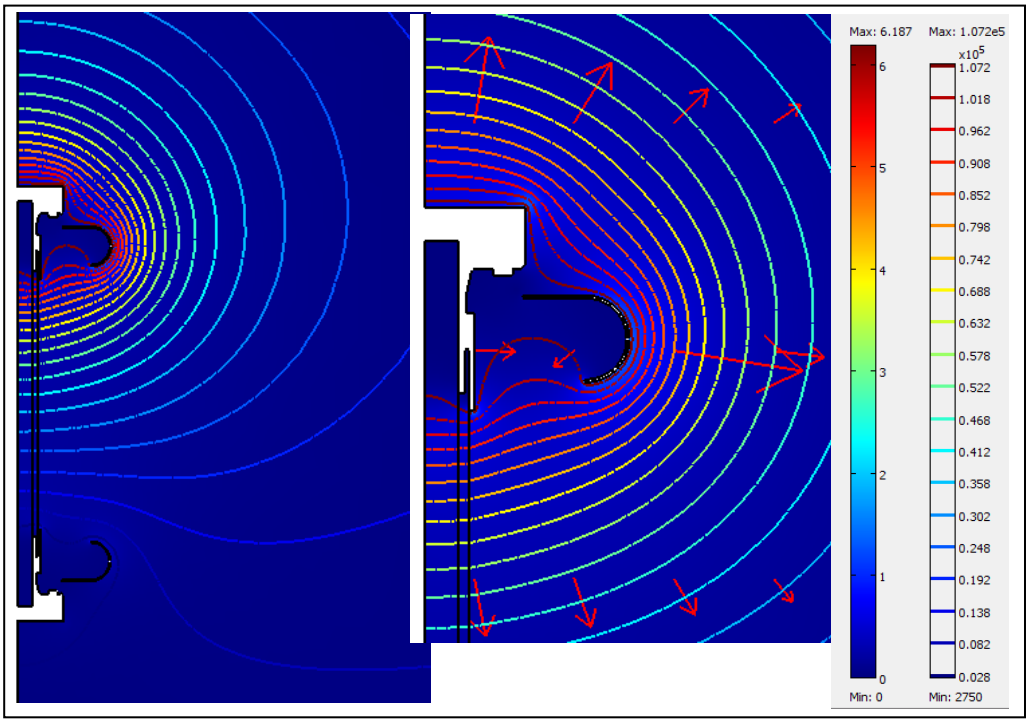

Figure IV-14: Generic case using the shield with the break sample.

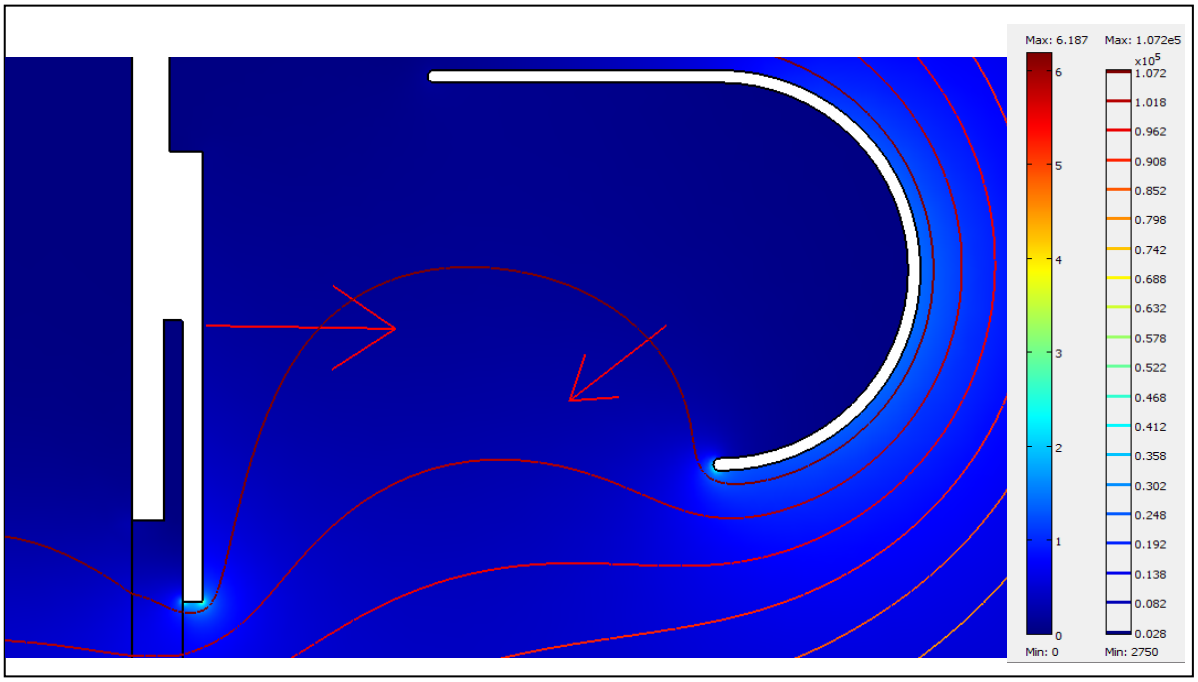

Figure IV-15: Particular of precedent case.

The Table IV-3 summarize the analysis done with COMSOL where only the y-coordinate (see Figure IV-13) varies respect to the flange.

Table IV-3: Comparison among analysis with the shield in a different position.

Distance y from the flanges [cm]	Electric Field [kV/mm] on point A	Electric Field [kV/mm] on point B
2	6.19	2.43
5	4.75	2.7
8	3.23	2.9
9.5	3.05	2.9

For the case where only the distance between the shields and the flanges can change it was possible to see that the more distance increase more the electric field decrease on point A and the point on the shield (point B) the electric field increases.

Next figure will show what happens if the shields are in a very low position, the fourth case of Table IV-3: the critical point will be the same between the stainless steel and the rubber tube, but the value of electric field on the lower side of the shield (see Figure IV-16) is increased. Even if we may have a low electric field peak, there will be the problem to how fix the shield, the stability cannot be assured because the distance is high from the flanges, so this can't be a good solution.

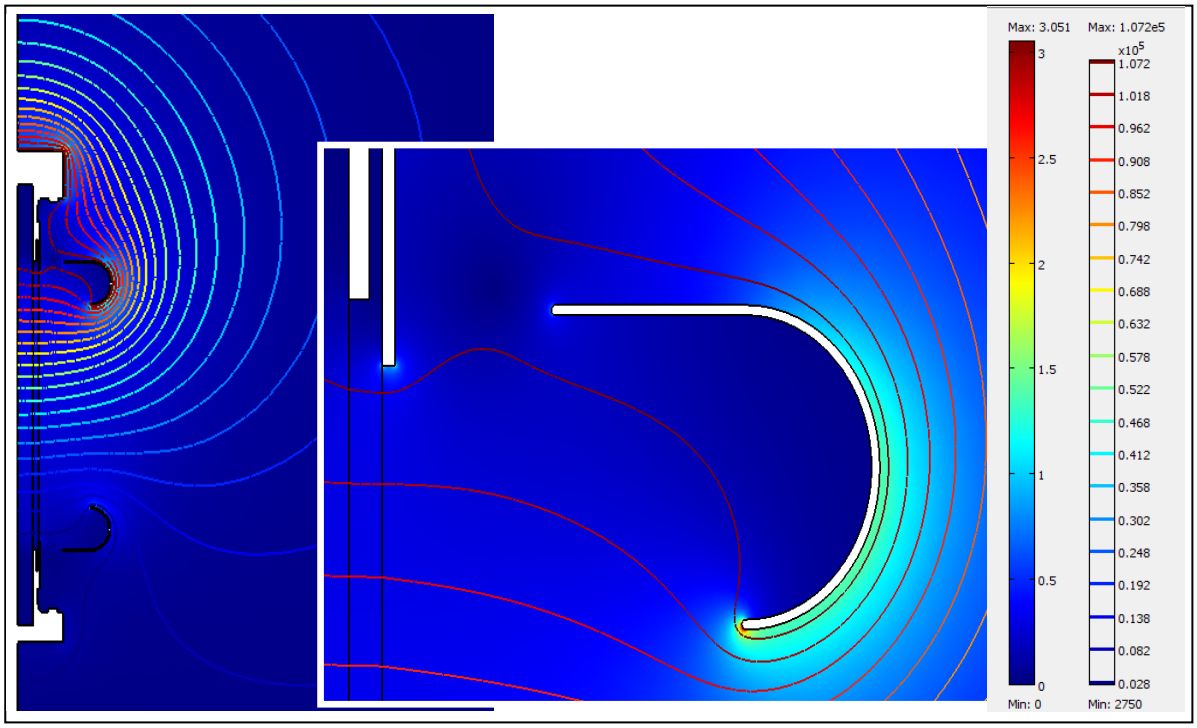

Figure IV-16: Case with shield in a very low position.

Even if the point of maximum electric field is too small, and the location where we can find it is the same, this is maybe caused from the geometry assigned during the design phase because for the solver. This point could be an edge point between two different regions, where the electric field can reach a very high value (theoretically infinite).

It is possible that the value of electric field obtained during all the analysis cannot correspond to the reality due to the different comparison between the real break and the break designed with COMSOL.

For the second kind if analysis, the evaluation changing the distance between the break and even between the flanges, it will be necessary to cut the shield in a half and then remove the part that won't need for the analysis.

A particular care during the comparison has been taken due to not stay too close to the break to avoid the possibility of electric discharges.

The next figures (Figure IV-17 and Figure IV-18) will show various cases of this analysis, and on Table IV-4 are summarized the results obtained.

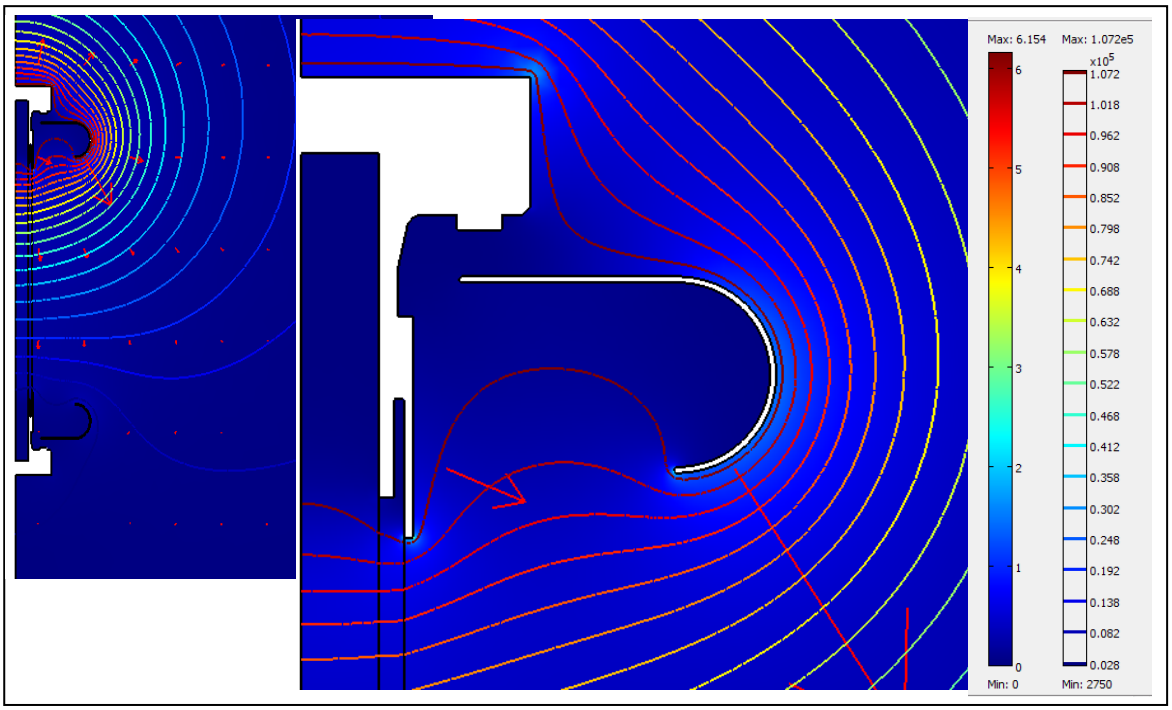

Figure IV-17: Generic case with different length of shield.

Even for this case we tried a solution with a substantial distance between the flanges and the shields, cutting a large part of the shield. This can permit to us to have a relevant distance from the break. The results are shown on Figure IV-18.

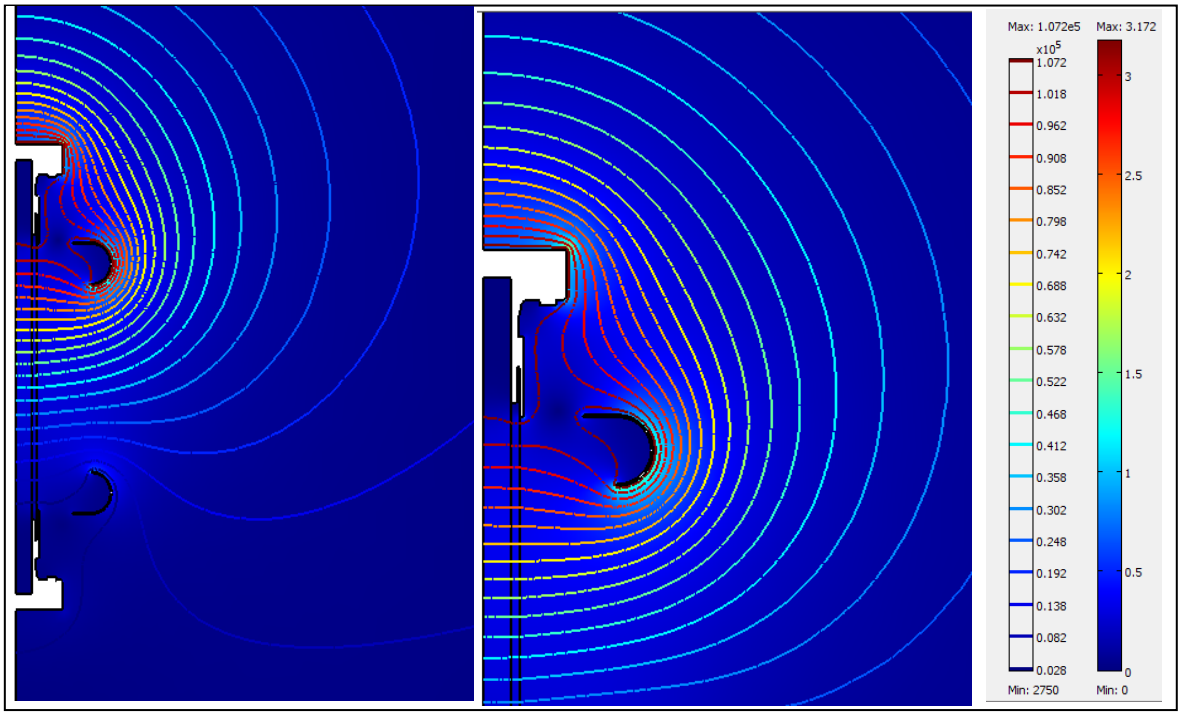

Figure IV-18: Case with high distance from the flanges and with cut shield.

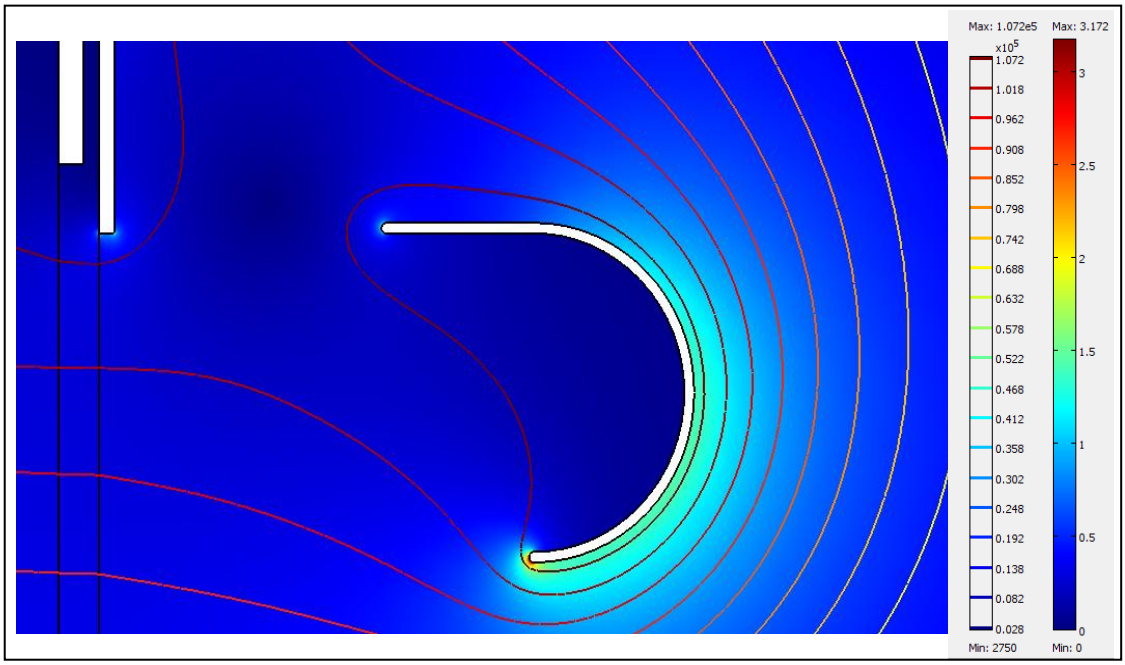

Figure IV-19: Particular of precedent figure.

Table IV-4 summarize the results obtained with the second type of analysis done with COMSOL.

Table IV-4: Comparison among analysis with different distances between shields and break.

Distance y from the flanges [cm]	Distance x from the break [cm]	Electric Field on point A [kV/mm]	Electric Field on point B [kV/mm]
2	2	6.15	2.4
5	1.5	4.74	2.64
10	1.5	2.97	2.68
10	3	3.17	3

As happened before, the critical point obtained is on the edge point between rubber and the stainless steel, but on the shield the value of electric field increases (see Figure IV-18 and Figure IV-19).
The critical point is the same for all the examples, but the values are similar to the precedent case, as is possible to see in the previous tables (see Table IV-3 and Table IV-4).
Even if tor this kind of evaluation the values are lower, the mechanical treatment on the shield could be more difficult than the first case.
In conclusion, the second kind of analysis offers a better opportunity to reduce the peak value. Even if all the values are closer it will be necessary to not put the shields in a lower position (the distance from the flanges is high), otherwise the function of the shields would be compromised and there could be problem regarding the connection and the stability of the same shields.
Thus the configuration that will be chosen if the shields are needed is the configuration with the shields where the distance from the flanges is 8 cm.
In the last figure it is possible to see the results with the shields in this configuration and with a sort of connection (see Figure IV-21, observable only on the upper part of the break) made using screws for example, a very simple thing only to see what happens near the connection.

The critical point is the same found before.
If tests on the break with voltage applied will show the need to use the shields, it will be preferred to move the shield only on the y coordinate (the first method of analysis), in order to make easy the shield working and the relative connections with the flanges.

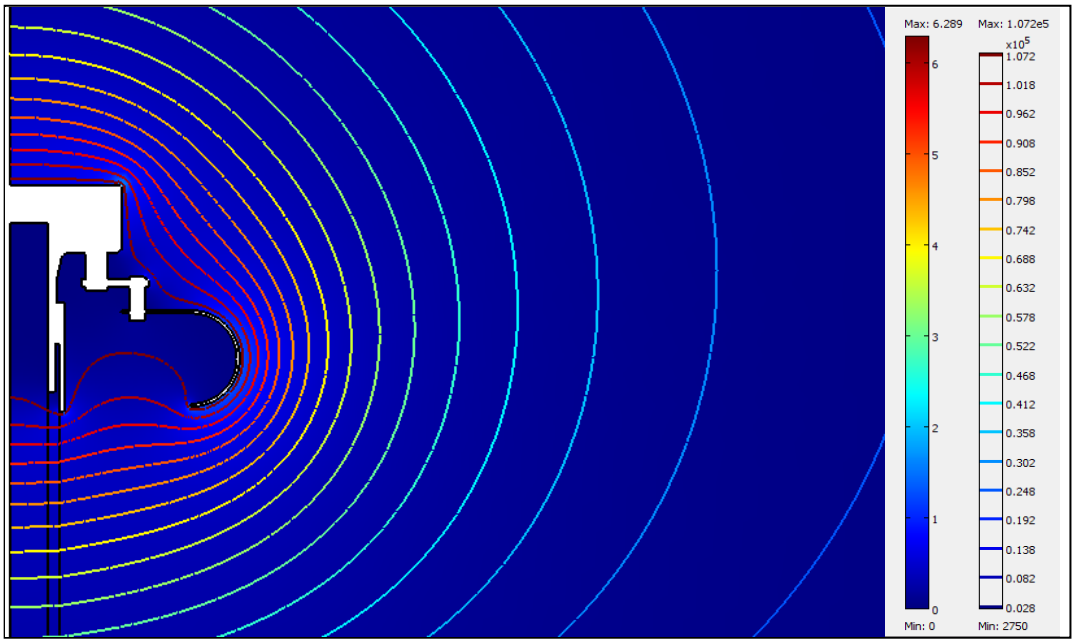

Figure IV-20: Case with the connection between the flange and the shield.

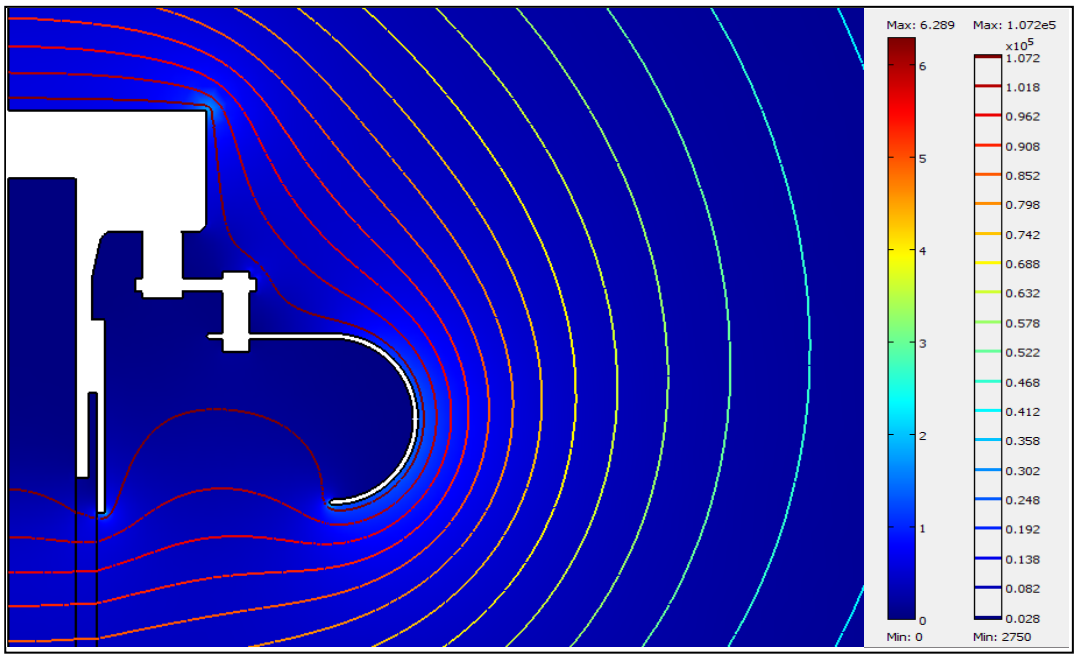

Figure IV-21: Particular of simple connection.

4.2.1.2. Results with break filled with ultrapure water

The further step to this analysis has been to add the ultrapure water inside the break to see the variation of electric field respect to the precedents studies done.
The most important difference between the previous analysis is that the air inside the break had electric constant that equals to $\varepsilon_r=1$; now for this analysis the break will be filled with ultrapure water that have an electric constant of $\varepsilon_r=82$.

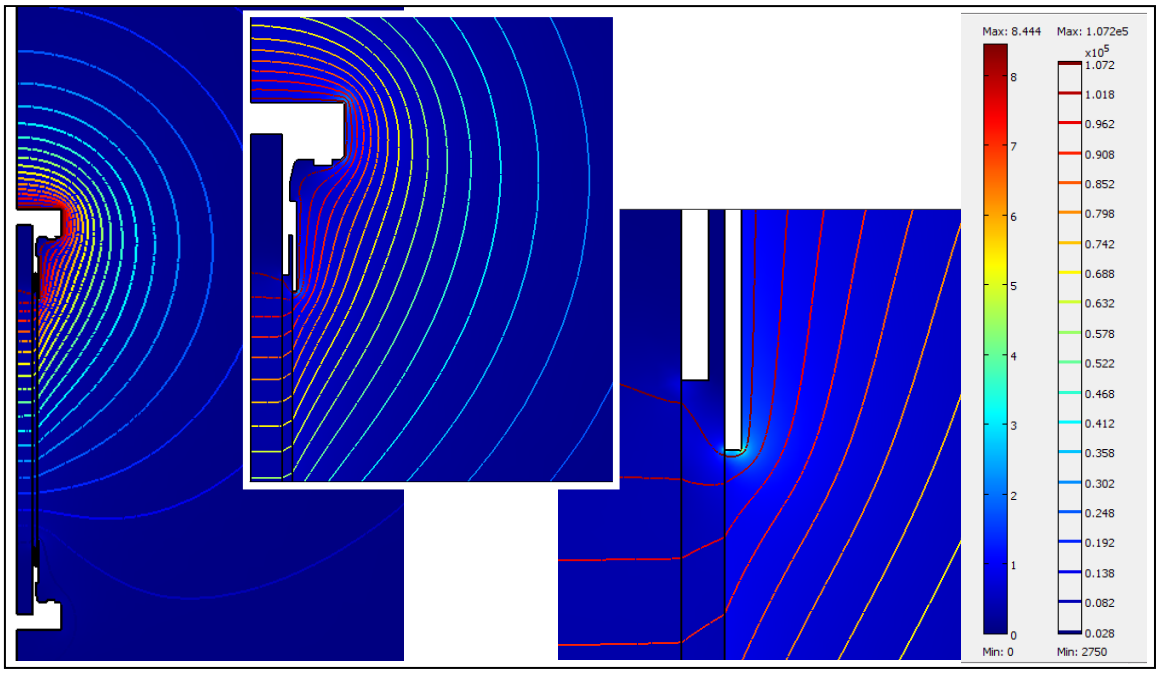

Figure IV-22: Results after analysis with break filled of ultrapure water.

Figure IV-22 shows the results after analysis done with the break filled of ultrapure water and without any shielding; the maximum electric field is reached on point A (see Figure IV-13) and the value is 8.44 kV/mm.
On Table IV-5 is shown the analysis done with the distance between the shields and the flanges of 8 cm, with the break filled of ultrapure water.

Table IV-5: Values of electric field reached during the analysis with the break filled of ultrapure water.

Distance from the flange [cm]	Electric Field on point A [kV/mm]	Electric Field on point B [kV/mm]
8	5.45	2.05

Figure IV-23 shows the analysis done with the conditions chosen in Table IV-5.

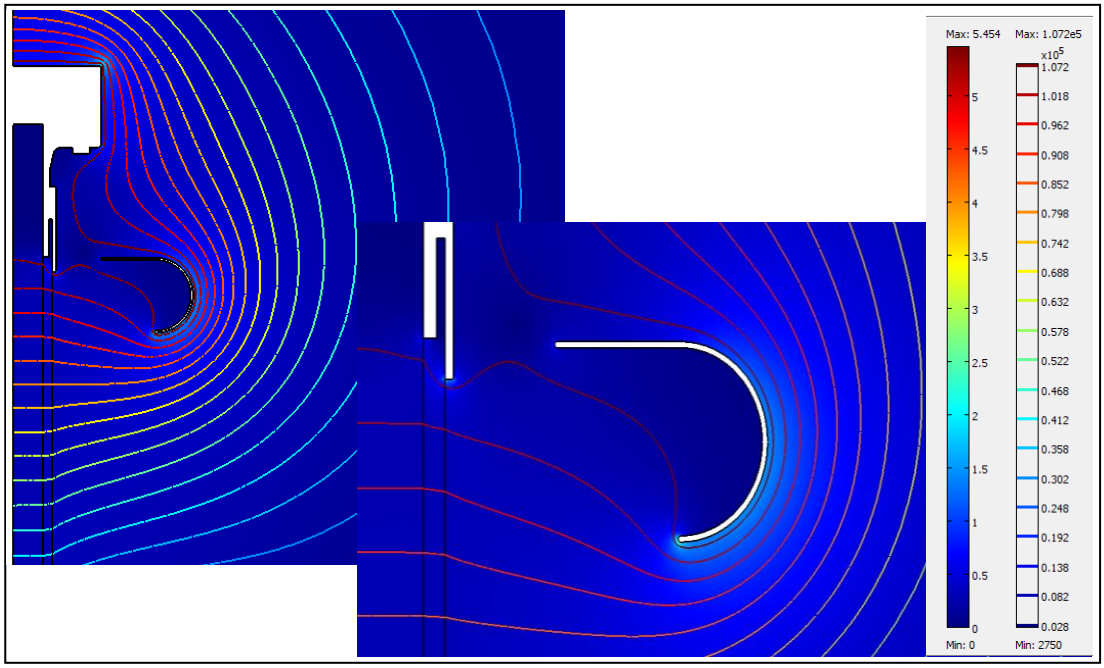

Figure IV-23: Results with break filled of ultrapure water with shields.

The electric field, respect to the same case with air inside the break, is increased on point A, but is decreased on point B. It is interesting to see that the electric field seems to benefit to the presence of ultrapure water inside the break.

Chapter V : Tests on insulating break samples

5.1. Introduction: Test setup

To perform high voltage test, ICE plant has been added by a specific part than can permit to use the power supply on break samples, without interacting with the remaining test section of ICE. On
Figure **V-1** it is possible to see the modifications done on ICE plant, where the output cable of power supply will be put on the top of the break and the bottom will be connected to ground potential and close the electric circuit with the power supply.
Before starting any practical activity, it has been necessary to clean every break that it will be used for the tests.
To avoid problems regarding the utilization of chemical cleaners that can damage the rubber inside the breaks, it has been chosen to use common soap and a thin broom to assure the good cleanliness especially inside the breaks. After this operation, all the breaks washed, were blown with nitrogen gas to perform a good removal of presence of dust particles and other materials.

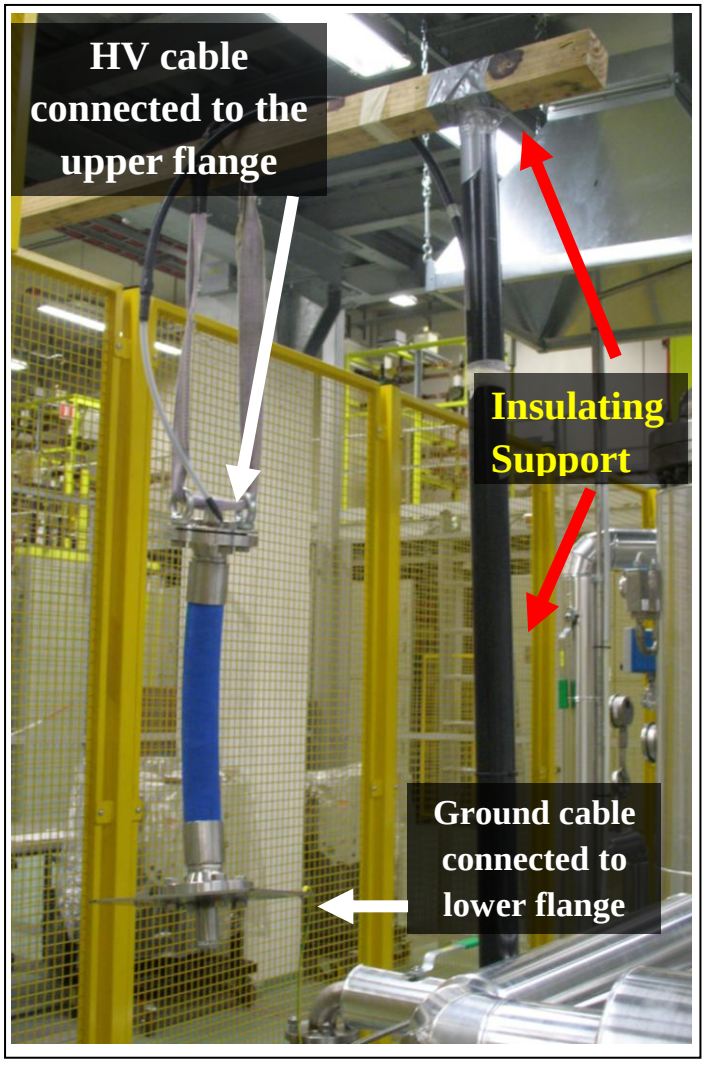

Figure V-1: High Voltage test section layout.

The power supply used for high voltage tests is basically an AC to DC power converter that can be remote controlled. Within the power supply, conversions of AC to DC then to high frequency AC, then to high voltage DC take place.
The power supply can supply up to 1200 Watt of DC power, the maximum voltage is 150 kV; the power can be supplied in two different ways:

- ✓ Voltage control: the output voltage regulator circuit maintains the voltage control.
- ✓ Current control: the output current regulator circuit maintains the current control.

The output is provided by a shielded high voltage output cable.

Figure V-2: Front of power supply.

5.2. Voltage test on insulating break in dry conditions

The electric scheme that summarizes the path of current for this kind of tests is shown in Figure V-3:

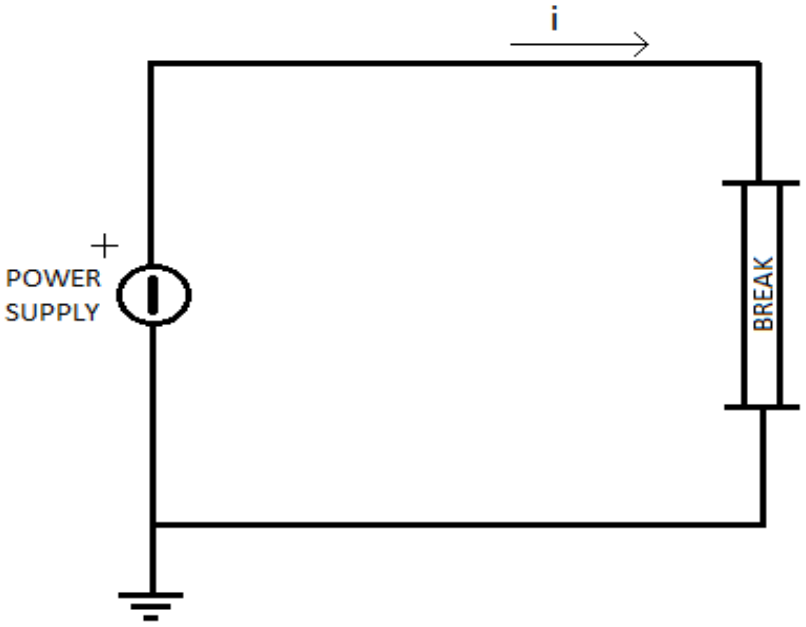

Figure V-3: Electric scheme of high voltage test done on empty breaks.

The break sample shown on
Figure **V-1** can be represented as shown on Figure V-4.
The Figure V-4 shows this simple scheme that represents the circuit in Figure V-3 where the resistance R_1 corresponds to the stainless steel flanges located at the top and the bottom of the break, R_2 represents the rubber between the flanges and R_3 represents the ultrapure water when will be present inside the break.
In case of break empty, R_3 won't be present in this scheme. The voltage applied is 110 kV.

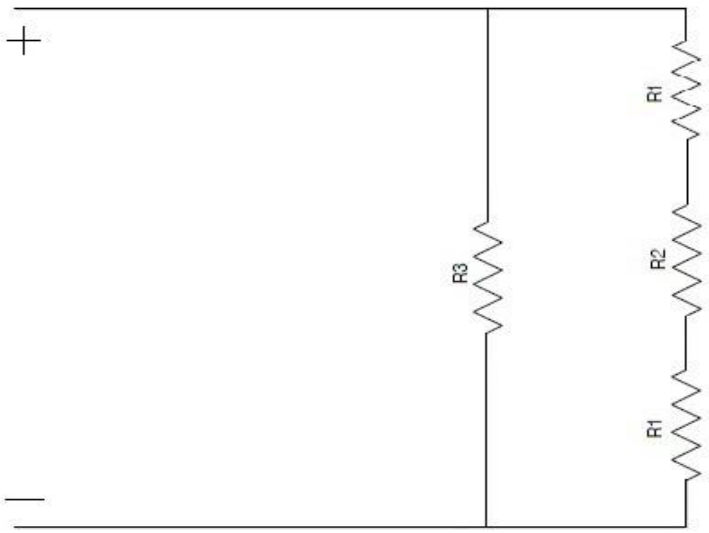

Figure V-4: Representation scheme of break under test voltage.

The values found for these parameters are:

- Restivity of Stainless Steel ≈ $0.75*10^{-6}$ Ω*m;
- Resistivity of rubber ≈ 10^{13} Ω*m;
- Resistivity of ultrapure water (when present) ≈ 2MΩ*cm [@ 25°C].

Without producer's datasheet the value of resistivity of rubber has been found on a text book [1]; it is necessary to underline that the value used is concerning to homogeneous rubber, and on the break there is not only rubber, but it is a composite material.
We can now calculate the resistance of each part of our test using the formula (2) previously used on paragraph 2.5:

$$\text{Resistance}=\text{Resistivity}*\frac{\text{Length}}{\text{Surface}} \qquad (2)$$

To evaluate the resistance of the rubber tube we used the specific measures given by the break's producers, the length is given (=0.40m) and the surface is calculated by a simple geometric formula because the tube surface is a circular corona $S=\pi*(R^2-r^2)$ where R is the major radius (=0,033m) and r is the minor radius (=0,025m):

$$S=\pi*(0.033^2-0.025^2) =0.00146m^2 \qquad (4)$$

Now it is possible to calculate the resistance R_2 using the formula (1):

$$R_2= 10^{13}*(0.42/0.00146) \approx 288.13*10^{13}\,\Omega \qquad (5)$$

It is possible to assume that the series of R_1, R_2 and R_3 equals to R_2 because this resistance is much higher than the other two (that corresponds to a conductive material, the Stainless Steel)
If we suppose that the break is empty, R_3 won't be calculated, the total resistance is $288.13*10^{13}$ Ω, using the Ohm's law the current will be:

$$I= V/R_2= 110000/288.13*10^{13}=3.82*10^{-11}\ A \qquad (3)$$

Due to this calculus, we can assume that a very low current will flows on the system, but it is important to compare this result to the tests that will be done afterward, because during the calculation of resistance, the assumptions done might be wrong.
To understand the real resistance of the break, a measure has been necessary to do: the measure is a normal measure of resistance with a specific megaohmmeter that can measure high resistances; the value measured was 30 GΩ, this will be the value of resistance of our break.
Comparing the value calculated with the value measured there is a significant difference that is why maybe the assumptions done during the calculation of resistance was wrong or the values of resistivity did not correspond to the materials used.

Figure V-5: A break sample during resistance measurement.

Once measured the resistance of the break, an application of voltage has been done to understand if the metallic connections used to support the break could be subjected to corona effects and evaluate if some parts of the upper side of the break has to be shielded or not.

During the test with the break empty the connection between the break and the insulating support in shown in Figure V-6:

Figure V-6: Connection of the support before test with empty break.

The power supply has been used with voltage control and it has been reached the value of 150 kV after further steps as it is possible to see on Table V-1, the maximum value of current reached is 0.22 mA, during this series of tests it has been noticed that in the side direct connected to the high voltage was subjected to corona effect, in particular the eyebolts and the small metallic parts that have function of support.

Table V-1: Values of voltage and current after first test with empty break.

Voltage [kV]	Current [µA]
110	70
120	90
130	130
140	150
150	220

An improving of the configuration has been done: the metallic parts subjected to corona effect were removed and the belt was used for the support of the break, the termination of high voltage cable were shielded with aluminium thin foil to avoid partial discharges to the mating flange.
Further test at the same voltage, with new configuration of connections, confirmed that the last solution adopted was the best because less corona effects were detected. Figure V-7 shows the different connection done after the first series of tests with empty break.

Figure V-7: Connection of the break's support after the modifications.

Table V-2 shows the values of current reached after the modifications done on the break support in order to limit corona effects noticed during the previous test.

Table V-2: Values of voltage and current after second test with empty break.

Voltage [kV]	Current [μA]
110	20
120	25
130	40
140	60
150	100

This configuration shown that the current is reduced comparing the valued measured in the precedent case.
These tests were done even for understand if the shielding studied with FEM analysis on previous chapter was necessary, the results given by the tests have revealed that the shielding were not necessaries and the tests can be conducted with the configuration done on Figure V-7.
The power supply can assure a maximum of current of 8 mA, but further tests will be done with the imposition of 6 mA to prevent the overcurrent that can stop the tests.
The purpose is to represent, to a limited degree, what will happen on SPIDER experiment during operative conditions (see paragraph 2.5 for further information about SPIDER operative conditions).
The voltage will depends from the variation of resistivity of column of water. In this sense Figure V-8 represents, respect particular values of resistivity, the function V(I).

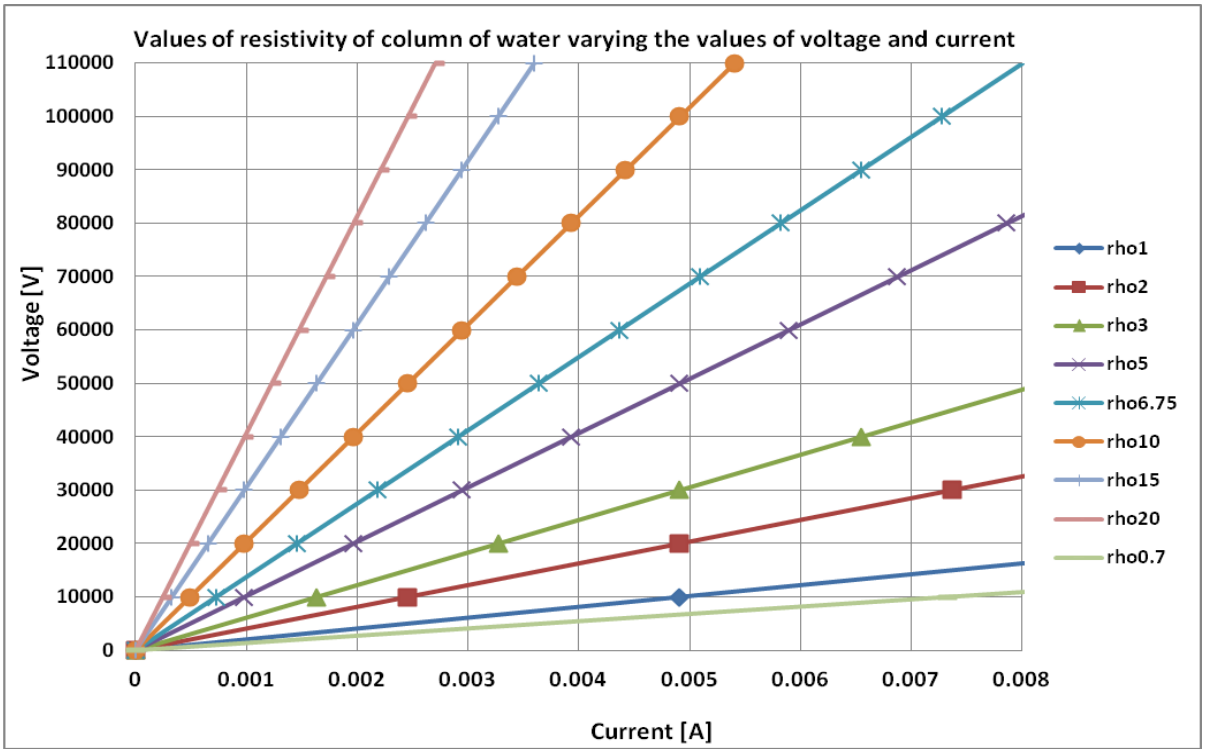

Figure V-8: Graph that shows at various values of resistivity the values of voltage and current that can be reached

The volume, or column, of water is given by the surface (19.64 cm^2) and the length (40 cm) of our break, so once the resistance is calculated with the Ohm's law, the resistivity of the column is easy to find using the reverse of (1).

The minimum value of resistance that can permit a flow of 0.008 A, applying -110 kV is:

$$110000/0.008 = 13.75\ M\Omega, \text{ that means a resistivity of } 6.75\ M\Omega*cm \quad (3)$$

This is a very high value of resistivity, considering the problems concerning the keeping of high values in ultrapure water.
Due to this high value necessary to reach -110 kV, the Figure V-8 can show various values of resistivity related to the column of water at different voltages and currents, this graph is necessary to understand the limits that could be achieved during the tests with the resistivity of water obtained after the filtration.
This chart needs to us only to realize the order of magnitude of our parameters, after that, what we found needs to be confirmed by the tests.
In the Figure V-8 the lower straight line represents the lower resistivity (almost 700kΩ*cm), and moving in the upper direction (or rotating in the counter clockwise sense) the resistivity increases, the maximum value considered is 20 MΩ*cm, only to see the limits of this case.
It's easy to see that the value of 6.75 MΩ*cm is the value that exactly reaches the maximum power output of the power source for our purposes (1200 W).

5.3. Tests on insulating break samples filled with ultrapure water

To perform these tests, the cell used to measure the water resistivity and temperature has been removed from the section for the purification water and put on the lower mating flange, directly connected to the ground potential, as it is possible to see on Figure V-9.
This has been done for all the tests done for all breaks.

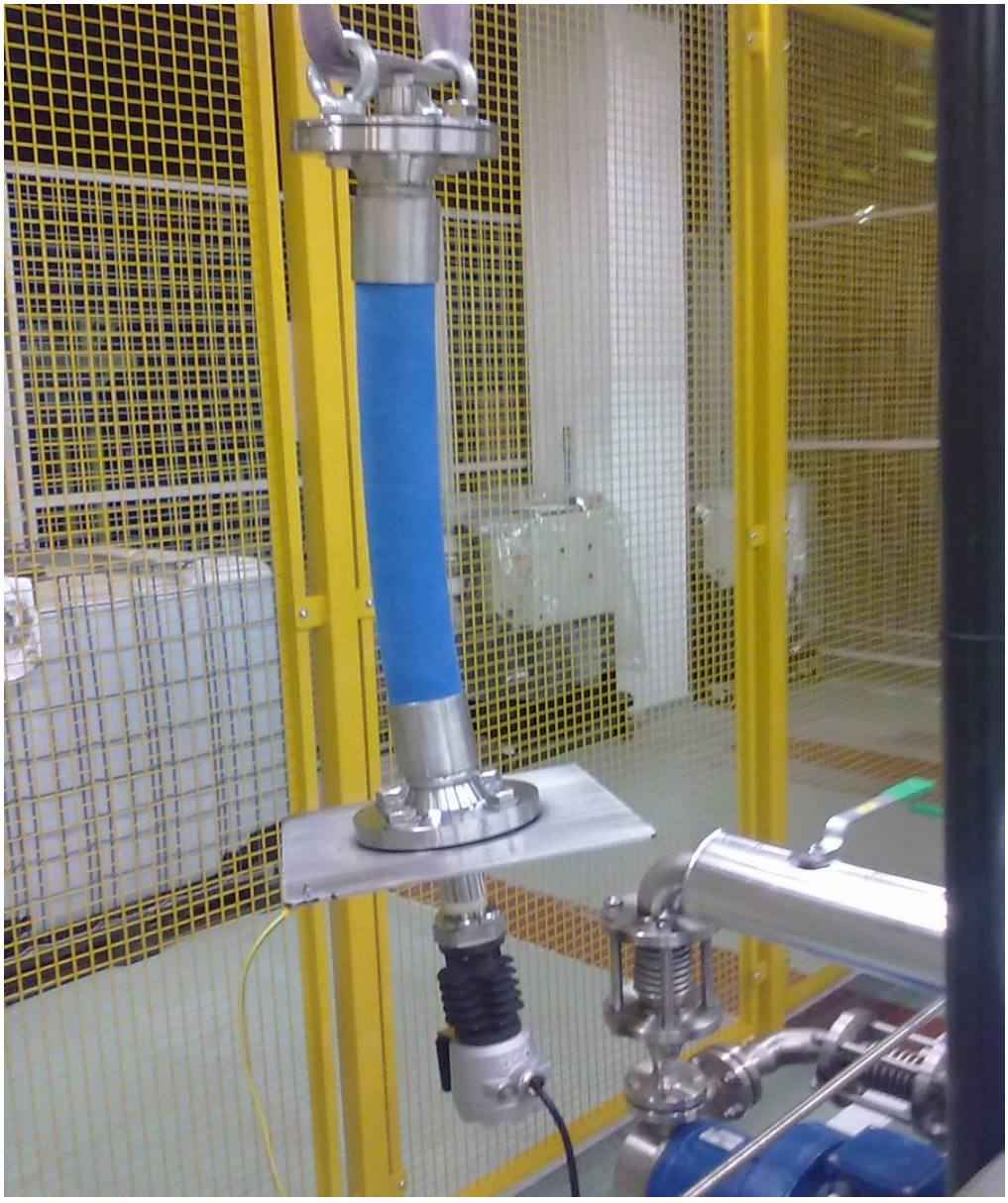

Figure V-9: Break with measure section added on the bottom.

5.3.1. Tests on first sample: break A

5.3.1.1. Water resistivity behaviour without voltage application

When the water has reached a stable level of resistivity during the purification analysis, in line with our requirements (ρ>2MΩ*cm), it has been possible to fill the breaks to evaluate the behaviour of ultrapure water when it enters in contact with other materials. It has to be remarked that it was difficult to stop the purification of the water always at the same value of resistivity, therefore following tests start at different value of resistivity, anyway always greater than the minimum value required.
We expect that the resistivity will decrease consistently, due to pollutant effect that materials have when are in contact with ultrapure water.

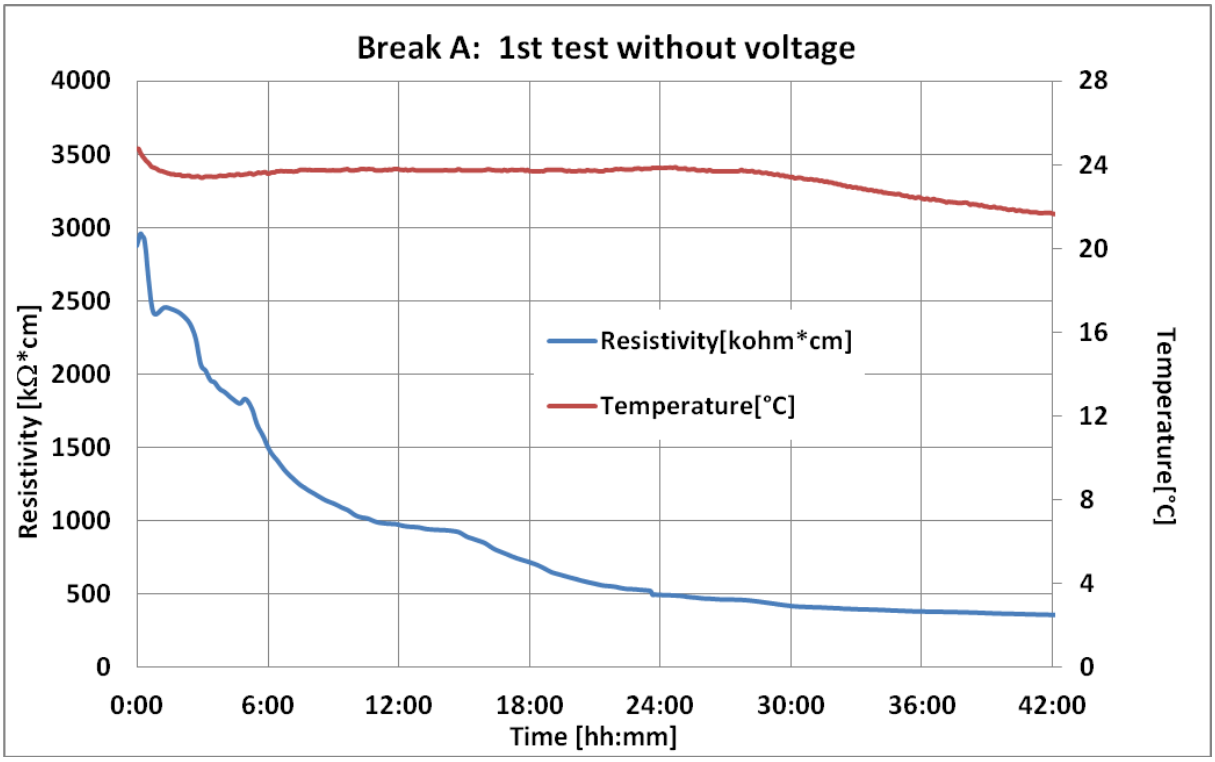

Figure V-10: Results after first test.

Figure V-10 reports the trend of ultrapure water resistivity measured on the lower side of the break, after two days. The first six/twelve hours from the beginning of the test, show that the decay of the resistance is very fast and sharp; the trend of resistivity in the remaining time is logically slow due to the slowing-down of solution process of water inside the break.
Similar results has been found in the further two tests, even if the starting value of resistance is not the same the trend seems be equal (Figure V-11 Figure V-12 and Figure V-13).
In this series of test we can see the different progressing of temperature, in fact the temperature varies with room temperature, but even in this case the resistivity does not affected from the temperature.

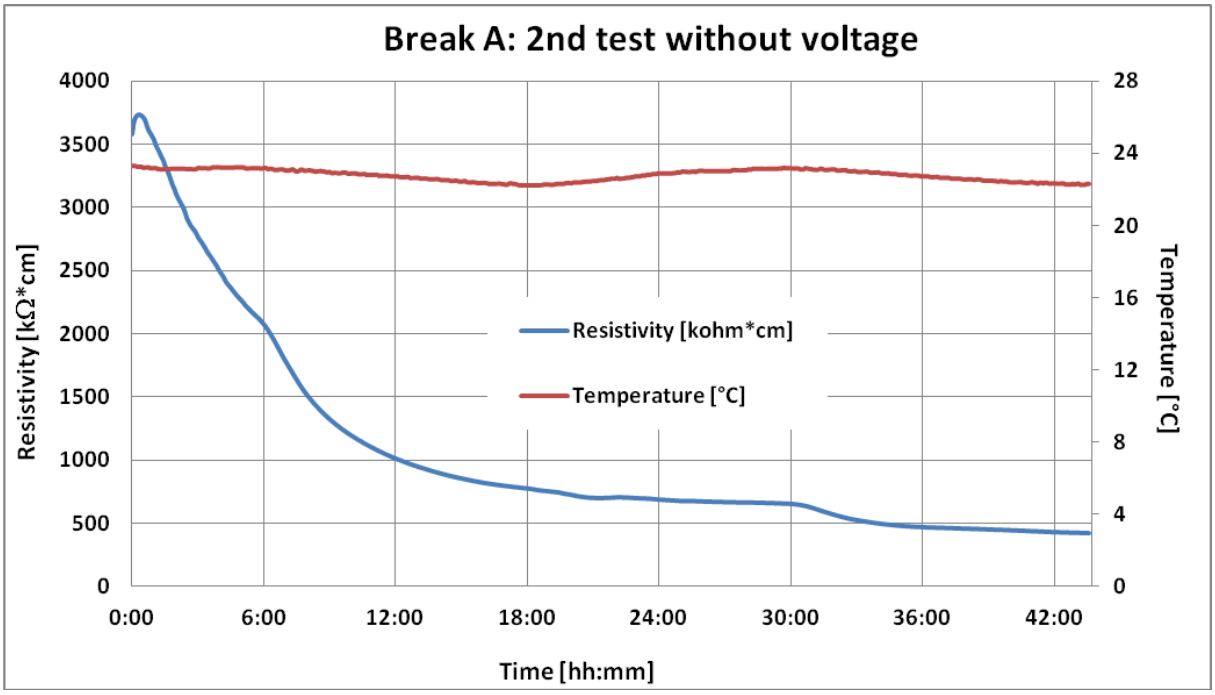

Figure V-11: Results after second test without applying voltage.

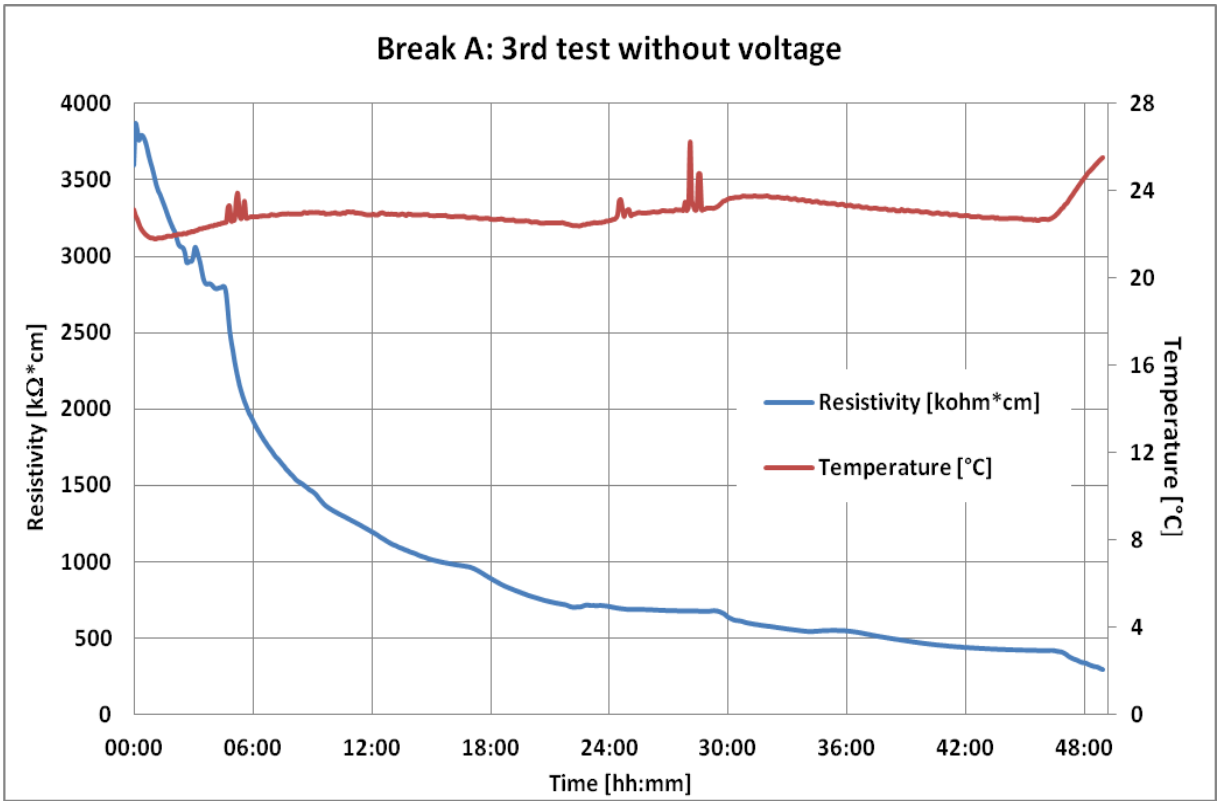

Figure V-12: Results of third test on break A.

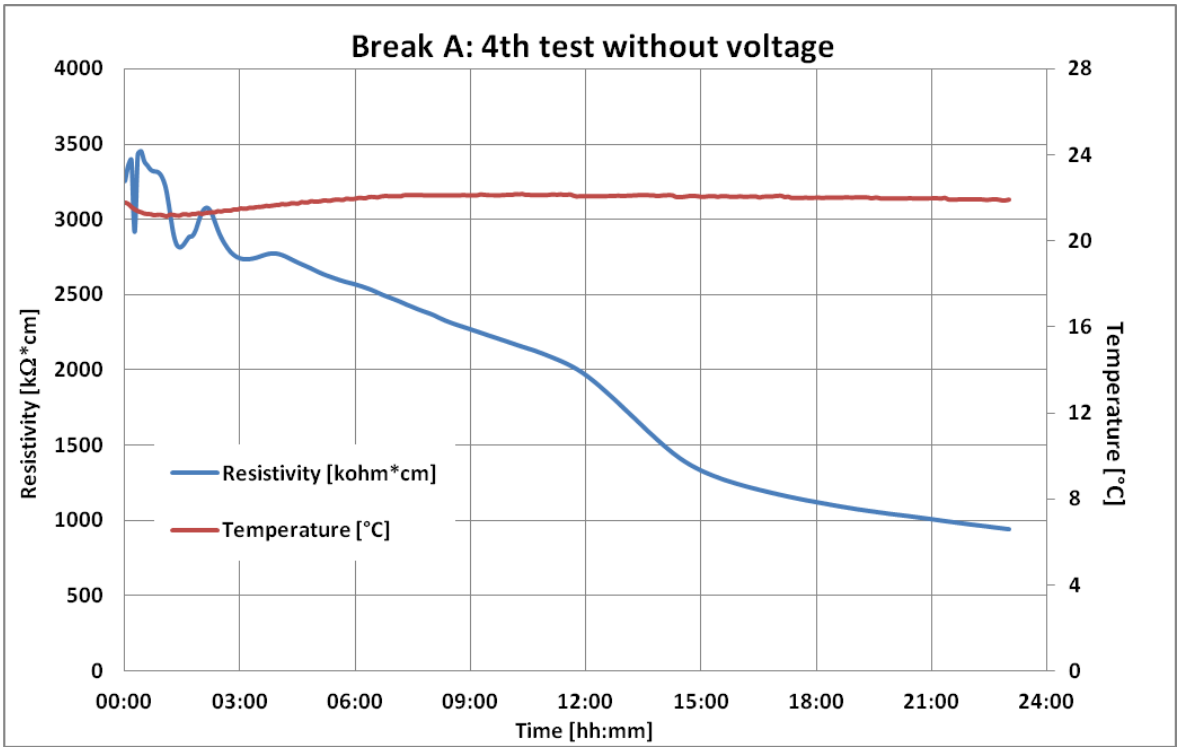

Figure V-13: Results after fourth test without applying voltage.

These tests show that, even if contained in a sealed volume, ultrapure water cannot maintain a stable value of resistivity, only after 48 hours the values are in a thin range and it is possible to say that the resistivity is stable, this is due to the easy and fast pollutant effect that material have when its become in contact with ultrapure water, as said before.

Ultrapure water is an unstable and delicate matter, in further and more important applications and experiments, it will be necessary to study a continuous filtration and purification system, in order to maintain water pure and suitable for the devices used in those applications.

5.3.1.2. Water resistivity trend with current circulation

To complete and understand the behaviour of ultrapure water for a possible use on a fusion experiment, even under voltage, and fully characterize the break that will carry ultrapure water it has been necessary to study the water resistivity variation with a current imposed by the power supply, for several hours.
These tests have been performed for eight hours of operation and with the power supply that supplies the power with the current control that deliver 6 mA of direct current constantly, than the voltage can vary in order to maintain stable the current. Figure V-14 shows the electric circuit for the voltage tests.

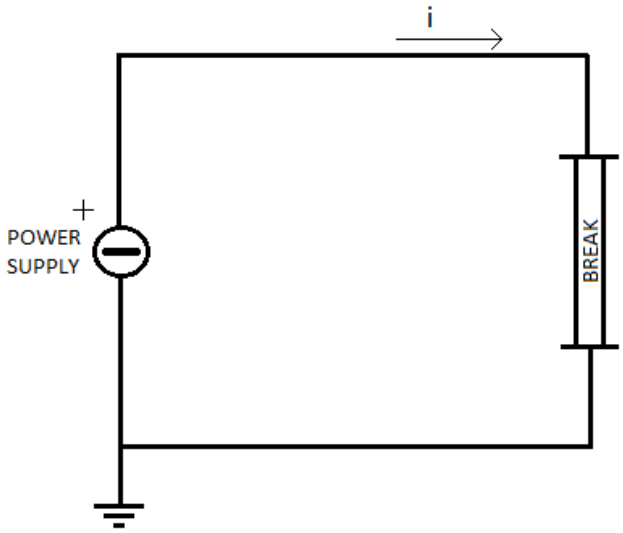

Figure V-14: Electric circuit for voltage tests.

It has been noticed that the power supply, with the current regulation, at low values of voltage becomes instable and consequently the current slowly increase as it is possible to see on Figure V-15:

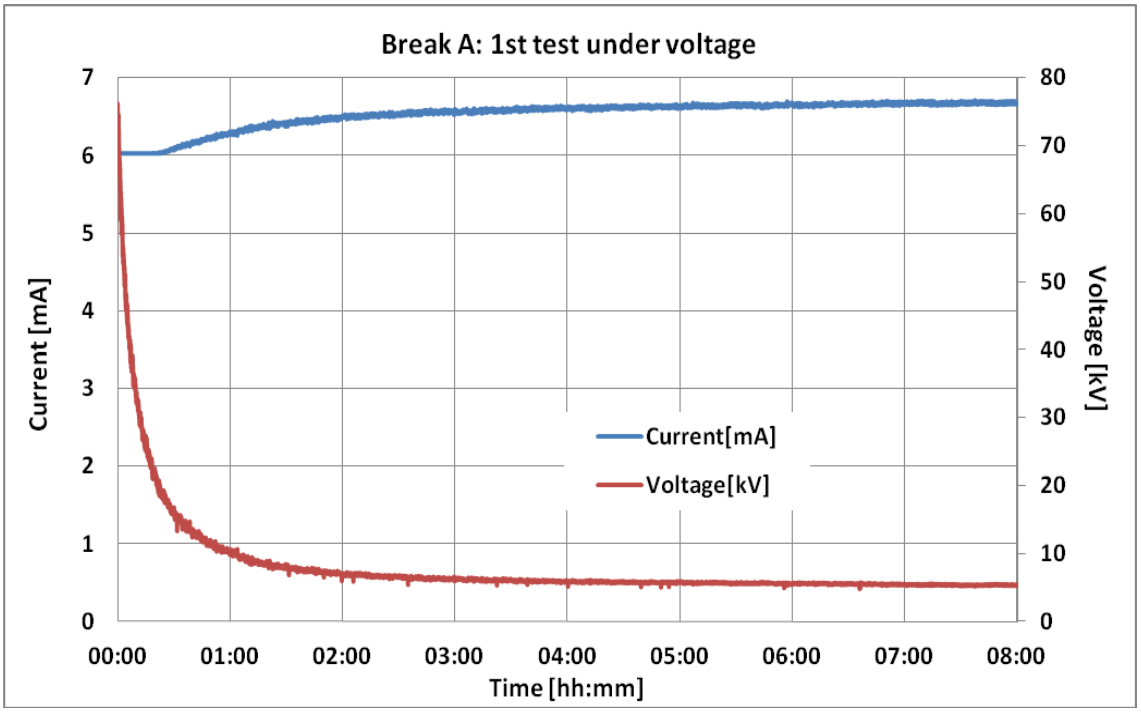

Figure V-15: Current and voltage during first test with voltage applied.

It is important to underline again that these test are done almost four times lower than SPIDER experiment (where are foreseen 27.5 mA with 110 kV), so the results are only to see what would happen with a current applied and try to study, and then find suitable countermeasures to resistivity degradation problems found during these high voltage tests.
Below, it's possible to see the trend of resistivity measured, resistivity calculated and temperature on Figure V-16:

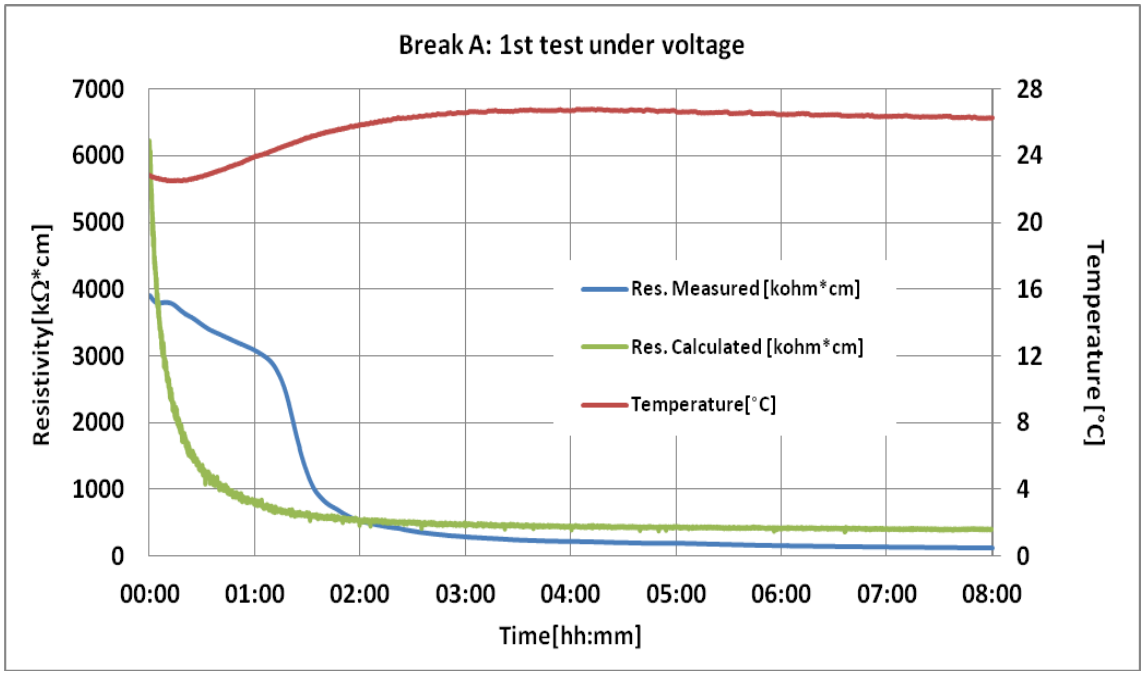

Figure V-16: Trends of resistivity and temperature during first test with voltage applied.

The difference between resistivity measured and calculated is that the first one is the resistivity measured by the cell and this is a value that represent a single point, precisely the bottom of the break, on the contrary the resistivity calculated is the calculus of medium resistivity of column of water obtained using the Ohm's law, more precisely the inverse of formula (1) applied before, for each value of voltage and current supplied by the power supply, it is clear that the resistivity calculated is proportional to the voltage trend because the current is constant.
It is possible to suppose that the measured resistivity is affected by the movement of water due to a temperature gradient, even if small that causes the particle movement, than the increasing of pollution of water that interact with internal faces of break and also releases contaminant particles.
After this first test with voltage applied, important results have been discovered: the resistivity decreases more than three times faster than the previous test without voltage, this fact is clear because the presence of a current accentuate the movement of particles inside water and the transport of charge phenomenon increase the decay of ultrapure water due to electrochemical effects correlated to current circulation.
In that sense, when resistivity decreases (so even the resistance), the voltage decreases sensibly because the current is maintained almost steady.

The following test confirm the same trend as shown in Figure V-17 and Figure V-18:

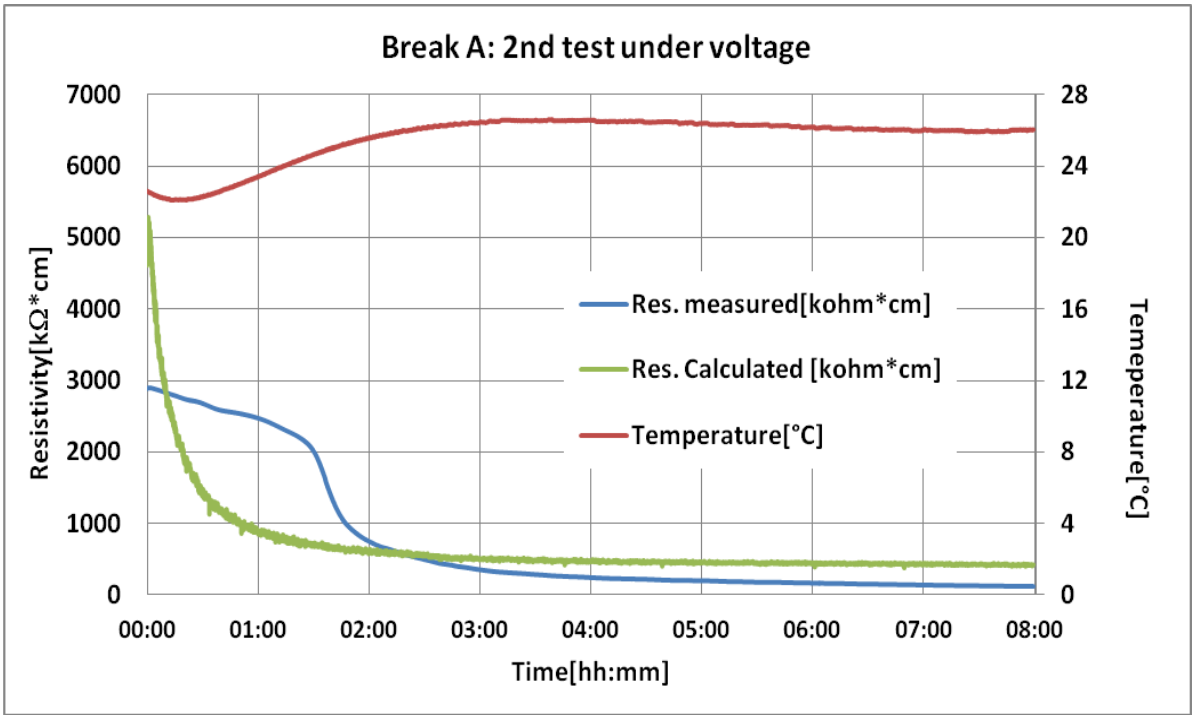

Figure V-17: Trend of resistivity and temperature.

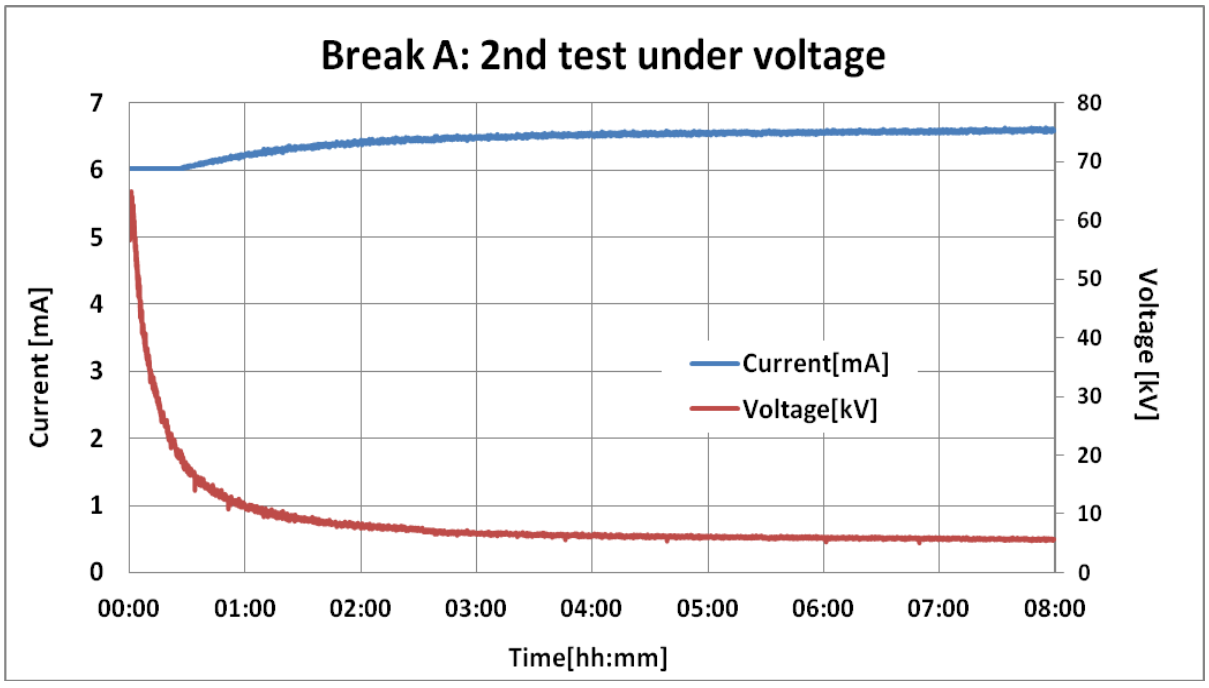

Figure V-18: Current and voltage during second test on break A.

The temperature during these tests is increased more than 4°C, this because the flow of a current, interacting with the water that have its resistance, causes the rising of temperature, as happens on electric circuit.
It is possible now to compare all the tests done in order to study and understand the behaviour of ultrapure water in different operative conditions. To simplify, the charts with results were plotted with normalized dimensions,

obtained dividing each value with the maximum value reached during the same test, to make easy the comparison among all tests studied.
On Figure V-19 the values of resistivity are absolute:

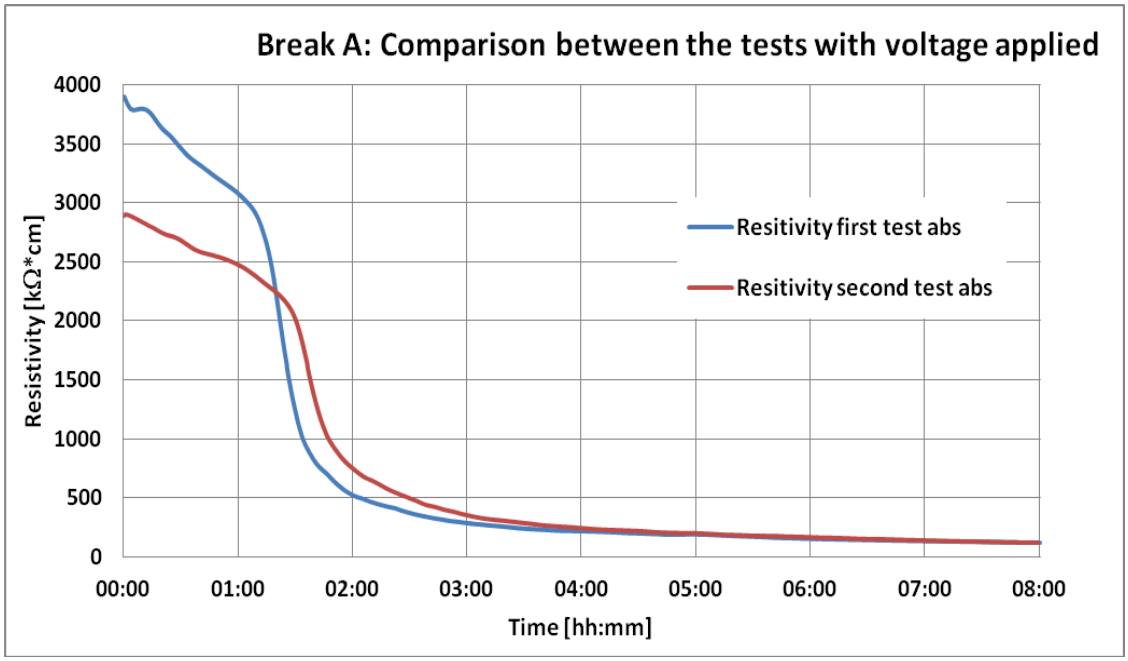

Figure V-19: Comparison of trend between the two tests done with voltage applied.

Even if the two tests did not start at the same value, the trend of decay is similar, it is possible to see it better on Figure V-20 where the values are normalized and the trend of reduction of resistivity is almost the same.
The charts on Figure V-20 and Figure V-21 show that the resistivity's decay during the first test is faster than the one of the second test, this lead again to the fact that during the first test there would be a sort of cleaning effect on the internal surface of the break.

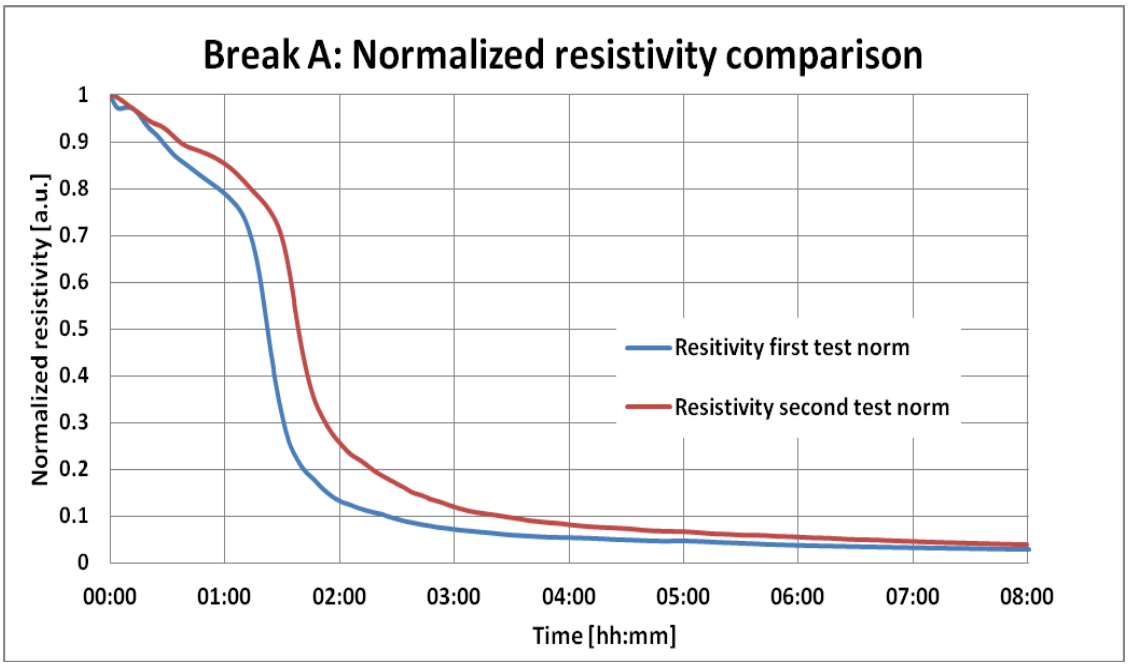

Figure V-20: Trend of normalized resistivity of two tests.

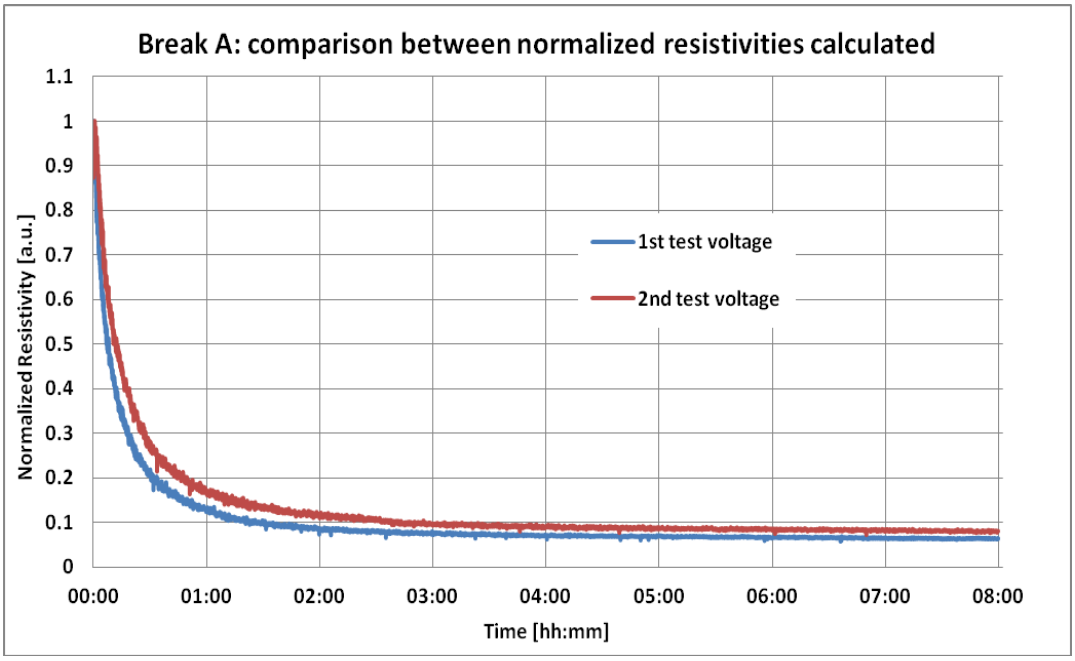

Figure V-21: Comparison between the calculated resistivity.

The chart below (Figure V-22) shows all tests done on break A, the presence of a current increase the reduction of resistivity, this is clear and the trend of all test done under the same conditions (with or without voltage) are similar and follow the same trend line.

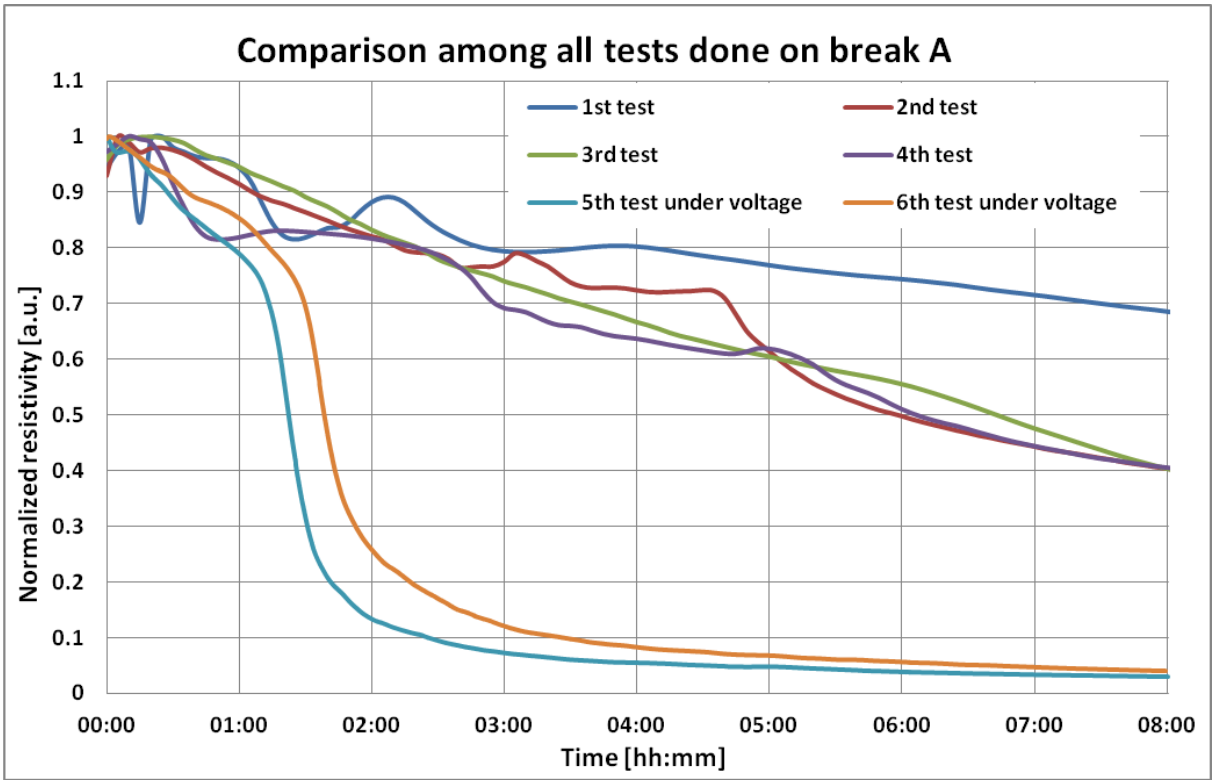

Figure V-22: Trend of all tests done with the first break.

It is interesting to see that, once the tests with current applied are done (after 8 hours), the resistivity of water increases and sets to a value near 300 kΩ*cm, as it is possible to see on Figure V-23: and Figure V-24::

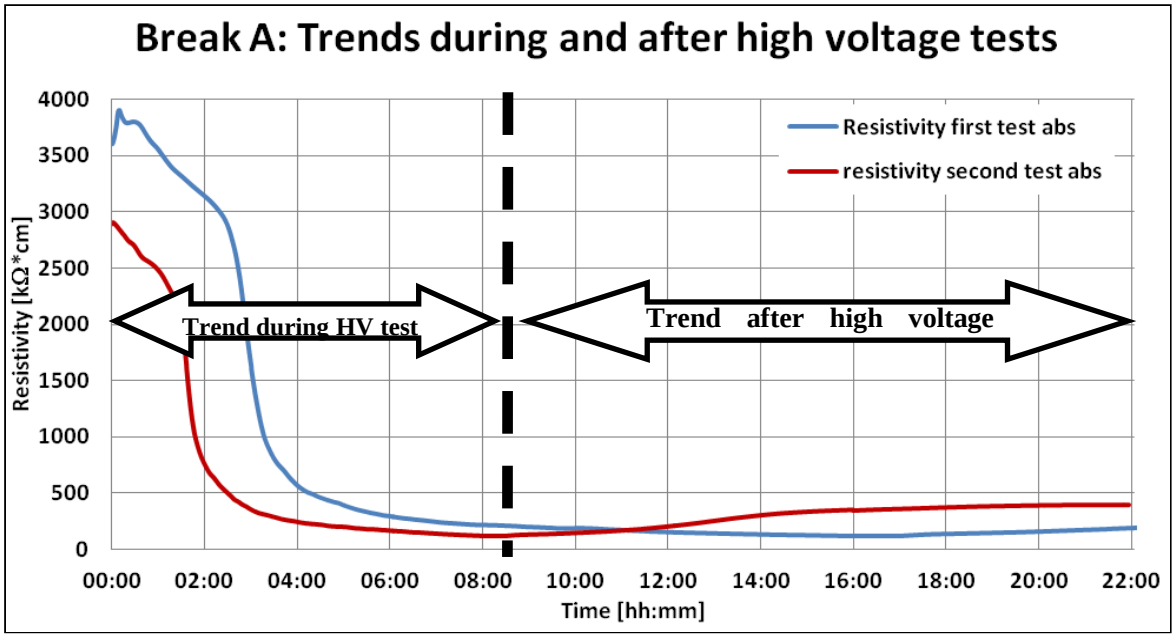

Figure V-23: Trend of resistivity during and after high voltage tests for break sample A.

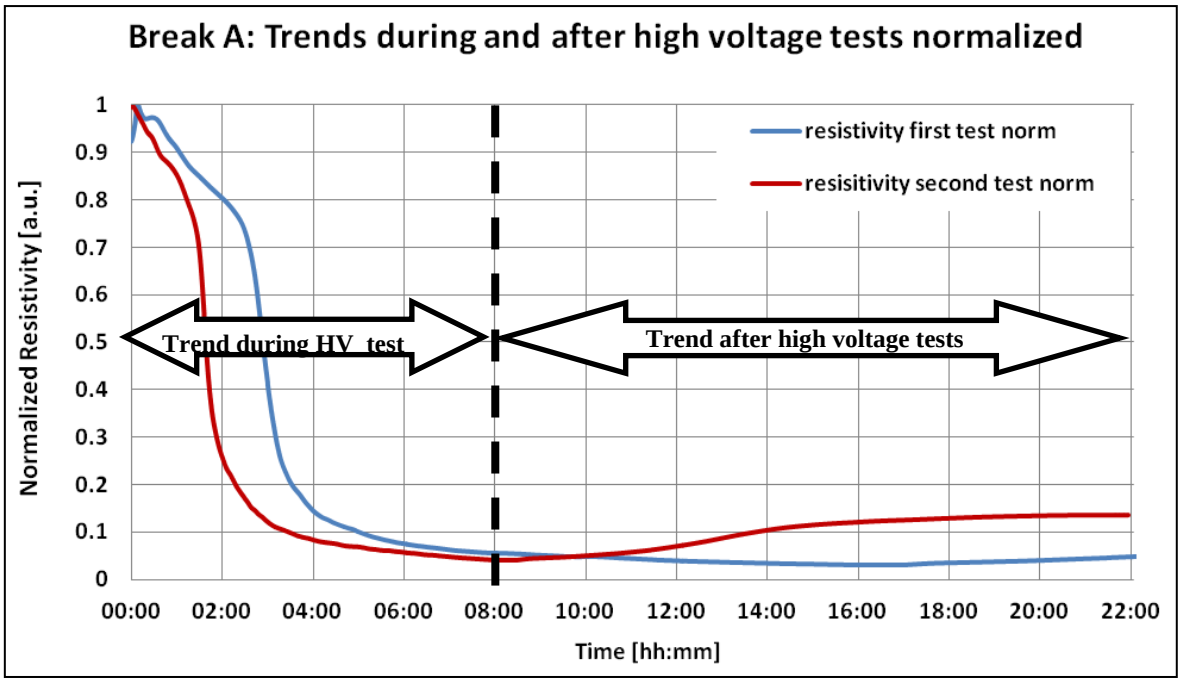

Figure V-24: Trend of normalized resistivity during and after high voltage tests for break sample A.

5.3.2. Tests on second sample: break B

5.3.2.1. Water resistivity behaviour without voltage application

In order to confirm the results obtained it has been decided to retry all tests done with a second break sample.
The tests done are the same for the first break sample, the following figures shows the results reached.
It is clear that the results obtained are similar to the ones obtained with the first break, the trend of decay is the same, the temperature has a different progress, but this depends from the room temperature evolution, nevertheless the range of variation of temperature during these tests is 4°C maximum.

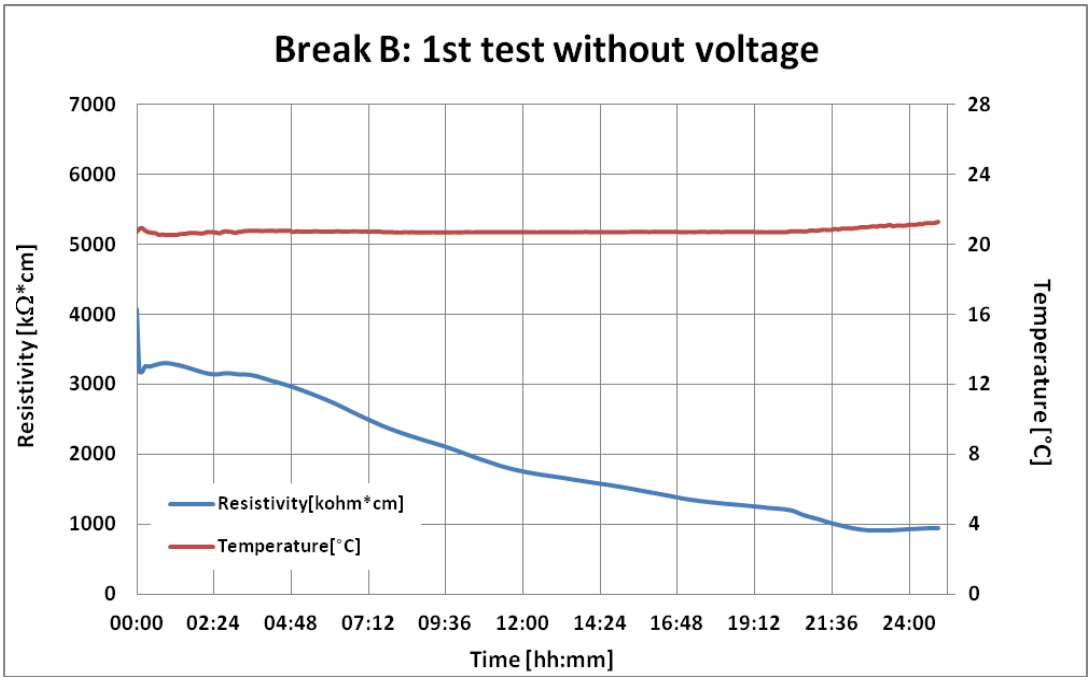

Figure V-25: Results obtained during the first test without voltage.

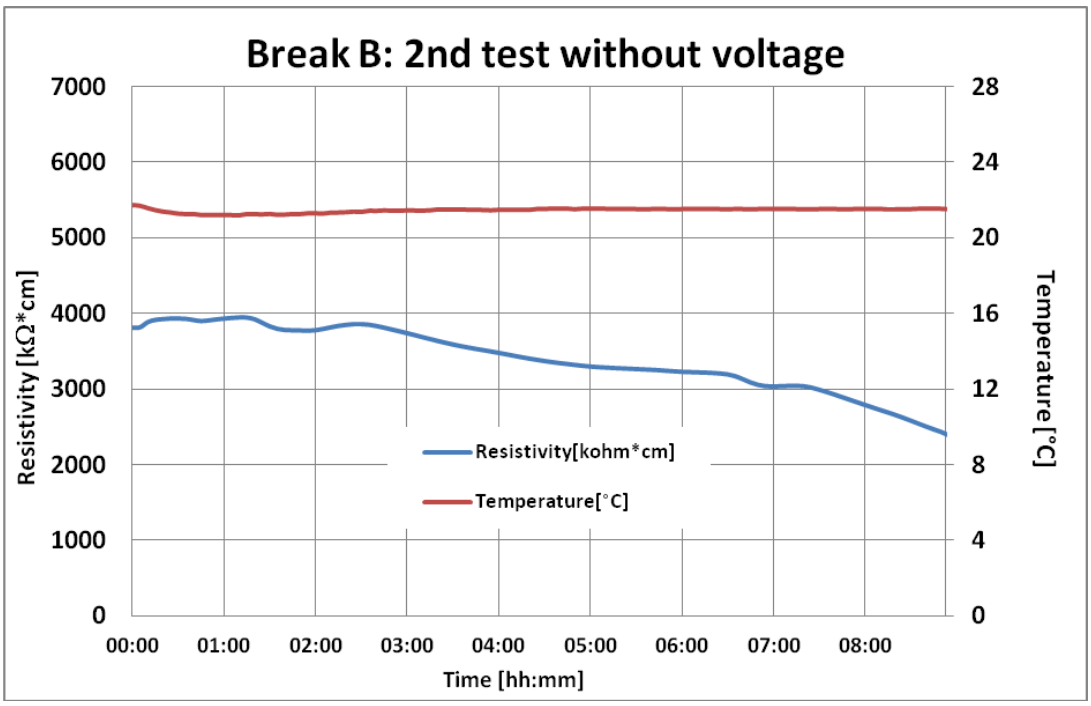

Figure V-26: Results during second test on second break.

5.3.2.2. Water resistivity trend with current circulation

The following charts will show the progression of voltage, current, resistivity and temperature during the three different tests done to confirm the results obtained with the first break.

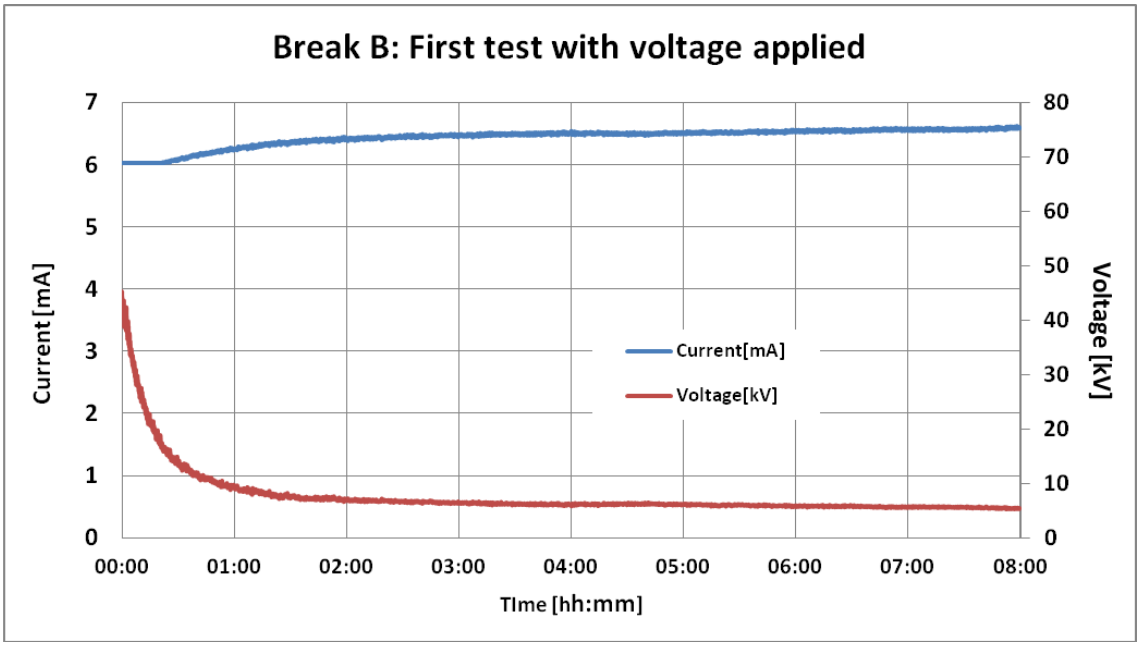

Figure V-27: Current and voltage progress during the first test on break B.

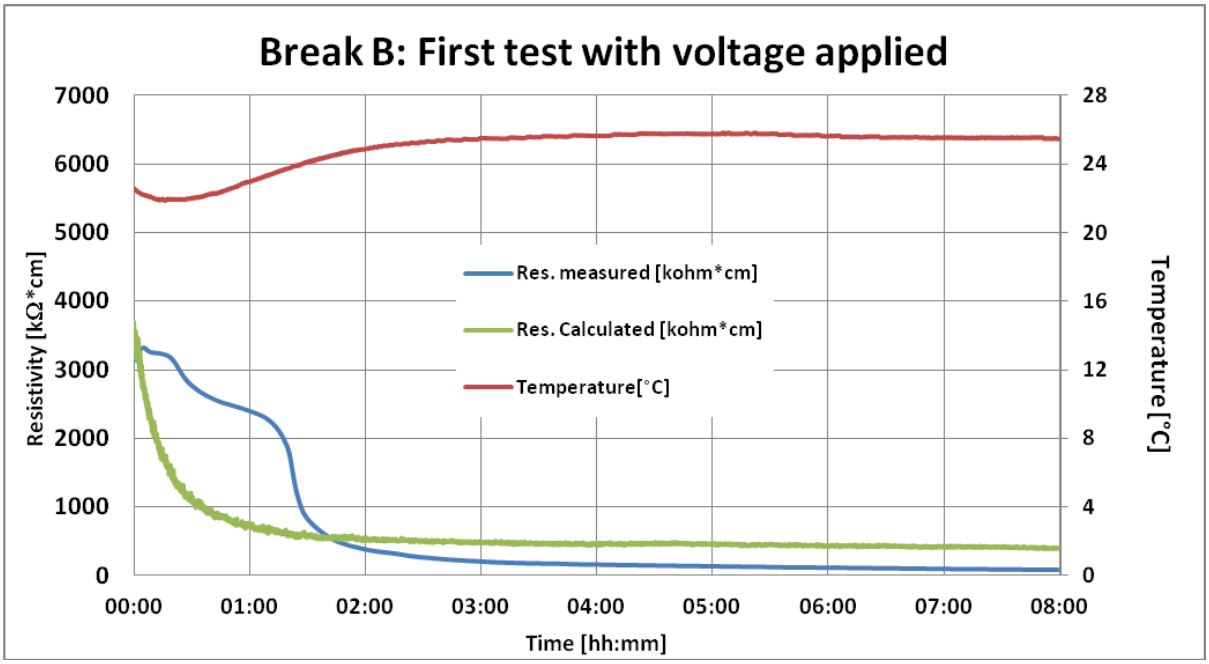

Figure V-28: Resistivity and temperature trend during the first test on break B.

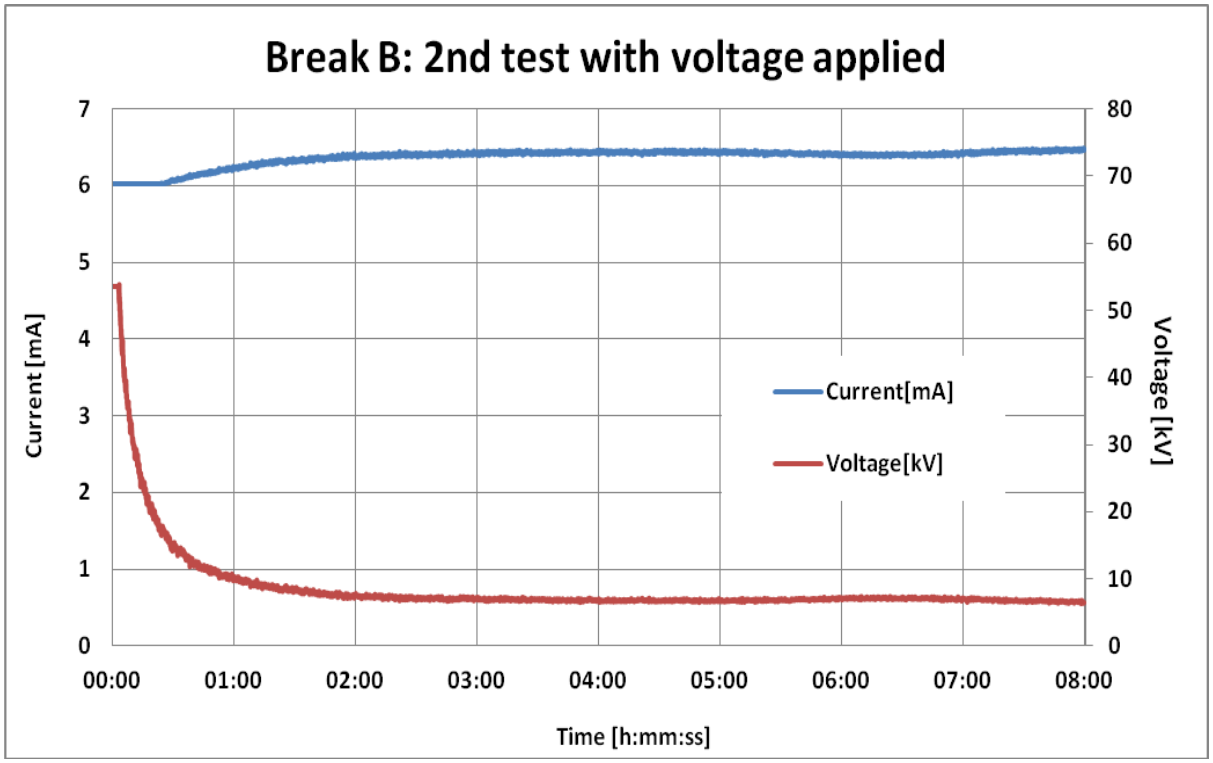

Figure V-29: Current and voltage trend after the second test on break B.

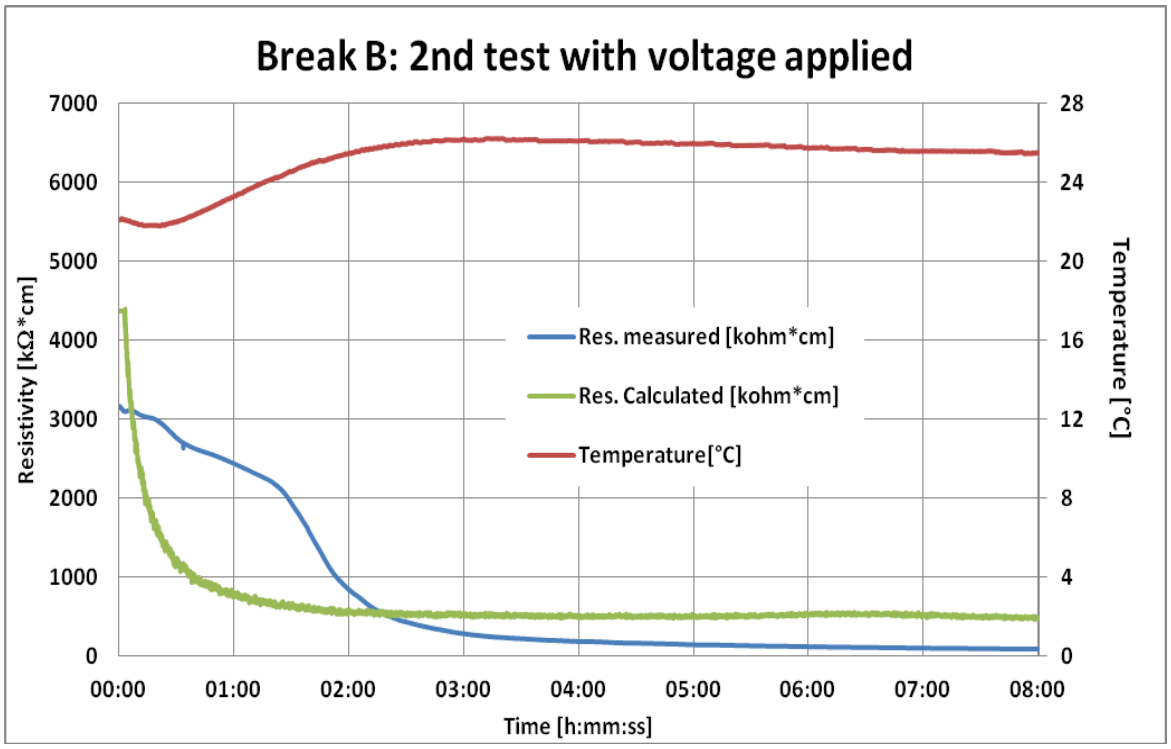

Figure V-30: Resistivity and temperature trend after the second test on break B.

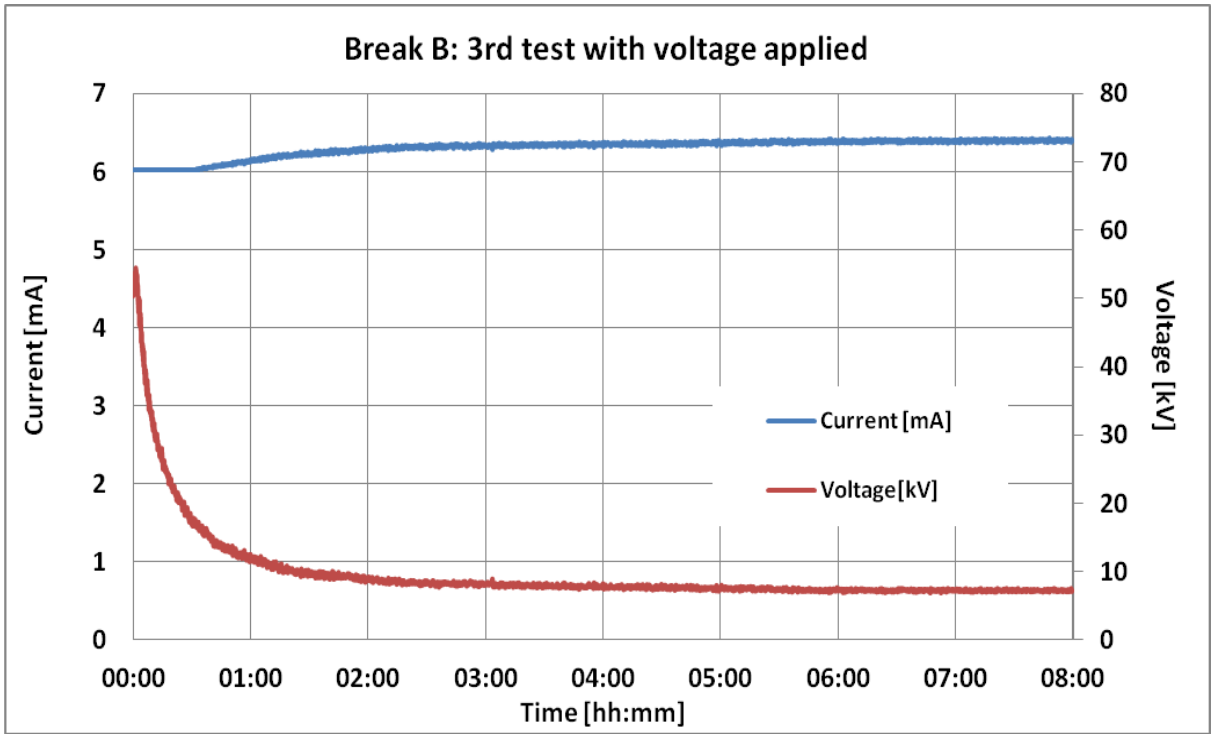

Figure V-31: Results after the third test on break B

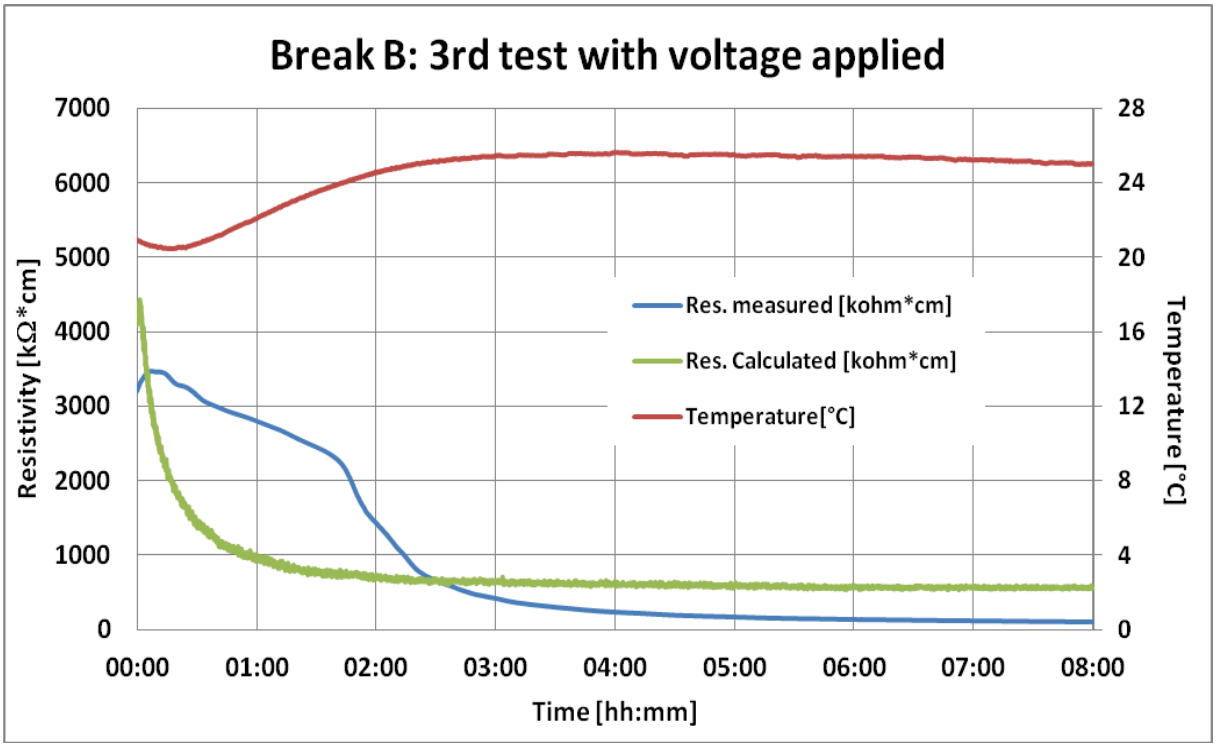

Figure V-32: Results after the third test with the second break.

Now it is possible to compare the results obtained in order to study the trends of resistivity and understand if these values follow the same trend line, and if they are similar to the results given by the results studied with the first break.

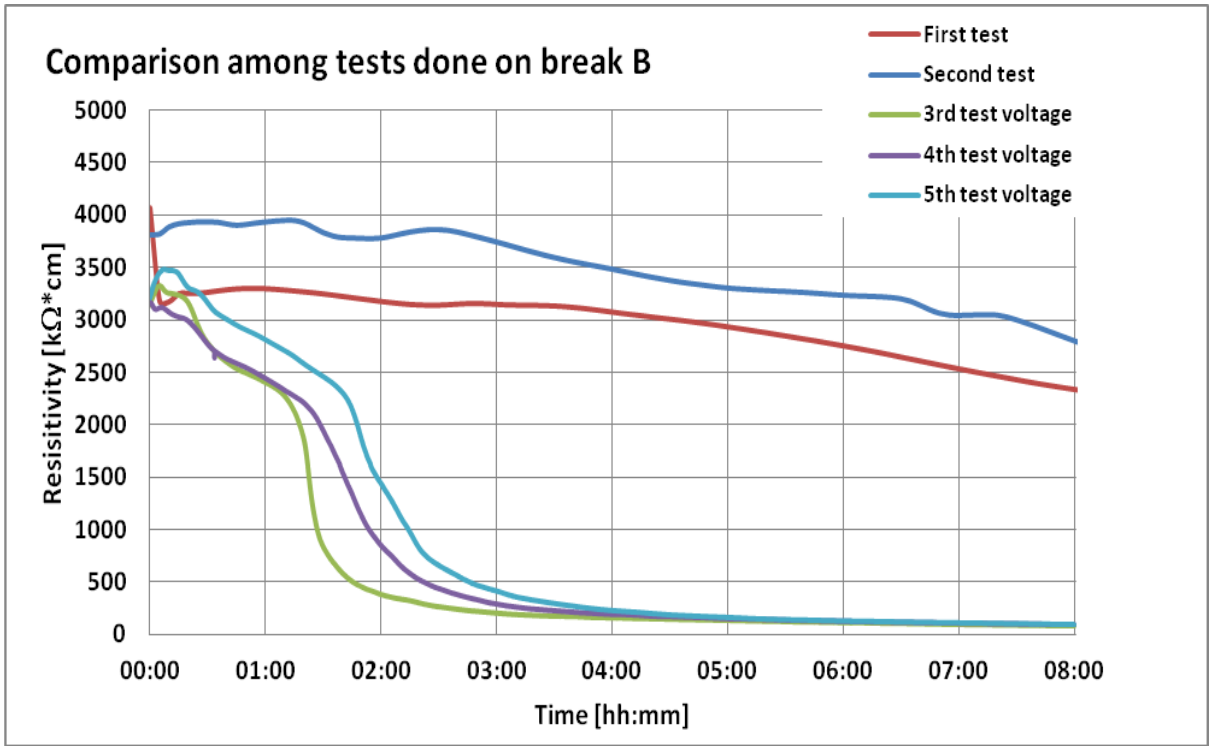

Figure V-33: Comparison among the normalized resistivity given by the tests done on break B.

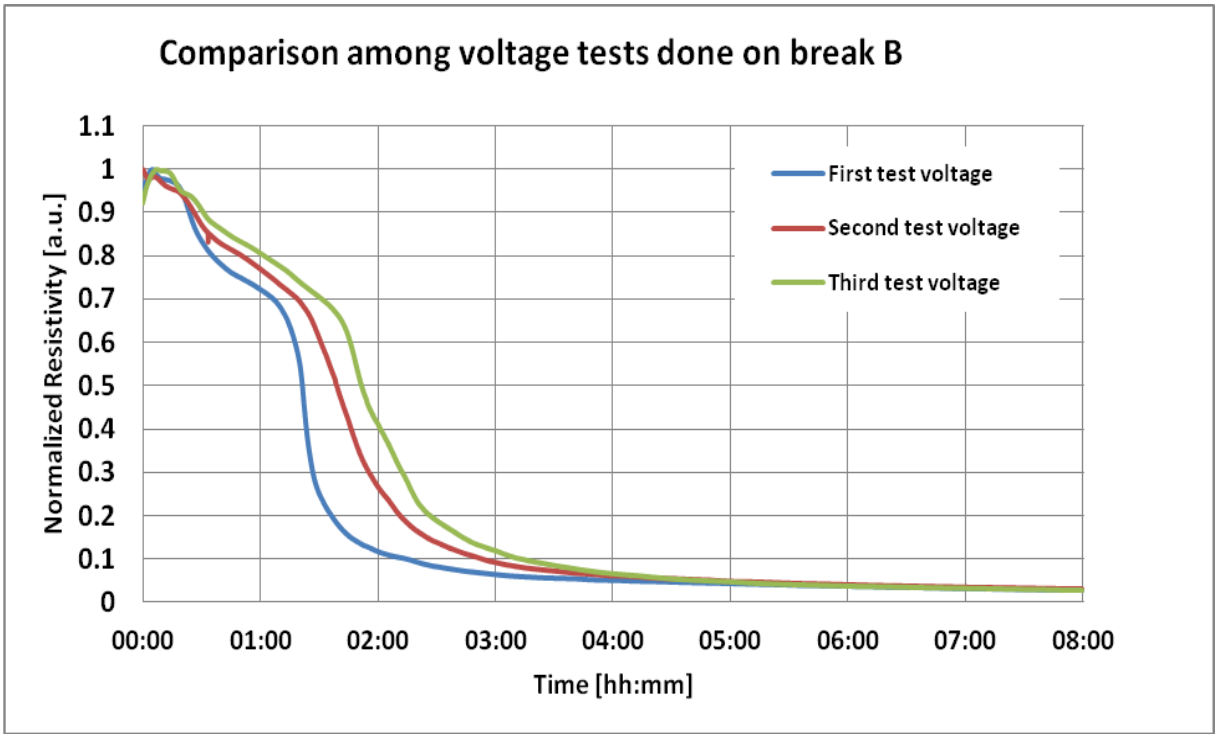

Figure V-34: Comparison among the normalized values of resistivity obtained during tests on break B.

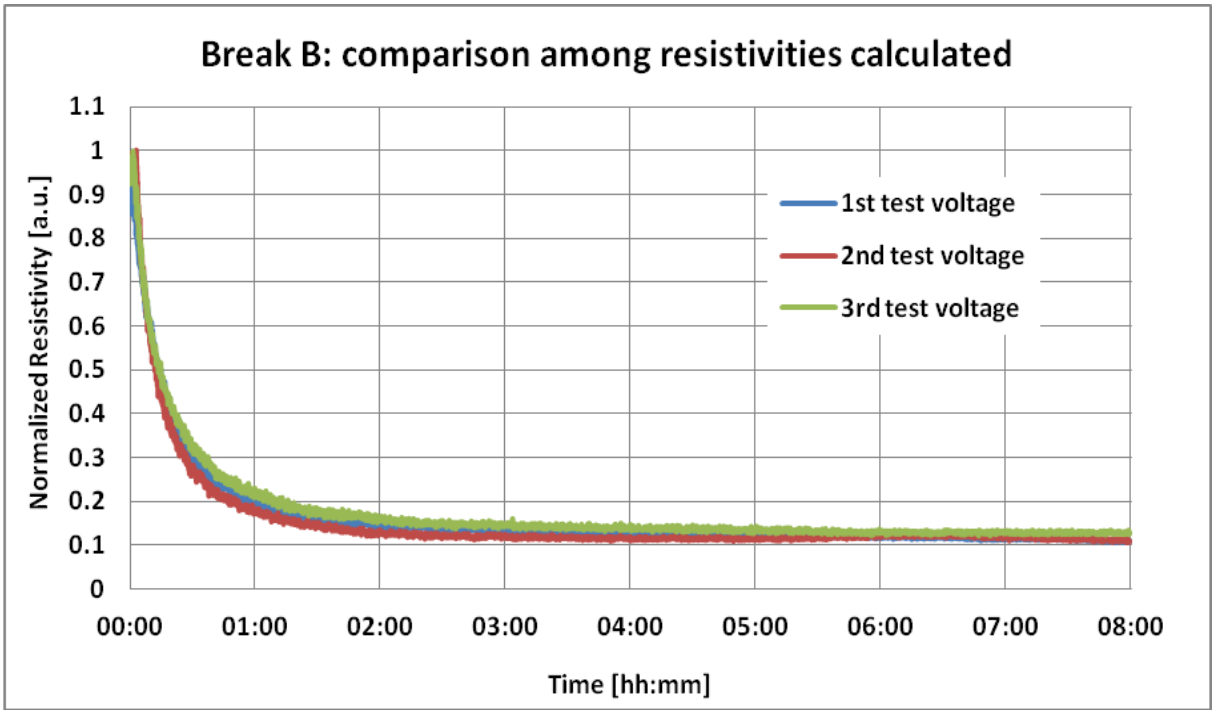

Figure V-35: Comparison among the normalized resistivity given by the tests done on break B.

Even for the second break, it has been noticed that the resistivity, after 8 hours of current applied, increases until the value of 300 kΩ*cm (see Figure V-36 and Figure V-37).

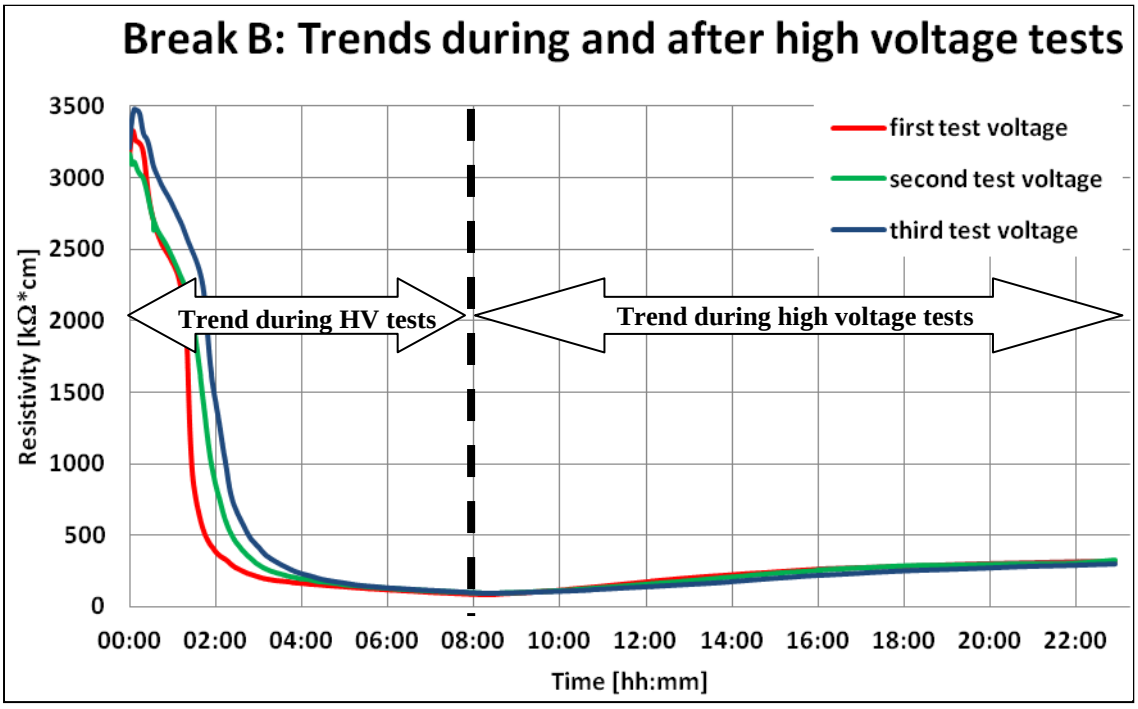

Figure V-36: Trend of resistivity during and after high voltage tests for break sample B.

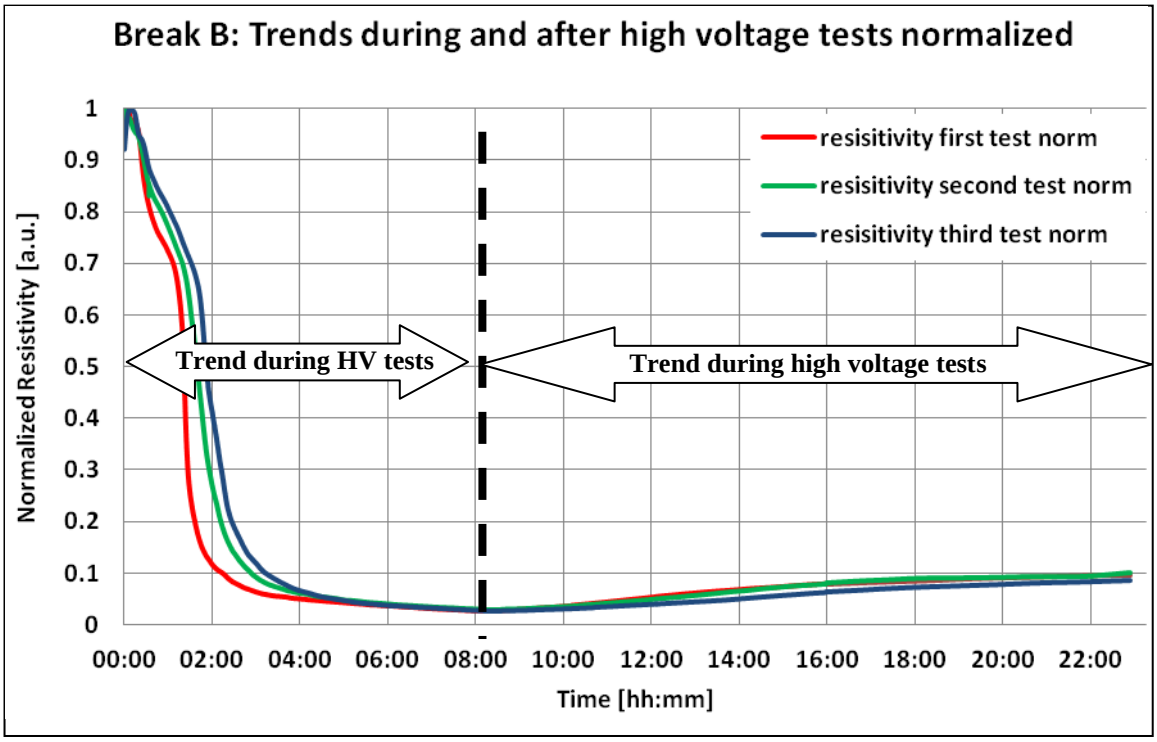

Figure V-37: Trend of normalized resistivity during and after high voltage tests for break sample B.

The results obtained show that the trends are similar between the two breaks, and the values reached are almost equal.

It is noticed that the trend of resistivity decay follow the fact that, test after test the resistivity decays slower when the number of proofs increases.

This is due maybe to the cleaning effect that removes the superficial particles inside the break.

5.4. Inspection after tests

Once all tests with the breaks were completed, the mating flanges on the breaks have been removed, the principal aim was to inspect the internal parts of the breaks to see if there were the presence of some effects created by the aggressive nature of ultrapure water, or by the application of current during the two different sets of tests.

5.4.1. First sample: break A

A deposition of a similar rust red-brown coloured has been found on inside region between the stainless steel flange and rubber as is possible to see on Figure V-38 and Figure V-39; this region is the part at grounded voltage (anodic region).

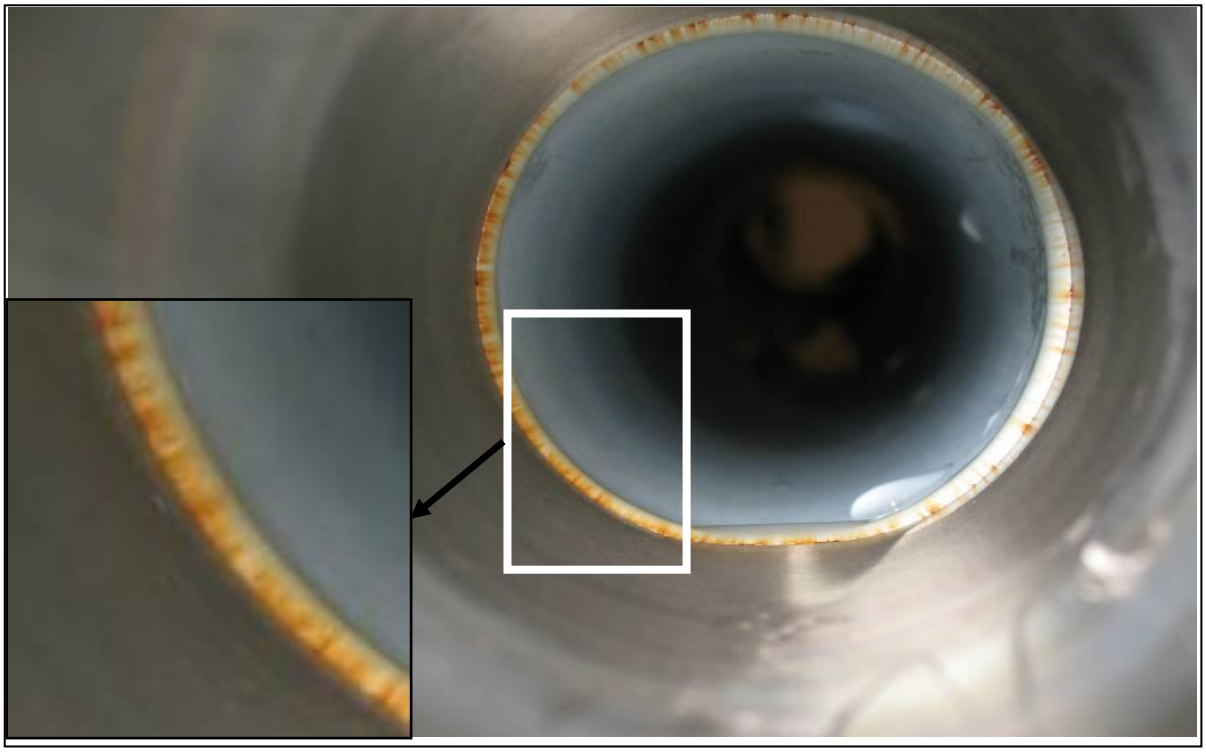

Figure V-38: Deposit similar to **r**ust found on the anodic side of the break A.

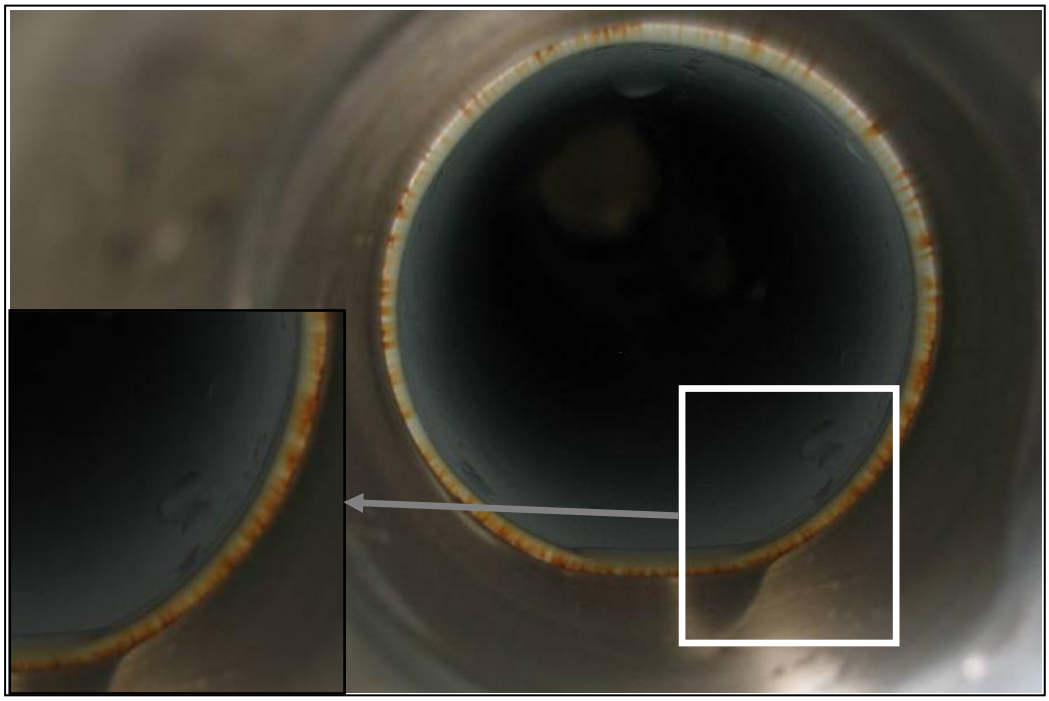

Figure V-39: Another view of the deposition found on the break A.

This rust deposition is probably due to the electrochemical effect created by the flowing current which creates transport phenomenon. The particles are extracted by the grounded flange and then, they moves to the cathodic region to permit the flow of the current; this particles also create a very pollutant effect for ultrapure water, this is referable to the fast decay of resistivity during the tests with current circulation.
In the same way, on the upper side of the break, it have been found a light-white discoloration (see Figure V-40) and this is probably due to the migration of metallic particles from this region, that is specular to the previous with the deposition of red particles, to the region at ground potential.

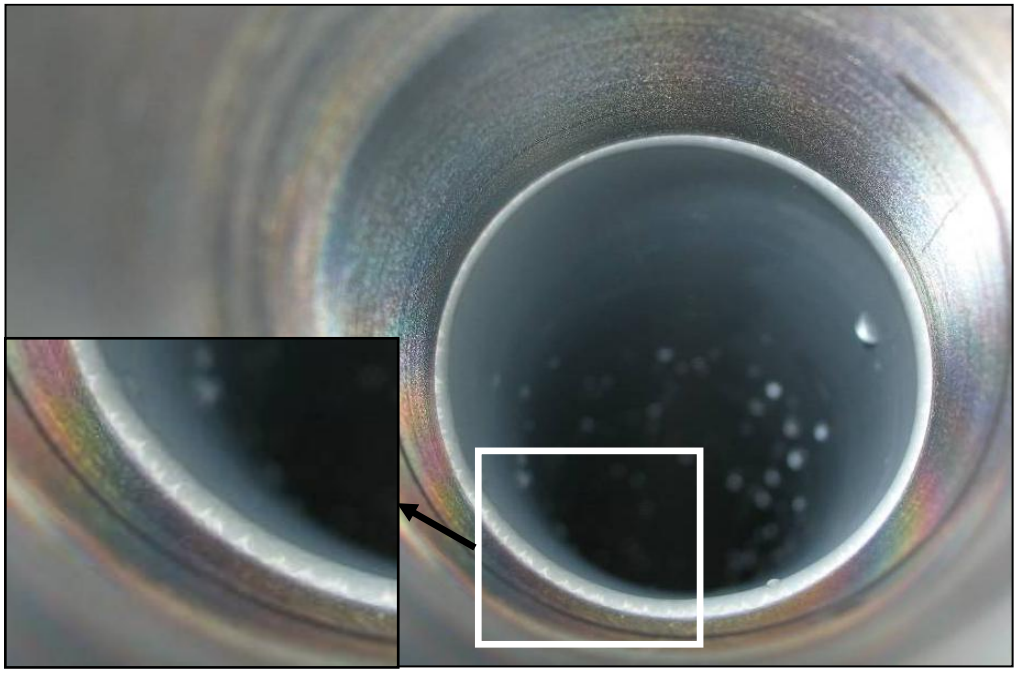

Figure V-40: White discoloration found on the cathodic side of break A.

5.4.2. Second sample: break B

The same procedure has been performed for the second break, after all tests, to confirm if the same process, with the same tests, gave the results found with the first break.
The same effects on the same regions have been found for this break, this means that for further operations, this kind of break needs a particular treatment after the installing on a cooling circuit that use ultrapure water, to avoid this effects and prevent the fast decay of ultrapure water during current circulation.
Below are shown (Figure V-41 and Figure V-42) what has been found during the inspection after the tests.

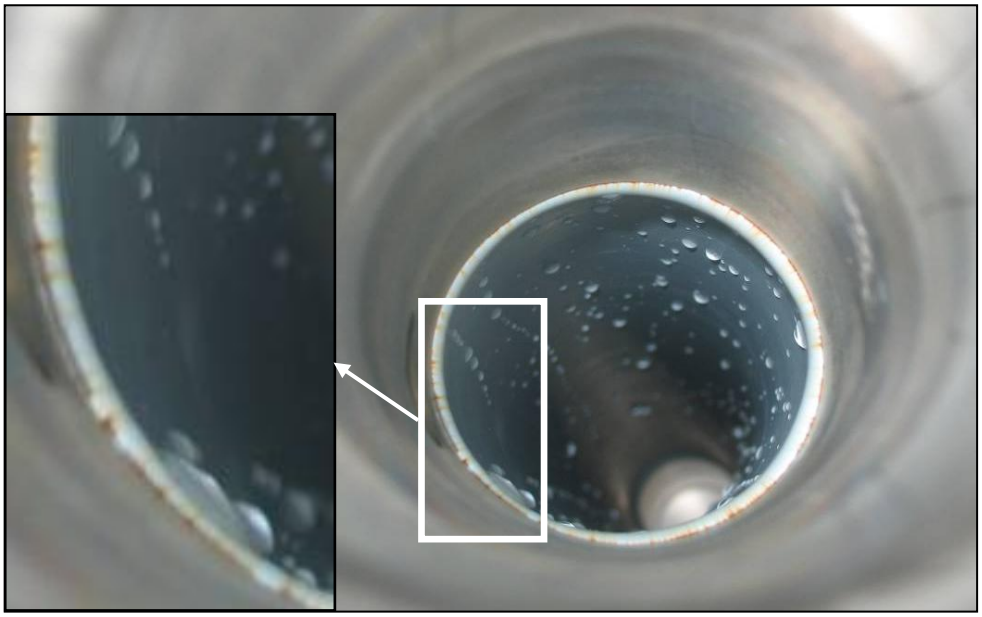

Figure V-41: Deposition found on the anodic side of break B.

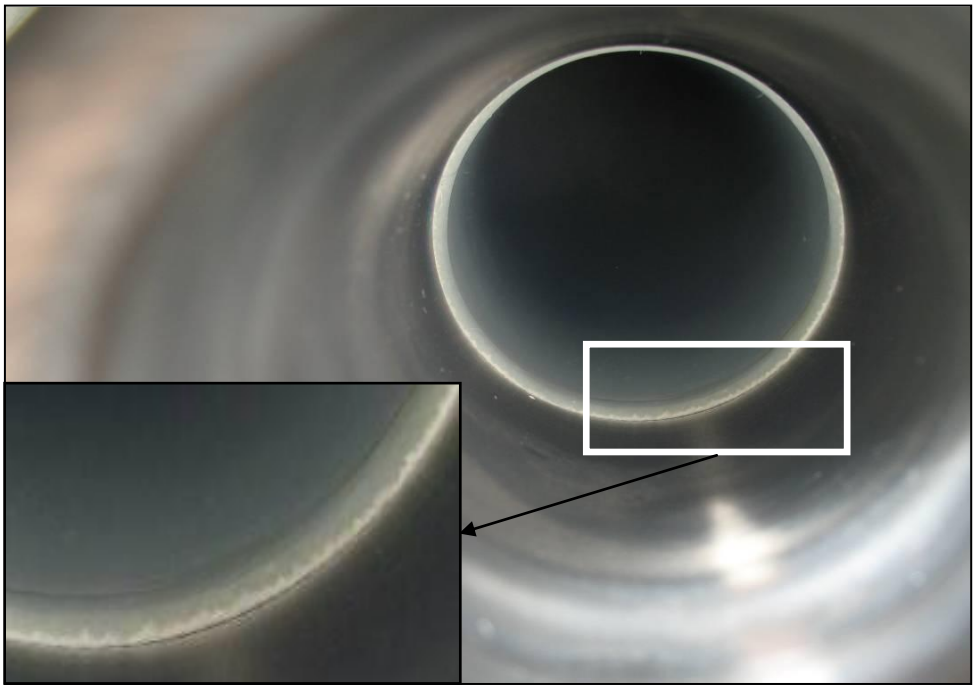

Figure V-42: Light white discoloration of cathodic side of break B.

5.5. Electrolytic considerations

The break, during the tests with the circulation of current is assimilabe to an electrolytic cell, where the electric energy supplied is used to make happen not natural reactions.
In our tests the negative pole (the cathode) is the upper side of the break, because the power supply supplies the voltage with negative polarity, and the side at ground potential is the positive pole (the anode).
When a current flows through an electrolytic cell, in the positive pole there is an oxidation process, and in the negative pole there is a reduction process; this could be assimilated to what is shown on previous figures. (See Figure V-41 and Figure V-42).
We tried to give an esteem of the rate of mass losses using the Faraday's first law of electrochemistry, the connection between the anodic current I_a and the rate of mass lost Δm during the time t is:

$$\Delta m = e_{eq} * q = e_{eq} * I_a * t \qquad (4)$$

Where:

Δm is the mass lost in the anodic region as a result of a flow of electric charge q;

e_{eq} is the electrochemical equivalent of corroded metal, and is given by:

$$e_{eq} = M/(z*F) \qquad (5)$$

M is the molar mass of metal used;
F is the Faraday constant equals to 96485 Coulomb;
z is the valence of the ion formed after the holding of the anodic reaction (z=2 in our case).

On the hypothesis that the principal reaction that happen inside the break is

$$Fe \longrightarrow Fe^{2+} + 2e^-$$

This reaction requires -0.44V of energy to happen, and this could be the worst condition because on the equation (5) z=2 is the worst condition under this hypothesis; there is another reaction that involves Iron:

$$Fe \longrightarrow Fe^{3+} + 3e^-$$

This reaction needs 0.771 V, higher than the previous reaction.
Under this hypothesis, the value of M is 55.8 and the electrochemical equivalent of corroded metal is:

$$e_{eq}=55.8/(2*96485)= 0.000289 \text{ g/C}$$

Now, we can calculate Δm:

$$\Delta m= 0.000289*0.006*(3600*8) \approx 0.05 \text{ g}$$

This is the rate of mass lost during 8 hour of test, we have to multiply this value by 2 because the test done under voltage for this first break amount to about 16 hours.

The total amount of mass removed is: $\Delta m_{tot}= 0.05*2= 0.1$ g

For long term operations it we have to expect that the amount of material removed will be proportional to the current applied because the current will be much higher and the operations time will be longer than these tests.
Another factor that was not taken in consideration is that on SPIDER and MITICA the ultrapure water is in movement inside the pipes, thus to the corrosion effect it will be necessary to add the erosion effect, and this particular process will rise the amount of particles inside the cooling plant and make worse the purity of water.

5.6. Water analysis

A water analysis, in order to study the composition of water inside the break samples, has been performed to understand the composition of this element after the high voltage tests and validate the amount of mass lost, under certain hypothesis, calculated in the previous paragraph.
Before the analysis of water samples it has been necessary use an acid, to remove some suspended particles found on the same water samples took from the breaks.
The analysis for the first break sample has shown that the average of elements found inside water was:

Table V-3: Average of elements dissolved inside water of break A.

Element	Chromium	Manganese	Iron	Cobalt	Nickel	Copper	Zinc	Molybdenum
Average mass [ppb]	37.13	6.40	25.37	0.13	18.74	11.64	25.16	0.56
Average mass [µg]	48.64	8.39	33.23	0.17	24.55	15.25	32.96	0.74

The total amount of element dissolved inside break A, where the total volume of water is to 1.31 litres, is 163.91 µg. This result, compared to the amount of mass lost calculated with the Faraday's law, show that there is an important difference of mass; a possible explanation is that the principal reaction hypothesized on previous paragraph is not the only that happens, because there is not only the presence of Iron.
This is an average because it has been performed more than one shot to analyze the water samples.
It is possible to suppose also, that the deposition process on the cathode side, that produced the light white discoloration (see Figure V-40 and Figure V-42) determined a sort of impoverishment of substances dissolved into ultrapure water and then this caused the reduction of concentration of same substances.
Another important fact found after the analysis is that there is the presence of elements that are not inside the chemical composition of Stainless Steel 316L, such as Copper and Zinc. The presence of these elements requires further studies because these elements might be entered on the circuit during the purification of water, from the filters or from the inox tank, there will be necessary to analyze the water outside the purification test section.
The analysis for the second break sample found the presence of these elements:

Table V-4: Average of elements dissolved inside water of break B.

Element	Chromium	Manganese	Iron	Cobalt	Nickel	Copper	Zinc	Molybdenum
Average mass [ppb]	77.97	7.89	22.50	0.26	26.97	5.45	19.24	1.56
Average mass [µg]	102.13	10.34	29.48	0.35	35.34	7.14	25.33	2.04

Even for this case the total amount of average mass lost is 212.15 µg, lower than the mass lost calculated, the reasons are the same described before. The analyses have been performed with a specific mass spectrometer described at page 111.

Chapter VI : Conclusions

On this work a prototype of hydraulic break has been characterized. This component will have the purpose to abduct ultrapure water (with resistivity $\rho > 2M\Omega*cm$) to cool high voltage components (up to -110 kV DC) for nuclear fusion experiments.

The break sample, previously studied with *Finite Elements Method*, has been tested with a voltage applied in order to study its dielectric strength. A voltage of -150 kV DC has been reached (maximum value of available power supply) without any problems. The results showed that the break can assure a good electric insulation, over the range of operation, since the operations will foresee a maximum voltage of -110 kV DC.

For further tests, ultrapure water has been obtained from deionized water (resistivity > 300 $k\Omega*cm$) commercially available. The purpose is to purify the water to a resistivity higher than $2M\Omega*cm$, value that is required in the cooling plant. Thus, the tests done on the break prototype filled with pure water showed that the resistivity has a fast decay during time. This phenomenon is due to the aggressive behaviour of pure water that dissolves substances with which it comes in contact.

The decay of resistivity during high voltage tests became faster than previous tests, without voltage applied, because the flow of a current, on the column of water, caused electrochemical phenomena.

Further investigations will be necessary in order to limit the fast decay of resistivity of pure water and to adopt some countermeasures for the correct running of the cooling plant.

Appendix

A.1 Water resistivity degradation

A.1.1 Rouge and rouging process

Stainless steel is often chosen as the material of construction of material processing because of its inherent corrosion resistance and the ease of use.
Under some environments, stainless steel is not inert and degradation of stainless steel may occur through different mechanisms. In ultrapure water the degradation of stainless steel often leads to the generation of particles, this is an undesirable phenomenon.
The process, know as rouging, beings with the formation of a thin yellow surface film, that if allowed to grow, will proceed (in color progression) to black, at which time, if the oxide layer is thick enough, the scale will spall and generate particles downstream. Essentially rouge is rust, which is the byproduct of corrosion that occurs on stainless steels surfaces that are exposed to a corrosive environment, in this case high purity water. The main constituents of rouge are iron oxides, but may include iron, chromium, nickel and other elements.
There were defined three different classes of rouge.
Class 1 appears as an orange/magenta film comprising particles that are electrostatically attached to the surface. The particles can be removed by ultrasonic cleaning. The following reactions have been proposed:

$$2Fe^{0}+4H_2O \longrightarrow 2FeO(OH)+3H_2$$

producing an orange discoloration, or

$$2FeO(OH)+2H_2O \longrightarrow Fe_2O_3+3H_2$$

or

$$Fe^{0}+3H_2O \longrightarrow Fe_2O_3+3H_2$$

producing a magenta discoloration.
Class 2 rouge typically occurs in the presence of chlorides. The scale that forms must be removed by mechanical or chemical means. The result is a red discoloration and the following mechanisms have been proposed:

$$C_2O_3+10Cl^{-}+2H_2O \longrightarrow 2CrCl_3+4HClO$$

$$2Fe^{0}+3ClO^{-} \longrightarrow Fe_2O_3+3Cl^{-}$$

Note that with class 2 rouge, both chromium and iron are active species in the degradation reaction.
For *Class 3* rouging, the species that forms is not Fe_2O_3 (hematite) but rather Fe_3O_4 (magnetite). Because of this, the scale is blue-black in color and cannot be removed by simple cleaning. The mechanism follows the expected reactions for magnetite:

$$Fe^{0}+H_2O \longrightarrow FeO+H_2(g)$$

$$2FeO+H_2O \longrightarrow Fe_2O_3+H_2(g)$$

$FeO+Fe_2O_3 \longrightarrow Fe_3O_4$

Because nearly all of above reactions include the oxidation of iron, the primary mechanism used to control the formation of rouge in clean water systems is to introduce chemical agents that reduce iron at the interior surface of the pipe, thereby preventing the formation of any iron oxide.[f]

As the temperature increases, the color becomes darker.

For stainless steel, rouging is a commonly observed long-term phenomenon, but it can also be degraded at a speed much faster than expected under certain environments. Insidious corrosion or corrosion that occurs in localized environments rather than generalized corrosion can be extremely destructive because of the difficulty in detecting the corrosion event.

Although rouge may be found in ambient water systems, it is more prevalent in hot high purity in water systems, in pure steam generators, and pure steam distribution piping.

Typical locations in water systems where rouge first appears include:

- Heat exchangers, particularly hot ends
- Pump casing and impellers
- Spray nozzle orifices and spray areas of water storage tanks
- Deadlegs and condensate collection areas
- Heat affected zone of welds
- Areas that have been ground or mechanically polished but not properly cleaned and passivated
- Valve diaphragms
- Stress Corrosion Cracking (SCC) affected areas

Rouge is the observed evidence of corrosion. The various types of corrosion that may occur in high purity water include:

- General corrosion due to chemical attack, normally uniform in nature. An example is corrosion from low pH, and aggressive cleaning and passivation chemicals that etch the stainless.
- Pitting corrosion, typically due to chlorides.
- Crevice corrosion, associated with dissimilar metals. Can also occur at weld boundaries when excessive heat alters the properties of the metal so that it is no longer stainless.
- Stress Corrosion Cracking, common when a chlorine or high chloride environment exists, especially at elevated temperature.
- Intergranular corrosion, such as in sensitized weld areas.
- Contact corrosion, due to surface contamination by deposited foreign particles from the surroundings, such as contact with carbon steel, grinding particles, or just plain grease and dirt.
- Erosion-Corrosion, typical in cavitation pumps, and in high velocity areas such as valves and orifices of spray balls and nozzles.
- Corrosion due to localized biological effect. Occurs under deposition and biofilm.

A.1.2 Understanding rouge

An useful approach to understanding rouge is to consider the various places where the stainless materials goes through, and what factors influence rouge formation in each phase. These phases are:

- The Mill and Material Composition
- Fabrication
- Process Environment
- Maintenance

- ***Mill and Material Composition***

On ICE the stainless steel used is 316/316L grade, this kind of stainless steel belongs to austenitic stainless steel and this family has a small amount of sulfur. Manganese sulfide inclusions may form during cooling of the melt at the mill. Pitting corrosion of stainless steel is related to these inclusions. Due to a difference in the cooling rate between the inclusions and the base metal, depletion of chromium occurs around the inclusion, rendering the alloy in that region to be no longer stainless.
Some mills may add aluminum to the melt in order to minimize porosity; traces of aluminum on the stainless surface become corrosion sites.
In general, the higher the chromium to iron ratio on the surface, the higher is the corrosion resistance.

Fabrication

Fabrication steps such as machining, shearing, welding, mechanical polishing and grinding all damage the passive film formed at the mill, and may result in surface contamination. Abrasive tools used in mechanical polishing, such as Silicon Carbide and Aluminum Oxide (corundum) are an example.
Small particles from fabrication tools or from the surrounding environment may become impeded in the stainless steel and become Contact Corrosion sites, unless removed during cleaning.
Welding produces oxides in the "heat affected" zone, this zone can have different metallurgy than the base metal, which results in Galvanic Corrosion. Sensitized weld areas are also susceptible to Intergranular Corrosion.

Process Environment

Rouge in this category is associated with the affect of the prevailing process environment on stainless steel process equipment and components. In addition to the high purity water the following process factor influence the susceptibility of stainless steel to rouging:

1) Feedwater pH and level of CO_2

Feedwater from reverse osmosis or some ion exchange systems, such as week acid beds, may have low pH, which is likely to cause rouging on the feed side of stills.

2) Chlorine in Feedwater

Of all possible causes of corrosion, chlorine is probably the most destructive, since it results in Stress Corrosion Cracking (SCC). Although rouge will appear in areas affected by SCC, the rouge problem become a mute issues, since SCC causes catastrophic failure that would call for replacing the affected areas, or part of, if not the whole piece of equipment. For these reasons, chlorine demands particular and careful attention.

3) Erosion-Corrosion

Some areas of the water system are subject to this type of corrosion, which can yield significant amounts of rouge. Typical examples of rouge contributors are pump cavitation and high velocity flow (velocities beyond the critical velocity for the material erode the surface and remove particles of metal, which corrode and turn into rouge).
It's important to note that metal particles removed by erosion are carried downstream and disperse throughout the system. This type of corrosion in more responsible for suspended rouge particles than, for example, rouge forming on a sensitized weld, which is more likely to remain adherent to the surface.

- ***Maintenance***

High Purity Water systems, during their lifetime, are subjected to repairs, alterations, cleaning and passivation.
Common sense and general practices call for cleaning and passivating newly installed piping runs or equipment before connecting to existing systems, this does not always happens.
Some de-rouging and cleaning chemicals are very aggressive and will etch stainless steel if the exposure time, temperature, and concentration are not controlled very carefully, which is not always easy to do.
Some de-rouging chemicals leave behind a blackish, greasy, carbonaceous deposit sometimes referred to as "Smut", which requires removal using alkaline and detergent type cleaners; if not effectively removed, smut-covered surfaces do not form a passive film, and can contaminate the system downstream.
One factor in the amount of suspended rouge build up in the tanks and circuits is the circulation/withdrawal ratio; accordingly, the more water that passes over the site, the more rouge is produced. In a one-way system, the water that passes over the site only once. In a circulation loop, the water may pass over the same site many times before leaving the system. With every pass, more rouge is picked up; if the amount of water withdrawn from the loop is small compared to that circulated, the concept of rouge build up in the system becomes obvious.

A.1.3 Rouge removal

Various chemicals and recipes are used to remove rouge.

- Effectiveness depends on:
  - Type of chemical or formulation
  - Concentration
  - Temperature
  - Exposure time
  - Method applied: Flooding/immersion, spraying, circulation, etc.

A.1.3.1 Rouge Removal Chemicals

- *Phosphoric acid*

- Does not etch the metal
- Fairly effective
- Best overall
- Often used as cleaning and passivating agent

Combining the effectiveness of phosphoric and that it does not etch the stainless; it is probably the best overall choice.

- *Citric acid*

- Slow acting
- Safe to handle
- Not effective on hard baked-on rouge

- *Oxalic acid*

- Very effective
- Quick acting
- Used for the worst cases of rouge
- Can, and often does etch stainless steel
- Length of exposure must be carefully controlled
- Passivation is required after an oxalic acid cleaning and rinse

- *Ammonium citrates*

- Similar to citric acid
- More often used as passivation agent

A.1.3.2 Rouge removal methods

One of the following methods or combination may be used depending on the type, size, and configuration of equipment or parts to be cleaned.

- Circulation
- One way intermittent flow
- Spraying
- Flooding
- Tank immersion
- Swabbing/wiping

A.1.4 Water resistivity measurement

As mentioned before, at 25°C, ultrapure water has a theoretical resistivity of 18.3MΩ*cm. If 1.0 µg/L of impurity, calculated as sodium chloride, is added to ultrapure water, the resistivity decreases 3.9% to 17.5 MΩ*cm. However at 100°C, where the resistivity of ultrapure water is 1.29 MΩ*cm, 1.0 µg/L of impurity decreases the resistance only 0.8 % to 1.28 MΩ*cm.
This discrepancy implied that at elevated temperatures the resistivity change for impurity levels below about 1 microgram per liter (µg/L or ppb) could not be calculated.
The theoretical conductivity of pure water, κ, and its reciprocal, resistivity, ρ, are related to its basic physical chemical properties according to

$$\kappa\ (S/cm) = 1/\rho = 10^{-3} d^{*}(C_{H}^{+}\lambda^{+}_{H} + C^{-}_{OH}\lambda^{-}_{OH})$$

Where d is the water density (g/cm^3). λ^{+}_{H} and λ^{-}_{OH} are the specific conductances of H^+ and OH^- (S*cm^2/mol), and C_{H}^{+} and C_{OH}^{-} are the respective concentrations of these ions (mol/kg water). In pure water, the only source of ions is due to auto-dissociation, which, are determined from the H_2O dissociation constant K_w and from the previous equation

$$\kappa\ (S/cm) = 1/\rho = 10^{-3} d^{*} K_w^{1/2} (\lambda^{+}_{H} + \lambda^{-}_{OH})$$

At 25°C the accepted values with their uncertainties for conductivity, κ and its reciprocal, resistivity ρ, are

κ=0.05501±0.0001 μS/cm at 25.00°C

ρ=18.18±0.03 MΩ*cm at 25.00°C

A.1.5 Temperature sensitivity of conductivity

Figure A.1 shows the importance of accurate temperature measurement. At 0°C the sensitivity of conductivity (or resistivity) of ultrapure water is 7.4%/°C.
Therefore an error of 0.1°C in temperature measurement is equivalent to a conductivity error of 0.74%. At 100°C this sensitivity drops to 2.3%/°C, a factor of three reduction. It might be inferred from Figure A.1 that accurate temperature measurement is less important at high temperatures, but the issue is more complex than this because the sensitivity of the measurement to impurity concentration has not been considered.

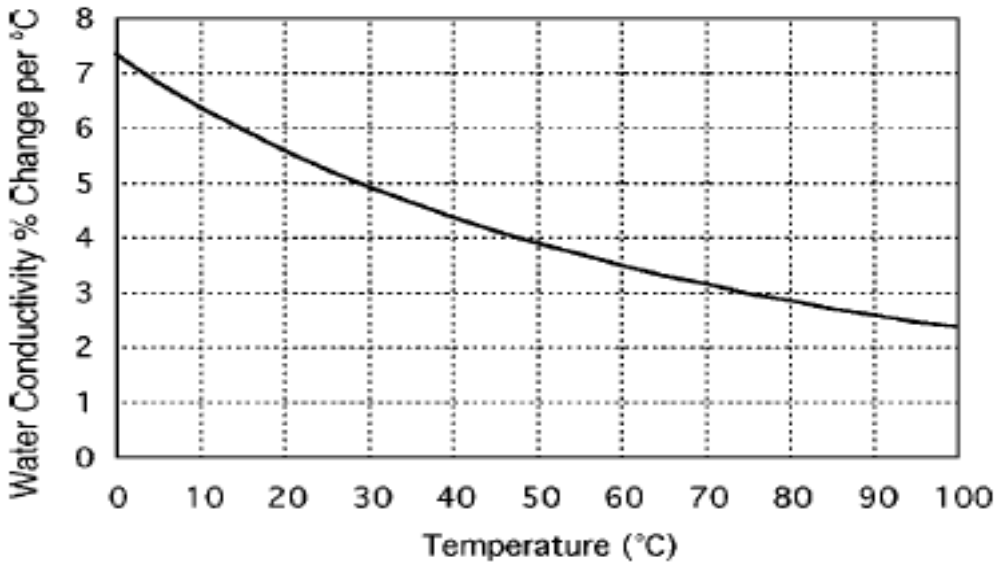

Figure A.1: Sensitivity of ultrapure water conductivity to changes in temperature.

The temperature dependence of the conductivity of the impurity and the sensitivity of the temperature compensation algorithm to temperature errors both has a major effect on temperature compensated conductivity measurements.
Figure 3.2 shows how this sensitivity changes with temperature, and shows a factor of 12 decrease in sensitivity when the temperature increases from 0 to 100°C. Most important, at 25°C the sensitivity is 4%/ppb while at 85°C it is 1%/ppb, so the instrument must be four times as accurate to be useful at 85°C as it is at 25°C.
This means cell constant calibration, instrument and sensor accuracy, and calculation procedures must all be four times as accurate.

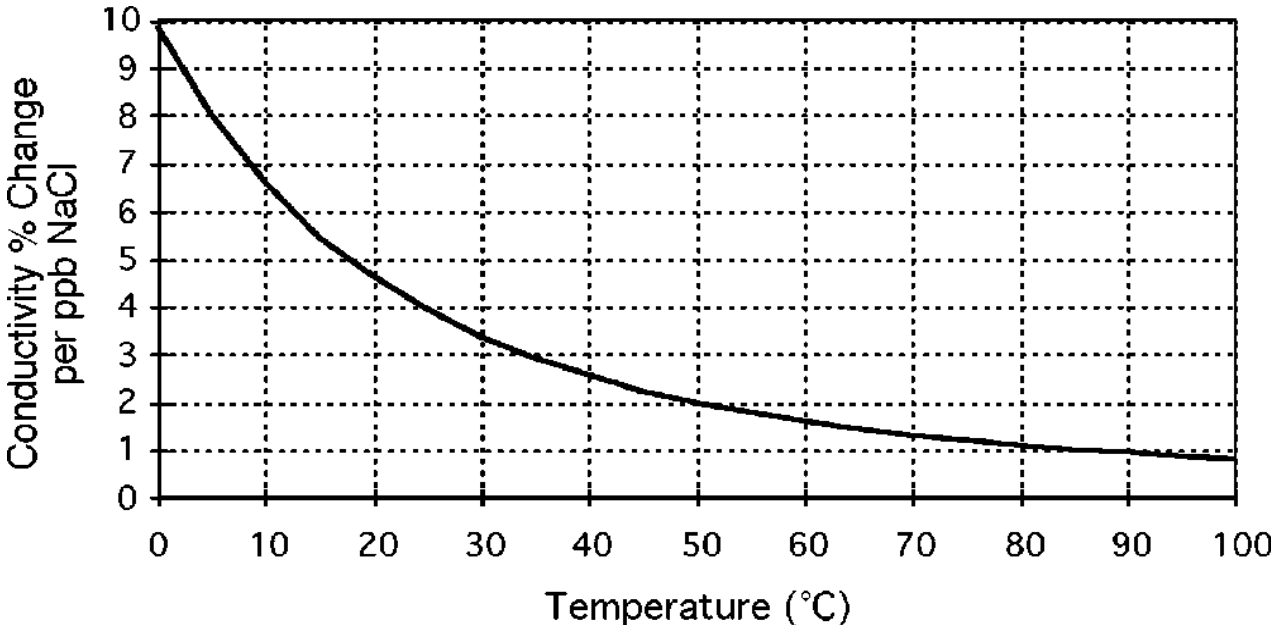

Figure A.2: Sensitivity of conductivity change to presence of impurities as a function of temperature.

The sensitivity of the compensated conductivity to the temperature measurement and to the conductance measurement is shown in Figure A.3. At 1°C temperature error at 25°C causes a 4.9% error in compensated conductivity, while at 100°C the same temperature error causes 11.6% error in compensated conductivity. Figure A.2 also shows that a 1% resistance measurement error causes about half the percentage error in compensated conductivity as a 1°C temperature error does. Figures A.1 and A.2 show that as temperature increases a temperature measurement error has less of an effect on the measured resistance but has a greater effect on the compensated conductivity. [g]

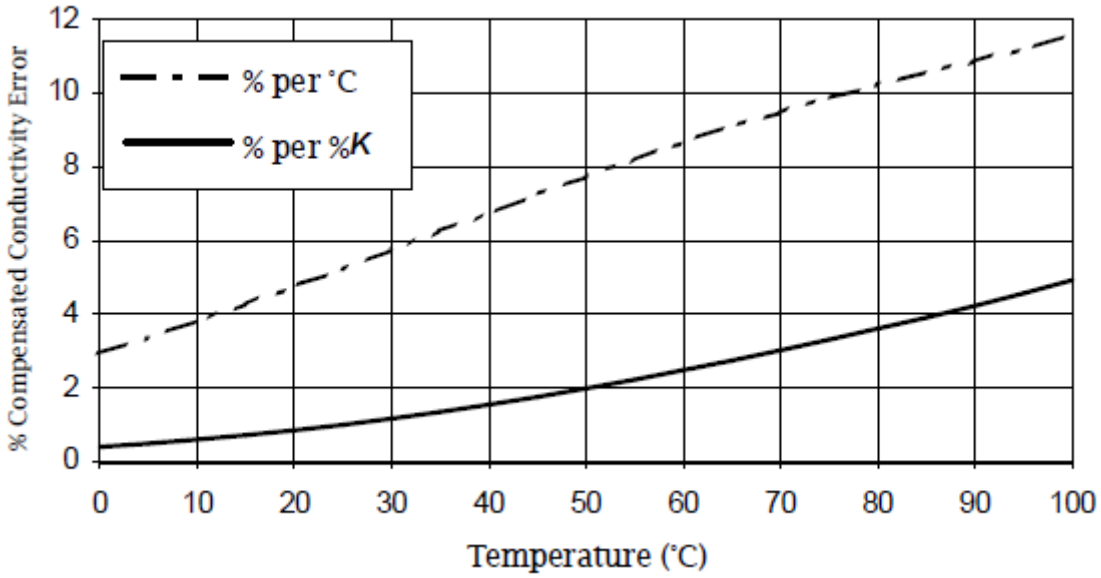

Figure A.3: Sensitivity of the compensated conductivity to errors in the conductance and temperature measurements.

Figures A.2 and A.3 show that at 85°C, temperature must be measured to within 0.1°C and conductivity to better than 1% to get even a rough measurement of impurity with a measurement sensitivity of 1 ppb. At 25°C it is

only needed to measure to about 3% accuracy to achieve the same instrument accuracy. Thus the temperature measurement only had to be accurate to about 0.5°C.

To illustrate the variety of detectable species, the resistivity of three different common chemicals – an acid, base, and salt – at very low concentrations at 25°C are shown in Figure A.4. At very low contaminant concentrations, 1-10 ppt (1 ppt=1ng/L), the resistivity is virtually unchanged. It is only at concentrations exceeding 100 ppt that acid and salt species lower the resistivity so that it is discernible from 1-10 ppt contaminant. And if the contaminant is slightly basic (NaOH impurity), then there is a slight increase in the resistivity until ~ 1000 ppt (1 ppb).

At higher temperatures, these concentrations become more difficult to detect.

The ability to detect the lowest concentrations of ionic species is controlled by three factors:

- ✓ the specific conductance of the ions,
- ✓ the sensitivity of the instrumentation,
- ✓ the absolute calibration of the resistivity system.[h]

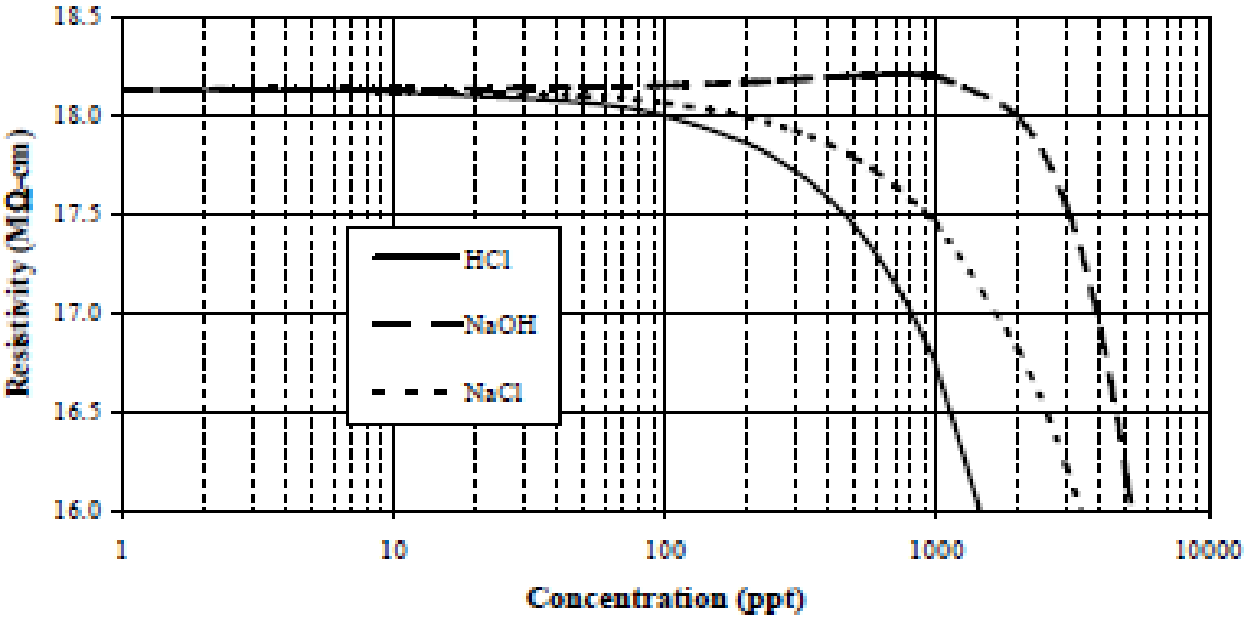

Figure A.4: Resistivity at trace concentrations of three common impurities at 25°C.

A.1.6 Cell calibration

Calibration of the sensor is also known as determination of the cell constant.
The accurate determination of the resistivity cell constant can be quite difficult in actual practice. Conceptually, the cell constant is sometimes idealized as two 1 cm^2 plates (area, *A*) that are separated by 1 cm (distance, *d*) as shown in Figure A.5.

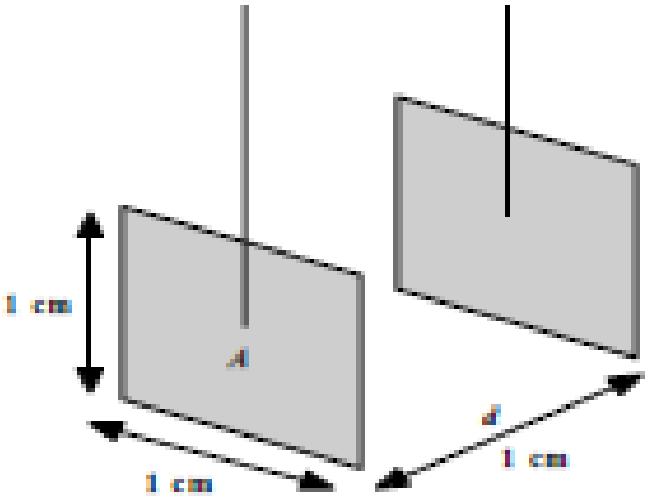

Figure A.5: Conceptual drawing of cell constant

The resistance of the water between the electrodes is the value measured by the meter. Since the resistance will increase with *d* and decrease with *A*, the resistance is normalized for these geometrical factors in order to measure the ionic quality, or resistivity, of the water. These geometrical or normalization factors are combined into one term called the cell constant, Φ. For the general case, Φ is defined in this equation:

$$\Phi = l/a \text{ with the units of } cm/cm^2 \text{ or } cm^{-1}$$

While an accurate measurement of the cell dimensions could yield the cell constant, there are some factors that make this approach impractical. First, this square plate model does not have the mechanical stability for in-line process applications. Sensors with concentric electrodes have become the most common design for in-line ultrapure water applications.

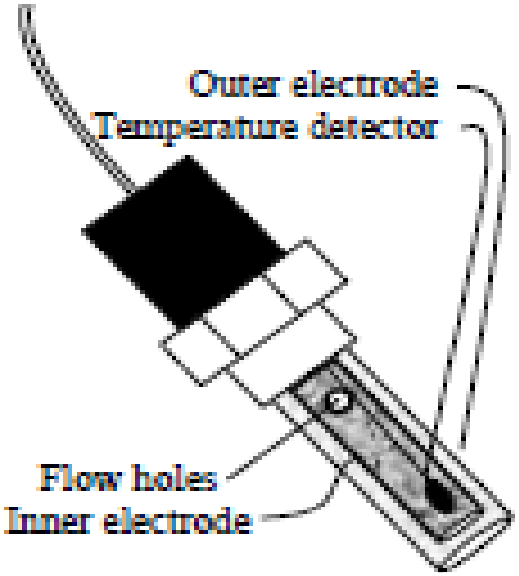

Figure A.6: Concentric cell design

The only practical method available to accurately determine the cell constant to 1% accuracy or better is by measuring the resistance of a standard reference solution.
The resistivity of the reference solution must be known with high certainty at the measurement temperature and the uncompensated resistivity and temperature of the fluid must be precisely measured.
The cell constant is then determined by:

$$\Phi = \frac{\text{Measured Resistance}(\Omega)}{\text{Reference Solution Resistivity}(\Omega * \text{cm})} = \text{cell constant } (\text{cm}^{-1})$$

Most modern conductivity or resistivity instruments either read a cell constant from a smart sensor or allow the user to enter either a cell constant or cell constant correction factor. Unfortunately, it is difficult to calibrate a conductivity cell for ultrapure water applications because there is no accepted standard solution that is suitable. A standard must have a resistivity in the same range as the solution being measured or there can be errors from a number of sources; examples include surface effects and measurement frequency and waveform. Higher resistivity solutions are generally not stable in the presence of air.
The cell should be initially calibrated in water at 40 to 50°C. It is easy to obtain ultrapure water at this temperature and the sensitivity to impurity is reduced, so the calibration can be more accurate.

Figure A.7: Cell used for resistivity and temperature measurements.

However, calibration depends on knowing the intrinsic resistivity in this temperature range, and there is still some uncertainty that limits the accuracy of high temperature calibration above 50°C.

The temperature of the water should then be reduced to 25°C where the resistivity of the water is accurately know to be 18.18 MΩ*cm on the basis of well-known physical parameters; the cell constant should be verified at 25°C.

Figure A.8: Particular of sensor cell used, it is possible to see that the constant cell is 0.01 cm^{-1}.

A.1.6.1 Cleanliness and aging

Sensor cleanliness is very important. A sensor newly installed in an ultrapure water system must typically operate for several hours before it can be used for reliable measurement; there is an initial aging effect that causes the cell constant to change slightly the first time it is used at high temperatures. Once this change has taken place there does not appear to be significant long term drift and the calibration will stay constant for many months. [i]

A.2 General Properties of Stainless Steel AISI 316L

Alloy 316L is molybdenum-bearing austenitic stainless steel which is more resistant to general corrosion and pitting/crevice corrosion than the conventional chromium-nickel austenitic stainless steels such as Alloy 304. Chemical composition as represented by ASTM A240 and ASME SA-240 specifications are indicated in the table below.

	Percentage by weight (maximum unless range is specified)
Element	**Alloy 316L**
Carbon	0.030
Manganese	2.00
Silicon	0.75
Chromium	16.00
Nickel	10.00
Molybdenum	2.00
Phosphorus	0.045
Sulfur	0.030
Nitrogen	0.10
Iron	Bal.

A.3 ICP-MS technical notes

The analysis relatives to the elementar concentration about water have been done on Istituto per l'Energetica e le Interfasi (IENI) located in Padua, using a mass spectrometer ICP-MS *X7 Series* made by Themo Elemental.

The Inductively Coupled Plasma Mass Spectrometry is a very sensible method that permits to determine different inorganic metallic and non-metallic substances with a concentration under one part per million (ppm).

The instrument uses a plasma torch ICP that produces the ionization and a mass spectrometer for the separation and the analysis of ion produced.

The ions are separated by their mass/charge ratio and the instrument produces a signal proportional to the concentration.

A quadrupole is composed by four parallel metallic bars. A direct voltage is applied to the bars, the diagonally opposite bars have the voltage with the same polarity, to this voltage is added an alternating current with frequency of some megahertz (radiofrequency).

The resulting electric field force the ions to cover an oscillating path different for each value of m/z. Varying this filed it is possible to select the value of m/z that belongs to ions that pass through the quadrupole, the ions with a value of m/z lower or higher to the selected value will be carried outside of electric field and they will not reach the detector.

The sample is introduced nebulised from the plasma torch to the detector's region using an argon flow that acts as carrier.

The concentration can be determined by means of calibration with known standard. On the specific case the standardization of instrument has been made by multi-elementary solutions certified by Accustandard.

References

[a] P.M. Bellan, "Fundamentals of plasma physics*"* pp.1-3, September 2004.
[b] Allen H. Boozer, "What is a stellarator?", *Physics of plasma*, vol.5,n.5,pp.1-9, May 1998.
[c] R.A. Krakowsky et al., "Compact Reversed-Field Pinch Reactors", *Nuclear Engineering and Design/Fusion 4*, pp. 75-120, 1986
[d] J.Wesson, *Tokamaks*, Oxford, Clarendon Press, 2004.
[e] P. Sonato et al., "The ITER full size plasma source device design", *Fusion Engineering and Design 84*, pp.269–274, January 2009.
[f] X. Dong et al., "Investigation of Stainless Steel Corrosion in Ultrahigh-Purity Water and Steam Systems by Surface Analytical Techniques", *Journal of Materials Engineering and Performance*, vol 19,n.1, pp. 135-141, February 2010.
[g] T.S. Light et al., "The Fundamental Conductivity and Resistivity of Water", *Electrochemical and Solid-State Letters*,
[h] K.R. Morash et al., "Measurement of the resistivity of ultrapure water at elevated temperature", *Ultrapure Water Journal*, pp. 1-13, December 1994.
[i] A.C. Bevilacqua, "Advances in Resistivity Instrumentation for UPW Systems of the Future", pp 1-15, March 2000.
[l] Serway, Raymond A. (1998). *Principles of Physics* (2nd ed ed.). Fort Worth, Texas; London: Saunders College Pub. p. 602

Ringraziamenti

Sono passati ben sette anni dall'inizio di questa lunga, lunghissima esperienza, ed ora ne sono giunto al termine; questi due anni di magistrale mi sono seviti come ulteriore maturazione e miglioramento e di questo non posso che esserne felice.
La fine di questa esperienza mi porterà nel mondo del lavoro, un mondo che oggi come oggi è difficile da vivere con fiducia e speranza per il futuro; quello che mi posso augurare è di riuscire a trovare un qualcosa che mi dia stabilità e che mi possa permettere di divenire sempre più indipendente.
Ma questa non è la parte per discutere del futuro che dipende solo da me, ma per ringraziare chi in questo periodo mi è stata sempre vicina.
Non posso che ringraziare per primi i miei genitori per avermi sostenuto soprattutto dal punto di vista economico ma anche nei momenti più critici.
Un menzione va a tutti i miei più cari amici per avermi sempre fatto passare attimi di spensieratezza tra cui non posso non nominare Filippo, Federico, Andrea Z., Andrea B., Igor, Valentina e Alessia.
Un ringraziamento speciale va a Giulia, che da quel lontano 29 Maggio mi ha rubato il cuore e ha portato la luce nella mia vita.
Un grazie anche ai compagni di corso con i quali abbiamo condiviso momenti critici ma che comunque assieme siamo riusciti a venirne fuori con aiuto reciproco, voglio ricordare Luca, Nicolò, Claudio e Christian.
Un altro ricordo va a chi non c'è più, a Marianna, spero che da lassù, o dovunque tu sia, possa guardarmi e renderti orgoglioso di me.
Un altro ringraziamento va ai miei correlatori Andrea e Marco, grazie per avermi supportato, ma soprattutto sopportato; un grazie anche al mio relatore il Prof. Sonato per avermi dato la possibilità di compiere questo lavoro di tesi molto importante.
Spero di aver nominato tutti,non me ne vogliano chi non ho potuto menzionare, in questi momenti ricordare tutti è difficile.